Universitat Rovira i Virgili (URV) and Universitat Oberta de Catalunya (UOC)

Master in Computational and Mathematical Engineering

FINAL MASTER PROJECT

Area: Ordinary Differential Equations

Numerical study of some bifurcation diagrams arising from ordinary differential equations

---

Oriol Llopis Almela

Supervised by Jordi Villadelprat Yagüe

Barcelona, January 29, 2024

Dr. Jordi Villadelprat Yagüe, certifies that the student Oriol Llopis Almela has elaborated the work under his direction and he authorizes the presentation of this memory for its evaluation.

Director's signature:

JORDI VILLADELPRAT YAGÜE - DNI 46627085J

Firmado digitalmente por JORDI VILLADELPRAT YAGÜE - DNI 46627085J
Fecha: 2024.01.29 09:40:40 +01'00'

FINAL PROJECT SHEET

Title:	Numerical study of some bifurcation diagrams arising from ordinary differential equations
Author:	Oriol Llopis Almela
Tutor:	Jordi Villadelprat Yagüe
Date (mm/yyyy):	08/2023
Program:	Master in Computational and Mathematical Engineering
Area:	Ordinary differential equations
Language:	English
Key words	ordinary differential equation, critical period, bifurcation

Abstract

Loud systems are a family of reversible quadratic centers depending on a bidimensional parameter $\mu = (D, F) \in \mathbb{R}^2$. Determining the bifurcation diagram of the period function by stating the exact number of critical periods for some regions of the space of parameters is still a matter of conjecture. As opposed to an analytical study, this work aims to tackle this question numerically with a view to provide solid evidence about the exact number of critical periods arising within these regions as well as analysing bifurcation curves. By compactifying the vector field of Loud systems to $\mathbb{RP}^2$, the period annulus remains bounded for all values of μ within the regions of interest, avoiding periodic orbits to escape to infinity, which may propagate numerical errors. Combining both 4th-order Runge-Kutta methods and other strategies of numerical integration, the period function and, subsequently, the number of critical periods will be determined for each value of μ with the intention of sketching the bifurcation diagram and comparing the results obtained with those proven analytically. Thus, the notion of criticality -number of critical periods in the period function- resembles Hilbert's 16th problem and the concept of cyclicity. Three different types of bifurcations will be identified: at the inner boundary of the period annulus, at the outer boundary and at the interior; and some conjectures will be verified in accordance with the limitation imposed by the computational cost of discretizing the space of parameters.

Keywords: ordinary differential equations, planar centers, period funcion, period annulus, bifurcation diagram

Contents

List of Figures

List of Tables

Chapter 1

Introduction

Loud systems are a bi-parametric family of differential equation systems defined within $\mathbb{R}^2$ whose expression is given by

$$\begin{cases} \dot{x} = -y + xy, \\ \dot{y} = x + Dx^2 + Fy^2, \end{cases} \tag{1.0.1}$$

where $\mu = (D, F) \in \mathbb{R}^2$. These systems have the property of reversibility with respect to the x-axis since transformation $(x, y, t) \longmapsto (x, -y, -t)$ preserves Loud form [14, 4]. It is well-known that Loud systems have a center at the origin for all values of $(D, F) \in \mathbb{R}^2$. Moreover, some works have proven previously that any planar differential system with this reversibility property can be brought, by an affine transformation and a reescaling of time, to (1.0.1) expression [6].

A singular point p of a planar differential equation systems is said to be a *center* if there exists a punctured neighbourhood of p which contains periodic orbits surrounding the singular point in its phase portrait. Given a center p, its *period annulus* P_a is the largest existing punctured neighbourhood with this property, which may be an unbounded subset of $\mathbb{R}^2$. By compactifying the period annulus to $\mathbb{RP}^2$ [23], since it may be unbounded, and denoting by ∂P_a the boundary of P_a, its inner boundary is the center p itself and its outer boundary is given by $\partial P_a \setminus p$. Associated with a center, its *period function* P maps each periodic orbit to its period and, as stated in [23], it is as smooth as the vector field inducing the differential equations system. Let $\{\gamma_x\}_{x\in(0,1)}$ be a parametrization of the set of periodic orbits within the period annulus. The period function contains a *critical period* in $x_0 \in (0, 1)$ if $P'(x_0) = 0$ and $P'(x) \neq 0$ for $0 < |x_0 - x| < \varepsilon$ and $\varepsilon > 0$ [23].

The bifurcation diagram of the period function displays regions within the space of parameters containing a certain number of critical periods and the different boundaries delimiting them where this number varies. The period function may undergo a bifurcation at the outer boundary of the period annulus [14, 23], at its inner boundary [4] or at the interior [14, 23]. Its study for the center at the origin of Loud systems and the maximum number of critical periods that the period function may contain have constituted the subject of study of many works, see for instance [4, 10, 11, 14, 23], which have tackled the problem analytically. In fact, this topic resembles Hilbert's 16th problem [22], which aims to study the maximum number of limit cycles that may arise for a planar differential equation system, in such a way that both of them try to find an upper bound for the concepts of *criticality* -number of critical periods in the period function- and *cyclicity* -number of limit cycles-, respectively.

Chicone and Jacobs studied the local bifurcation diagram of the period function of Loud systems near the center [4], where the period function extends analytically, i.e. at the inner boundary of the period annulus, the period function admits a Taylor expansion. Moreover, Chicone conjectured in [24]

that the period function associated to the center at the origin from (1.0.1) contained, at most, two critical periods. Subsequent work (for instance [9, 14, 23]) has progressed in this direction with results that make this conjecture more solid. On the other hand, the study of the local bifurcation diagram of Loud systems at the outer boundary of the period annulus, where the period function does not extend analytically and whose shape varies as a function of $(D, F) \in \mathbb{R}^2$, has been the topic of many subsequent studies [14, 23].

At this juncture, there is a solid evidence of a bifurcation diagram in the space of parameters $D - F$, $(D, F) \in \mathbb{R}^2$. It displays several regions containing a number N of critical periods. These regions are separated by the so-called *bifurcation curves*, some of them have already been proved analytically while others are just conjectured. Furthermore, there exists curves such that only its initial and final germs are known but not their complete shape.

This project seeks to address the problem of analysing the bifurcation diagram of the period function of the centre at the origin in Loud systems from a numerical point of view as opposed to all the analytical and theoretical studies mentioned above. In this line, assess how the numerical approach fits the theoretical results and whether it adds more strength to the conjectures made in all the aforementioned works will be the cornerstones of this thesis. It is worth pointing out that, beyond attempting to reproduce exactly the theoretical results, this work intends to clarify the scope of numerical computation techniques.

Numerical methods for ordinary differential equations are the keystone among techniques used in order to tackle the problem. Therefore, the period function of the center at the origin of system (1.0.1) will be studied by numerical integration of system (1.0.1) using 4th-order Runge-Kutta methods or by direct integration of the period function using integration numerical methods such as composite Simpson's rule [12]. Besides, some numerical methods to find zeros of a function such as Newton's method will also be useful for some purposes. On the other hand, since the period annulus of the center at the origin in (1.0.1) may be unbounded for some values of $\mu = (D, F)$, dealing with periodic orbits escaping towards infinity will be a constant. From a numerical point of view, these orbits may induce propagation of numerical errors leading to falsified results. To overcome this issue, change of coordinates by compactification will avoid periodic orbits escaping to infinity giving rise to bounded period annulus whose boundary contains two connected components: the center itself and a polycycle identified with the outer boundary. This fact will facilitate the numerical study.

This work is divided into 8 different chapters which constitute the core of this project and, additionally, four appendices that expand on some of the topics covered and contain the algorithms used for the numerical study. This first chapter is devoted to introduce the problem to be analysed by stating previous results found in this field and the progresses made in the topic of study. Likewise, the objectives that the project aims to achieve will be outlined as well as the temporary planning carried out to develop all the tasks.

Second chapter provides the theoretical background on ordinary differential equations with the objective of establishing a starting point towards the analysis of the period function and its bifurcation diagram for Loud systems. Basic definitions, the classification of singular points and some fundamental theorems related to the local study of the phase portrait for planar systems are stated and referenced. Subsequently, third chapter focuses on the theory of planar centers, introducing notions such as first integrals, invariant algebraic curves and some results about the Darboux theory of integrability.

Chapter four outlines one of the most useful techniques for the numerical study of the period func-

tion: compactifications. For this purpose, and with the aim of getting a better understanding of the concept, the development of Poincaré-Lyapunov compactification will be explained and its advantages and disadvantages to review Loud systems will be considered. Then, $\mathbb{RP}^2$ compactification, the one that will be used will be explained and important equations and expressions will be remarked.

Moving on to the fifth chapter, it focuses on Loud systems and analyses the most important features by proving the existence of the center at the origin, the existence of a first integral and the existence of invariant algebraic curves. Besides, the most important results about the bifurcation diagram of the period function of the center at the origin will be referenced as well as the most important existing conjectures with a view to provide new evidence to confirm them.

Chapter six contains the methodology used to tackle numerically the problem and the criteria employed and chapter seven displays the numerical results obtained when analysing the bifurcation diagram in the space of parameters $D - F$. Specifically, it focuses on regions that are still nowadays a matter of discussion and their features rely on conjectures, i.e. regions which are conjectured to be associated to period functions containing, exactly, two critical points. Bifurcation curves and the different types of bifurcations will be analysed.

Finally, the eighth chapter exposes the conclusions achieved and appendices develop the 4th-order Runge-Kutta numerical method, a result about line integrals and contain the algorithms implemented in C language used to reach the numerical results.

Below, the main objectives that this thesis tries to fulfil are listed:

- **Consolidate and expand all the knowledge acquired during the Master's studies.** Be able to make use of the new insight, specially in the field of numerical methods and dynamical systems. Combine both the theoretical approach with the computational one with a view to develop an algorithm that allows analysing the bifurcation diagram of the period function of the center at the origin for Loud systems.
- **Determine the scope of the numerical approach to study Loud's period function.** Analyse the principal factors that contribute to get numerical results consistent with those proven analytically and investigate how well the numerical study of the bifurcation diagrams gets. Compare between different approaches and being able to discern among their advantages and disadvantages.
- **Provide evidence on existing conjectures**. The exact number of critical periods in some regions within the bifurcation diagram of the period function of the center at the origin are still under conjectures and, thus, this thesis aims to verify whether they could be certain or not. In this line, regions conjectured to have exactly two critical periods will be the cornerstone and boundaries between them, the so-called bifurcation curves, will also be analysed and compared to the proven results.
- **Analyse critically the results obtained and develop research techniques**. Be able to select the important information from important mathematical publications and understand the evolution of the problem throughout years. Extract powerful conclusions about the study.

The temporary planning of the project is displayed in the Gantt diagram in figure 1.1. All the implicated work has been carried out during six months, from November 2022 to January 2023 and from June 2023 to August 2023, with a pause since March 2023 until May 2023 due to personal reasons. Tasks developed are the following ones:

- **Research**. Bibliographical enquiry concerning the topic in question by reading and understanding papers and reference books.
- **Code implementation in C**. Development of the algorithm and its implementation using C language performing modifications and providing new possible useful ideas.
- **Software verification**. Certification of the proper functioning of the implemented algorithm by comparing the results of simple cases with already known ones.
- **Computations**. Executing the planned numerical runs of the code in order to obtain the results.
- **Written memory**. A long process that includes writing important and useful results, analysing the numerical results obtained and explaining them and creating a well-structured document.
- **Video presentation**. Summarise the most important contents of the thesis in a series of slides.
- **Evaluation**. Self-assessment about the personal work carried out.

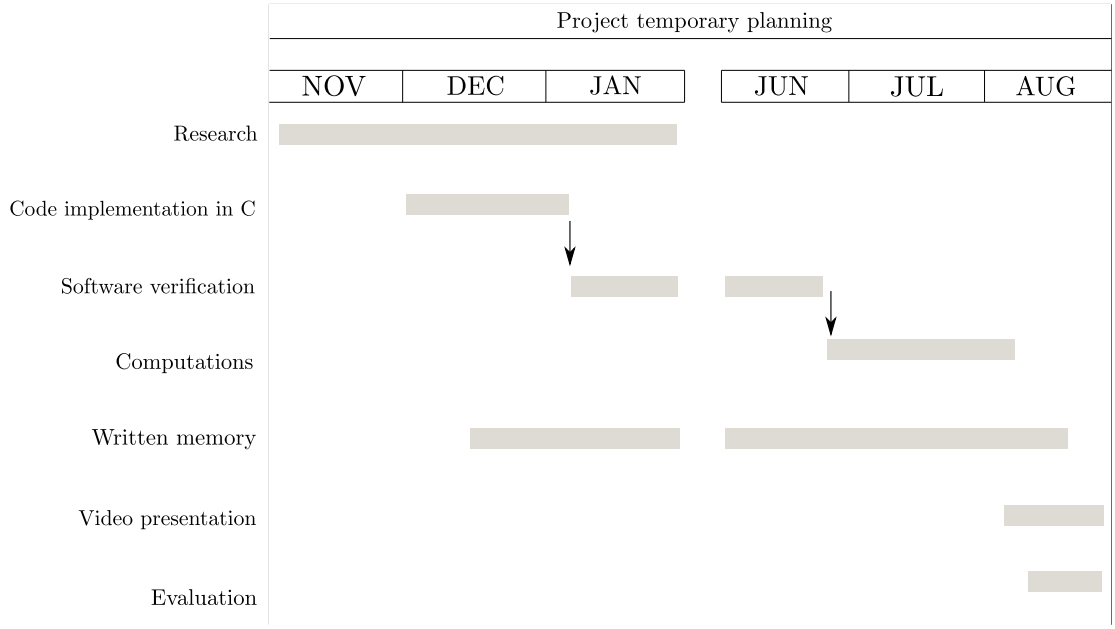

Figure 1.1: Gantt diagram displaying the temporary planning of the project.

Chapter 2

Fundamental results on differential equations

This section intends to provide an introduction to the basic notions and main results of the theory of ordinary differential equations with the intention of creating a solid theoretical framework for further study. All the results presented here are extracted from chapters 1 and 2 of [15].

2.1 Basic results

Let $\Delta \subseteq \mathbb{R}^2$ be an open subset of the real plane and $X : \Delta \longrightarrow \mathbb{R}^2$ a $\mathcal{C}^r$ vector field defined on it, where r can be either $r \in \mathbb{Z}^+$, $+\infty$ or $r = \omega$. When $X \in \mathcal{C}^\omega$, the vector field is a real analytic function, i.e. for every $x_0 \in \Delta$ there exists a neighbourhood of x_0 in which the function can be expressed in the form of a power series which is convergent within the given neighbourhood. This notion is local. Hereafter, whenever a vector field is $\mathcal{C}^r$, r will refer to one of the three previously mentioned possibilities. Vector field X can also be expressed in its differential form as

$$X = X_1 \frac{\partial}{\partial x_1} + X_2 \frac{\partial}{\partial x_2}, \tag{2.1.1}$$

where x_1 and x_2 are the coordinates in the euclidean plane $\mathbb{R}^2$ and $X(x_1, x_2) = (X_1(x_1, x_2), X_2(x_1, x_2))$. It can be associated to a differential equation in such a way that

$$\dot{x} = X(x), \tag{2.1.2}$$

where $\dot{x} = dx/dt$ and t is the temporal variable. The differential equation is said to be autonomous if its associated vector field has only dependence on the spatial coordinates x_1 and x_2 and not on the temporal variable t. The following definition makes a distinction among the different kind of points in the domain associated to (2.1.1).

Definition 2.1.1. *Let $x \in \Delta$ be a point in the domain of X. Then x is said to be a singular (respectively, regular) point if $X(x) = 0$ (respectively, $X(x) \neq 0$).*

Solutions of (2.1.2) are differentiable curves $\varphi : I \longrightarrow \Delta$, where $I \subseteq \mathbb{R}$ is an interval in which the curve is defined, satisfying

$$\frac{d\varphi(t)}{dt} = X(\varphi(t)). \tag{2.1.3}$$

Solution $\varphi(t)$ such that $\varphi(0) = x_0$ where $x_0 \in \Delta$, defined on an interval $I \subseteq \mathbb{R}$, is said to be a maximal solution if, given any other solution of (2.1.2) denoted by $\phi : J \longrightarrow \Delta$ such that $I \subset J$ and $\varphi = \phi|_I$,

then $I = J$ and $\varphi = \phi$. In this case, I is said to be a maximal interval in which the solution φ is defined and it is denoted by $I = I_{x_0}$ due to its dependence to the initial condition. Given a maximal solution $\varphi(t)$ and $x_0 \in \Delta$ a regular point such that $\varphi(0) = x_0$, the subset $\gamma_\varphi = \{\varphi(t) : t \in I\} \subset \Delta$ is the orbit with orientation induced by φ.

Given $x \in \Delta$, we denote by $\varphi(t, x) = \varphi_x(t)$ the unique solution of (2.1.3) passing through x at time $t = 0$, i.e. such that $\varphi(0, x) = x$. It can also be defined the following subset: $\Omega = \{(t, x) : x \in \Delta, t \in I_x\}$, where recall that, for each $x \in \Delta$, I_x stands for the maximal interval of definition of $\varphi(t, x)$. Moreover, $\varphi : \Omega \longrightarrow \mathbb{R}^2$ is the flow generated by the vector field X and associated to any given $x \in \Delta$ and any time $t \in I$, the point on the euclidean plane $\mathbb{R}^2$ which is the image of the solution curve passing through x at time t.

The following theorem provides a solid basis to ensure existence and uniqueness of maximal solutions and continuity with respect to initial conditions. It can be found in [15] as well as its proof.

Theorem 2.1.2. *Let X be a vector field with the properties defined previously. Then the statements below hold.*

(i) For every $x \in \Delta$, there exists an open interval I on which a unique maximal solution φ of the differential equation (2.1.2) satisfying $\varphi(0) = x$ is defined.

(ii) Let Ω be the domain of the flow introduced beforehand. Then Ω is an open subset of $\mathbb{R}^3$ and $\varphi : \Omega \longrightarrow \mathbb{R}^2$ given by $\varphi(t, x) = \varphi_x(t)$ is a $\mathcal{C}^r$ map ($\varphi_x(t)$ denotes the solution curve passing through x, which is unique due to statement (i)). Moreover, φ satisfies

$$\frac{\partial}{\partial t}\frac{\partial}{\partial x}\varphi(t, x) = DX(\varphi(t, x))\frac{\partial}{\partial x}\varphi(t, x)$$

for every $(t, x) \in \Omega$, where DX is the linear part of X.

Given a point $x \in \Delta$, φ_x is the orbit of the vector field X passing through point x and it is the image of the maximal solution with maximal interval I and orientation induced by φ if the solution is regular. Let $x_1 \in \varphi_x$, then there exists $t_1 \in I$ such that $\varphi(t_1, x) = x_1$. Due to uniqueness of solutions given by theorem 2.1.2, $\varphi_x = \varphi_{x_1}$ and therefore, two different orbits coincide or they are disjoint.

In order to try to classify orbits, the next theorem provides three different options defining three different types of orbits, i.e. curve solutions of system (2.1.2). Its proof can be found in [15].

Theorem 2.1.3. *Let $\varphi(t)$ be a maximal solution of (2.1.2). Then one of the three statements holds.*

(i) φ is a bijection onto its image.

(ii) φ is a constant function, $I = \mathbb{R}$ and γ_φ contains a single point.

(iii) φ is a periodic function of period τ and $I = \mathbb{R}$.

A periodic function of period $\tau > 0$ is such that $\varphi(t+\tau) = \varphi(t)$ for all $t \in I$. Moreover, given $t_1, t_2 \in I$ such that $|t_1 - t_2| < \tau$, it is always true that $\varphi(t_1) \neq \varphi(t_2)$. The third statement of the theorem accounts for the existence of periodic orbits.

The set of oriented orbits of the vector field X, consisting of constant orbits (singularities) and regular orbits, is defined as the phase portrait of X. The orientation is induced by each solution φ in the sense of increasing t. Therefore, assuming $I \subseteq \mathbb{R}$, theorem 2.1.3 provides the different elements in the phase portrait of a vector field.

2.2 Topological conjugacy and equivalence

Notions introduced in this section are of great relevance in classifying the elements of a phase portrait and comparing phase portraits of different vector fields. Indeed, concepts of topological conjugacy and equivalence allow sorting vector fields into equivalent or conjugate depending on the topological structure of their phase portraits.

Let X_1 and X_2 be two different vector fields defined in open subsets $\Delta_1, \Delta_2 \subseteq \mathbb{R}^2$ and their associated flows $\varphi_1 : \Omega_1 \longrightarrow \mathbb{R}^2$ and $\varphi_2 : \Omega_2 \longrightarrow \mathbb{R}^2$.

Definition 2.2.1. *Vector fields X_1 and X_2 are said to be topologically equivalent if there exists a homeomorphism $h : \Delta_1 \longrightarrow \Delta_2$ sending orbits of X_1 to orbits of X_2 preserving their orientation. Let $x_0 \in \Delta_1$ and γ_{x_0} the orbit passing through x_0 of X_1. Then $h(\gamma_{x_0})$ is an oriented orbit of X_2 passing through $h(x_0)$. In this case, h is said to be a topological equivalence.*

Definition 2.2.2. *Vector fields X_1 and X_2 are said to be topologically conjugate if there exists a homeomorphism $h : \Delta_1 \longrightarrow \Delta_2$ such that $h(\varphi_1(t, x)) = \varphi_2(t, h(x))$ for every $(t, x) \in \Omega_1$, which requires the maximal intervals of φ_1 and φ_2 to be equal. In this case, h is said to be a topological conjugcay.*

From the definition of topological equivalence, an equivalence h maps singular points from X_1 to singular points from X_2 and periodic orbits are also mapped between them. Particularly, a conjugacy preserves the period of periodic orbits. The following lemma provides a characterisation of conjugacies and it is a very powerful tool to identify if a given homeomorphism h is a conjugacy between two vector fields. The proof can be found in [15].

Lemma 2.2.3. *Given a $\mathcal{C}^r$ diffeomorphism $h : \Delta_1 \longrightarrow \Delta_2$ with $r \geq 1$ and two $\mathcal{C}^r$ vector fields $X_1 : \Delta_1 \longrightarrow \mathbb{R}^2$ and $X_2 : \Delta_2 \longrightarrow \mathbb{R}^2$, h is a conjugacy between X_1 and X_2 if and only if*

$$Dh_x(X_1(x)) = X_2(h(x)), \quad \forall x \in \Delta_1$$

The flow box theorem allows to get insight of the phase portrait of any given vector field in the neighbourhood of any given regular point, i.e. non singular. Before stating the theorem, the transverse section notion must be introduced. Let $f : A \longrightarrow \Delta$ be a $\mathcal{C}^r$ map where $A \subset \mathbb{R}$ and $\Delta \subset \mathbb{R}^2$ are open subsets. Then f is said to be a transverse local section of X if for all $x \in A$, $f'(x)$ and $X(f(x))$ are linearly independent. Moreover $\Sigma = f(A)$ is a transverse section of vector field X if $f : A \longrightarrow \Sigma$ is an homeomorphism. Both the statement of the flow box theorem and its proof below are extracted from [15].

Theorem 2.2.4. (Flow Box Theorem) *Let p be a regular point of a $\mathcal{C}^r$ vector field $X : \Delta \longrightarrow \mathbb{R}^2$ and $f : A \longrightarrow \Sigma$ a $\mathcal{C}^r$ transverse section of it such that $f(0) = p$. Let $\varepsilon > 0$ and B be an open interval with center at the origin of $\mathbb{R}^2$. Then there exists a neighbourhood $V \subset \Delta$ of p and a $\mathcal{C}^r$ diffeomorphism $h : V \longrightarrow (-\varepsilon, \varepsilon) \times B$ such that:*

i) $h(\Sigma \cap V) = \{0\} \times B$

ii) h is a $\mathcal{C}^r$-conjugacy between $X|_V$ and the constant vector field $X_1 : (-\varepsilon, \varepsilon) \times B \longrightarrow \mathbb{R}^2$ defined by $X_1 = (1, 0)$.

Proof. Denote by φ the flow of the vector field X with domain Ω and define $\Omega_A = \{(t, u) : (t, f(u)) \in \Omega\}$. The map $F : \Omega_A \longrightarrow \Delta$ defined by $F(t, u) = \varphi(t, f(u))$ moves parallel lines into solution curves

of X. The justification consists on proving that in $(0,0) \in \mathbb{R}^2$, F is a local diffeomorphism. First,

$$D_1F(0) = \frac{d}{dt}\varphi(t, f(0))|_{t=0} = X(\varphi(0,p)) = X(p) = X(f(0))$$
$$D_2F(0) = \frac{d}{du}\varphi(0, f(u))|_{u=0} = \frac{d}{du}f(u)|_{u=0} = f'(u)|_{u=0} = f'(0)$$

where D_1 denotes the time derivative and D_2 the derivative with respect to u. From the definition of local transverse section, $D_1F(0)$ and $D_2F(0)$ are linearly independent and therefore, they span $\mathbb{R}^2$. Consequently, $DF(0)$ is an isomorphism and, by the inverse function theorem, there exists $\varepsilon > 0$ and a neighbourhood B in $\mathbb{R}$ of the origin such that $F|_{(-\varepsilon,\varepsilon)\times B}$ is a diffeomorphism on an open set $V = F((-\varepsilon,\varepsilon) \times B)$. Choosing $h = (F|_{(-\varepsilon,\varepsilon)\times B})^{-1}$, $h(\Sigma \cap V) = \{0\} \times B$ since $F(0,u) = f(u) \in \Sigma$ for all $u \in B$. Using h^{-1},

$$\begin{aligned} Dh^{-1}(t,u)X_1(t,u) &= DF(t,u)(1,0)^T = D_1F(t,u) = X(\varphi(t,f(u))) \\ &= X(F(t,u)) = X(h^{-1}(t,u)) \end{aligned}$$

for all $(t,u) \in (-\varepsilon,\varepsilon) \times B$. Therefore, by lemma 2.2.3, h^{-1} conjugates X and X_1. □

It must be taken into account that this is a local result and in any case it can be inferred from it that a vector field containing only regular points is globally conjugate to a constant vector field.

2.3 ω-limit and α-limit subsets

Let X be a $\mathcal{C}^r$ vector field and $x_0 \in \Delta \subset \mathbb{R}^2$. Let φ_{x_0} be the solution curve of X through point x_0 defined in the maximal interval $I_{x_0} = (\omega_-(x_0), \omega_+(x_0))$ such that $\omega_-(x_0) > -\infty$ and $\omega_+(x_0) < \infty$. Then it can be proved that $\varphi_{x_0}(t)$ tends to $\partial\Delta$ when $t \to \omega_\pm(x_0)$, i.e. the boundary of Δ [15]. In other words, $\varphi_{x_0}(t) \to \partial\Delta$ means that, for every compact $K \subset \Delta$, there exists $\varepsilon > 0$ such that $\varphi(t, x_0) \notin K$ for all $t \in (\omega_+(x_0) - \varepsilon, \omega_+(x_0))$.

On the other hand, when the extremes of the maximal interval are given by $\omega_-(x_0) = -\infty$ or $\omega_+(x_0) = \infty$, it is possible to define, respectively, the two following sets:

$$\omega(x_0) = \{x \in \Delta : \text{there exists a sequence } \{t_n\} \text{ with } t_n \to \infty \text{ and } \varphi(t_n) \to x \text{ when } n \to \infty\}$$
$$\alpha(x_0) = \{x \in \Delta : \text{there exists a sequence } \{t_n\} \text{ with } t_n \to -\infty \text{ and } \varphi(t_n) \to x \text{ when } n \to \infty\}.$$

These sets (that may be empty) are known, respectively, by the ω-limit and the α-limit and allow a characterisation of the future and the past of a given orbit. It must be noticed that if $x_1, x_2 \in \Delta$ and $x_1, x_2 \in \gamma$, where γ is an orbit of a vector field X, then $\omega(x_1) = \omega(x_2)$ and $\alpha(x_1) = \alpha(x_2)$. Then sets α-limit and ω-limit coincide for every point in the same orbit. The following result defines an important property of these sets [15].

Lemma 2.3.1. *ω-limit and the α-limit sets are invariant for X, that is to say, any orbit passing through a point contained in one of each sets, the entire orbit is contained in the set.*

Proof. The proof will be sketched only for the ω-limit set. Let $x \in \omega(x_0)$, $\phi : I_x \longrightarrow \Delta$ the solution curve through x and $x_1 = \phi(t_0)$ for a given time t_0. From the definition of ω-limit, there exists a sequence $\{t_n\}$ such that $t_n \to \infty$ and $\phi(t_n) = \varphi(t_n, x_0) \longrightarrow x$ when $n \to \infty$. Given the continuity of the flow φ,

$$\begin{aligned} x_1 = \varphi(t_0, x) &= \varphi\left(t_0, \lim_{n\to\infty} \varphi(t_n, x_0)\right) \\ &= \lim_{n\to\infty} \varphi(t_0, \varphi(t_n, x_0)) = \lim_{n\to\infty} \varphi(t_0 + t_n, x_0). \end{aligned}$$

The sequence $\{t_0 + t_n\}$ satisfies $t_0 + t_n \longrightarrow \infty$ when $n \to \infty$ and $\varphi(t_0 + t_n, x_0)$ tends to x_1 as $n \to \infty$, which, by definition, means that $x_1 \in \omega(x_0)$. As x_1 is an arbitrary point of the orbit passing through x, the whole orbit is contained and therefore the set is invariant. □

2.4 Local phase portrait of singular points

As aforementioned in former subsections, let X be a $\mathcal{C}^r$ vector field with $1 \leq r \leq \infty$ or $r = \omega$. For the sake of simplicity, consider X is a planar vector field given by $X = (P, Q)$ and take p a singular point, i.e. $X(p) = 0$. Singular points of a vector field can be classified locally according to their linear part, defined as follows:

$$DX(p) = \begin{pmatrix} \dfrac{\partial P}{\partial x}(p) & \dfrac{\partial P}{\partial y}(p) \\ \dfrac{\partial Q}{\partial x}(p) & \dfrac{\partial Q}{\partial y}(p) \end{pmatrix}. \tag{2.4.1}$$

This matrix is the linear part of vector field X evaluated at singular point p and its eigenvalues allow a classification in accordance with the subspace their associated eigenvectors span. Let λ_1 and λ_2 be eigenvalues of matrix $DX(p)$. Below, different cases are listed:

- $\lambda_1 \neq 0$ and $\lambda_2 \neq 0$. Singular point p is said to be *non-degenerate*.
- $\mathrm{Re}(\lambda_1) \neq 0$ and $\mathrm{Re}(\lambda_2) \neq 0$. Singular point p is said to be *hyperbolic*.
- $\lambda_1 = 0$, $\lambda_2 \neq 0$ or $\lambda_1 \neq 0$, $\lambda_2 = 0$. Singular point p is said to be *semi-hyperbolic*.
- $\lambda_1, \lambda_2 = 0$ but $DX(p) \not\equiv 0$. Singular point p is said to be *nilpotent*.
- $DX(p) \equiv 0$. Singular point p is said to be *linearly zero*.
- λ_1 and λ_2 are purely imaginary and $\lambda_1, \lambda_2 \neq 0$. Singular point p is said to be *linearly a center*.

Last case will be the most important in this thesis and makes up one of the most complicated problems in the qualitative theory of planar differential equations: distinguishing between a center and a focus when the singular point is linearly a center. Section 3 will develop the center case and some of the most important results.

Denote by $\det(DX(p))$ the determinant of the linear matrix at singular point p, $\mathrm{tr}(DX(p))$ its trace and $\Delta(p) = \mathrm{tr}(DX(p))^2 - 4 \cdot \det(DX(p))$ its discriminant. Then [15],

- $\det(DX(p)) \neq 0$. Singular point p is non-degenerate and either linearly a center or hyperbolic.
- $\det(DX(p)) = 0$ but $\mathrm{tr}(DX(p)) \neq 0$. Singular point p is semi-hyperbolic.
- $\det(DX(p)) = 0$ and $\mathrm{tr}(DX(p)) = 0$. Singular point p is linearly zero or nilpotent. It depends on whether $DX(p)$ is the zero matrix.

2.5 The Poincaré-Bendixson theorem

Poincaré-Bendixson theorem is a powerful result which allows discerning the composition of the ω-limit set of a given point in terms of the points contained on it. In this way, under a few hypothesis for a vector field X, the ω-limit is fully described as this theorem gathers all possible situations. The version of the theorem given in here follows from the description that can be found in [15]. Therefore,

the notation used is in accordance with that in the aforementioned citation.

Let X be a $\mathcal{C}^r$ vector field where $1 \leq r \leq \infty$ or $r = \omega$ and X is defined in an open subset $\Delta \subset \mathbb{R}^2$. Let $\varphi(t) = \varphi(t, p)$ be a solution curve of vector field X, i.e. an integral curve of X with the property of passing through point p and defined for all $t \geq 0$. Before stating the theorem, four lemmas will be stated without proof in order to sketch the proof of the Poincaré-Bendixson theorem. They are extracted from [15] and, for their proofs, refer to it.

Lemma 2.5.1. *Let Σ be a transverse section of vector field X and $\gamma = \{\gamma(t)\}$ an orbit contained in $\mathbb{R}^2$. If $p \in \Sigma \cap \omega(\gamma)$, then there is a sequence of points $\gamma(t_n)$ contained in Σ as $t_n \to \infty$ such that p is its limit.*

Lemma 2.5.2. *Consider γ an orbit of vector field X and $p \in \Sigma \cap \gamma$, where Σ is a transverse section to X which is contained in the subset of definition of X, Δ. Let $\gamma_p^+ = \{\varphi(t, p) : t \geq 0\}$. Then, intersection points of γ_p^+ with the transverse section form a monotonic sequence that can be either finite or infinite.*

Lemma 2.5.3. *A transverse section Σ of a vector field X intersects $\omega(p)$, where $p \in \Delta$, in at most one point.*

Lemma 2.5.4. *If $\omega(\gamma)$ contains regular points, where γ is an orbit of X such that $\gamma \subset \omega(p)$, $p \in \Delta$ and γ_p^+ is contained in a compact set, then γ is a closed orbit satisfying $\omega(p) = \gamma$.*

Bearing in mind all the former lemmas, the statement of Poincaré-Bendixson theorem reads as:

Theorem 2.5.5. (Poincaré-Bendixson) Let $\gamma(t) = \gamma(t, p)$ an orbit of vector field X defined for positive times satisfying the property of γ_p^+ being contained in a compact set $K \subset \Delta$. Assume X has, at most, a finite number of singularities contained in this compact set. Then, three different situations may arise and one of them always holds:

i) $\omega(p)$ is a periodic orbit if it only contains regular points.

ii) If $\omega(p)$ contains both regular and singular points, then $\omega(p)$ contains a set of orbits each of them tending to one of the singular points in $\omega(p)$ as $t \longrightarrow \pm\infty$.

iii) $\omega(p)$ is a unique singular point if $\omega(p)$ does not contain regular points.

Proof. *i)* Assume $\omega(p)$ only contains regular points. Since the ω-limit set is invariant, given $q \in \omega(p)$ and γ_q the orbit through q, one must necessarily have $\gamma_q \subset \omega(p)$. Moreover, since $\omega(p)$ is a compact set, by definition $\omega(\gamma_q) \neq \emptyset$. It readily follows from lemma 2.5.4 that $\omega(p) = \gamma_q$, where γ_q is a closed orbit. Thus, in this case, the ω-limit is a periodic orbit.

ii) Assume $\omega(p)$ contains both singular and regular points. Let γ be a regular orbit such that $\gamma \subset \omega(p)$ following the same argument as in *i)*. Since ω-limit set and α-limit set are connected sets, from lemma 2.5.4, both $\omega(\gamma)$ and $\alpha(\gamma)$ must contain singular points.

iii) Assume $\omega(p)$ does not contain regular points. Since $\omega(p)$ is connected and X can only have finitely many singularities in $\omega(p)$, the fact that $\omega(p)$ is a unique singular point follows readily. □

2.6 Normal forms for the main singularities

It is possible to find canonical vector fields for hyperbolic and semi-hyperbolic singular points, i.e. vector fields such that any other vector field can be brought, by means of an appropriate $\mathcal{C}^r$ coordinate change, to this standard form. The theory describing this family of vector fields is the so-called Normal Form Theory. In practice, this description offers the advantage of determining the behaviour of elementary singular points in terms of the eigenvalues of the linear part of a vector field.

Formally, let $X = A + f$ be a $\mathcal{C}^\infty$ vector field defined in $\mathbb{R}^n$ such that A contains the linear part and f is a $\mathcal{C}^\infty$ function. Assume, moreover, $f(0) = 0$ and $Df(0) = 0$. Normal Form Theory aims to find a family of vector fields $X' = A + f'$ such that $f' \in F_n$, where F_n is a family of non-linear functions the simplest as possible, for every linear vector field A. In this situation, an appropriate $\mathcal{C}^\infty$ coordinate change brings vector field X to X'.

This theory requires an extensive and meticulous analysis and development which escapes the scope of this thesis. Thus, just with the goal of formalising the classification of hyperbolic and semi-hyperbolic singularities, two summarising theorems are stated below. They fully characterise the local phase portrait in a neighbourhood of a given hyperbolic or semi-hyperbolic singularity for analytic systems. The following theorems are extracted from chapter 2 in [15]. For a complete description and proofs, refer to it.

Theorem 2.6.1. (Hyperbolic singularities theorem). *Let $(0,0)$ be an isolated singularity of a given vector field X with the following expression:*

$$\begin{cases} \dot{x} = ax + by + A(x,y), \\ \dot{y} = cx + dy + B(x,y), \end{cases} \tag{2.6.1}$$

where A and B are analytic functions in a neighbourhood of the origin satisfying $A(0,0) = B(0,0) = DA(0,0) = DB(0,0) = 0$. Denote by λ_1 and λ_2 the eigenvalues of matrix (2.4.1) when evaluated at the origin. One of the following statements hold:

i) $\lambda_1, \lambda_2 \in \mathbb{R}$ and $\lambda_1\lambda_2 < 0$. The origin is a saddle. Let E_1 and E_2 be the eigenspaces spanned associated to λ_1 and λ_2 respectively. Then there exists two invariant analytical curves tangent to E_1 and E_2 at the origin such that on one of them points are attracted towards the origin and on the other are repelled. Vector field X is $\mathcal{C}^\omega$ linearizable on these curves.

Then there exists a $\mathcal{C}^\infty$ coordinate change bringing (2.6.1) to the normal form for the saddle case, given for $\lambda_2/\lambda_1 \in \mathbb{R} \setminus \mathbb{Q}$ and $\lambda_2/\lambda_1 = -k/l \in \mathbb{Q}$ with $k, l \in \mathbb{N}$ coprimes, respectively, by

$$\begin{cases} \dot{x} = \lambda_1 x, \\ \dot{y} = \lambda_2 y, \end{cases} \qquad \begin{cases} \dot{x} = x(\lambda_1 + f(x^k y^l)), \\ \dot{y} = y(\lambda_2 + g(x^k y^l)), \end{cases} \tag{2.6.2}$$

where f and g are $\mathcal{C}^\infty$ functions. In both cases, (2.6.1) is $\mathcal{C}^0$ conjugate to

$$\begin{cases} \dot{x} = x, \dot{y} = -y, \end{cases} \tag{2.6.3}$$

which is the simplest vector differential equations systems such that the origin is a saddle.

ii) $\lambda_1, \lambda_2 \in \mathbb{R}$ satisfying $|\lambda_2| \geq |\lambda_1|$ and $\lambda_1\lambda_2 > 0$. Then the origin is a node. If $\lambda_1 > 0$ (respectively $\lambda_1 < 0$), then it is a repelling or unstable node (respectively attracting or stable). There exists a

$\mathcal{C}^\infty$-coordinate change transforming (2.6.1) to the following normal forms,

$$\begin{cases} \dot{x} = \lambda_1 x, \\ \dot{y} = \lambda_2 y, \end{cases} \qquad \begin{cases} \dot{x} = \lambda_1 x, \\ \dot{y} = \lambda_2 y + \delta x^m, \end{cases} \tag{2.6.4}$$

for $\lambda_2/\lambda_1 \notin \mathbb{N}$ and for some $\delta = 0, 1$, $\lambda_2 = m\lambda_1$ with $m \in \mathbb{N}$, $m \leq 1$, respectively. In this case, system (2.6.1) are $\mathcal{C}^0$-conjugate to

$$\begin{cases} \dot{x} = \delta x, \\ \dot{y} = \delta y, \end{cases} \tag{2.6.5}$$

with $\delta = \pm 1$ and $\lambda_1 \delta > 0$.

iii) If $\lambda_1 = \alpha + i\beta$ and $\lambda_2 = \alpha - i\beta$ with $\alpha, \beta \neq 0$, then the origin is a "strong" focus. For $\alpha > 0$ (respectively $\alpha < 0$), it is a repelling or unstable (respectively, attracting or stable). There exists a $\mathcal{C}^\infty$-coordinate change transforming (2.6.1) into the normal form

$$\begin{cases} \dot{x} = \alpha x + \beta y, \\ \dot{y} = -\beta x + \alpha y. \end{cases} \tag{2.6.6}$$

In this case, system (2.6.1) is $\mathcal{C}^0$-conjugate to

$$\begin{cases} \dot{x} = \delta x, \\ \dot{y} = \delta y, \end{cases} \tag{2.6.7}$$

with $\delta = \pm 1$ and $\alpha\delta > 0$.

iv) If $\lambda_1 = i\beta$ and $\lambda_2 = -i\beta$ with $\beta \neq 0$, then the origin is a linear center, topologically, a weak focus or a center.

Theorem 2.6.2. (Semi-Hyperbolic singularities theorem). *Let $(0, 0)$ be an isolated singular point of a given vector field X with the following expression:*

$$\begin{cases} \dot{x} = A(x, y), \\ \dot{y} = \lambda y + B(x, y), \end{cases} \tag{2.6.8}$$

where A and B are analytic functions in a neighbourhood of the origin satisfying $A(0, 0) = B(0, 0) = DA(0, 0) = DB(0, 0) = 0$ with $\lambda > 0$. Denote by $y = f(x)$ the solution of equation $\lambda y + B(x, y) = 0$ in a neighbourhood of the origin and let $g(x) = A(x, f(x))$ with expression $g(x) = a_m x^m + o(x^m)$, where $m \geq 2$ and $a_m \neq 0$. Then, there exists an invariant analytic curve tangent to $x = 0$ at 0 such that X is analytically conjugate to

$$\dot{y} = \lambda y. \tag{2.6.9}$$

This curve is called the strong unstable manifold and the former equation has a repelling behaviour since $\lambda > 0$. Moreover, the following statements hold.

i) The origin is topologically a saddle for m odd and $a_m < 0$. There exists a unique invariant $\mathcal{C}^\infty$ curve which is tangent to $y = 0$ and on which vector field X is $\mathcal{C}^\infty$-conjugate to

$$\dot{x} = -x^m(1 + ax^{m-1}), \tag{2.6.10}$$

for some $a \in \mathbb{R}$. The invariant curve is the so-called center manifold. Vector field X is $\mathcal{C}^\infty$-conjugate to

$$\begin{cases} \dot{x} = -x^m(1 + ax^{m-1}), \\ \dot{y} = \lambda y, \end{cases} \tag{2.6.11}$$

and it is $\mathcal{C}^0$-conjugate to

$$\begin{cases} \dot{x} = -x, \\ \dot{y} = y. \end{cases} \tag{2.6.12}$$

ii) The origin is topologically a unstable node for m odd and $a_m > 0$. There exists an invariant $\mathcal{C}^\infty$ curve, the so-called center manifold, which is tangent to $y = 0$ at the origin and such that every point not lying on the strong unstable manifold is contained on it. Moreover, X is $\mathcal{C}^\infty$-conjugate to

$$\dot{x} = x^m(1 + ax^{m-1}), \tag{2.6.13}$$

for some $a \in \mathbb{R}$ on the center manifold. The system given by vector field X is $\mathcal{C}^\infty$-conjugate to

$$\begin{cases} \dot{x} = x^m(1 + ax^{m-1}), \\ \dot{y} = \lambda y, \end{cases} \tag{2.6.14}$$

and it is $\mathcal{C}^0$-conjugate to

$$\begin{cases} \dot{x} = x, \\ \dot{y} = y. \end{cases} \tag{2.6.15}$$

iii) The origin is a saddle-node for m even. Assume $a_m > 0$ modulo changing x into $-x$. Every point to the right of the strong unstable manifold lies on an invariant $\mathcal{C}^\infty$ curve (center manifold) which is tangent to $y = 0$ at the origin and on which X is $\mathcal{C}^\infty$-conjugate to

$$\dot{x} = x^m(1 + ax^{m-1}), \tag{2.6.16}$$

for some $a \in \mathbb{R}$. Center manifolds are infinitely tangent to the origin for $x \leq 0$ and all of them coincide in this range. At most one of them can be analytic. Vector field X is $\mathcal{C}^\infty$-conjugate to

$$\begin{cases} \dot{x} = x^m(1 + ax^{m-1}), \\ \dot{y} = \lambda y, \end{cases} \tag{2.6.17}$$

and is $\mathcal{C}^0$-conjugate to

$$\begin{cases} \dot{x} = x^2, \\ \dot{y} = y. \end{cases} \tag{2.6.18}$$

Normal Forms theory, as deduced from the former results, allow a characterisation of singularities by using the notion of conjugacy. Furthermore, the phase portrait in a neighbourhood of hyperbolic singularities can be described in terms of the linear part of a vector field X given by (2.4.1). The following result, known as the Hartman-Grobman theorem, provides a powerful shortcut to sketch the phase portrait locally around a hyperbolic singularity. Its proof can be found in chpater 2 of [15].

Theorem 2.6.3. (Hartman-Grobman). *Let X be a $\mathcal{C}^\infty$ vector field and consider p a hyperbolic singularity of X. Then at p, X is locally $\mathcal{C}^0$-conugate to its linear part $DX(0)$.*

Chapter 3

Planar centers

3.1 Basic definitions

According to the definitions introduced formerly, a vector field (2.1.1) has a singular point, linearly a focus or a center, if eigenvalues of the linearized matrix are purely imaginary. Consider a vector field with a singular point at the origin. Performing a suitable linear change of variables [15], system (2.1.1) can be brought to:

$$\begin{cases} \dot{x} = \lambda x + y + p(x, y), \\ \dot{y} = -x + \lambda y + q(x, y), \end{cases} \tag{3.1.1}$$

where $p(x, y)$ and $q(x, y)$ are analytic functions with terms of order 2 or higher [15]. Case $\lambda = 0$ implies, when the origin is linearly a focus or a center, that it is a weak focus or a center.

A singular point p of vector field (2.1.1) is said to be a centre if there exists a punctured neighbourhood of p in which all the orbits contained within it are periodic. The largest punctured neighbourhood of p containing closed orbits is the period annulus of the center, which is an open subset of $\mathbb{R}^2$ and it may be unbounded [23]. By compactifying the period annulus to $\mathbb{RP}^2$ [23], the inner boundary of the period annulus consists of the center p itself while the outer boundary is $\partial\mathcal{P} \setminus p$, where $\partial\mathcal{P}$ denotes the period annulus boundary. The outer boundary is usually a polycycle, i.e. the disjoint union of singular and regular points.

Within the period annulus, each orbit of the system can be associated to its period. The period function of a center maps each periodic orbit to its period. In order to identify periodic orbits, a parametrization must be used. A commonly used parametrization is, for instance, a transverse section such as the one given by the orbits of the orthogonal vector field $X^{\perp}$. Taking the definition in [23], let $\{\varphi_s\}_{s\in(0,1)}$ be the parametrization of the orbits within the period annulus of p, where orbits with parameter s near to zero are the ones near p and $s \approx 1$ the ones near the outer boundary of the period annulus. Thus, the period function may be defined as:

$$\begin{array}{rccc} P: & (0,1) & \longrightarrow & (0,+\infty) \\ & s & \longmapsto & P(s) := \{\text{period of } \varphi_s\}. \end{array} \tag{3.1.2}$$

It must be clarified that, for the future purposes of this thesis, the subset for the parametrization has been chosen to be $(0, 1)$, where s near 0 corresponds to orbits near the center and s near 1 corresponds to orbits near the outer boundary of the period annulus. However, generalising, any subset U containing the definition domain of any parameter s fits for the definition. The Implicit Function theorem provides a proof of the smoothness of function P, which is equal to that of vector field X [23].

Moreover, function P extends analytically to $s = 0$ if the vector field defining the system is analytic and the center p is non-degenerate [23]. However, it is not the case of s near 1, i.e. near the outer boundary of the period annulus, where the period function does not extend analitically.

Isolated critical points of the period function P are the so-called *critical periods* and they will be the cornerstone of this thesis. Orbits φ_s satisfying $P'(s) = 0$ are critical periodic orbits of vector field (2.1.1).

Another characterisation of a center is described in terms of a boundary neighbourhood parametrization [15]. Let

$$\begin{array}{rccc} \rho: & \mathbb{S}^1 & \longrightarrow & \mathbb{R}^2 \\ & e^{2\pi i t} & \longrightarrow & \rho(e^{2\pi i t}) \end{array} \tag{3.1.3}$$

be an injective regular parametrization of the circle where ρ is a $\mathcal{C}^1$ injective function with $\rho' \neq 0$ at every point of $\mathbb{S}^1$. In other words, consider a $\mathcal{C}^1$ function $\Psi : \mathbb{R} \to \mathbb{R}^2$ with $\Psi(t) = \rho(e^{2\pi i t})$, $\Psi'(t) \neq 0$ and such that restricted to the real interval $[0, 1)$ it is injective. Let $n(t) = (-\Psi_2'(t), \Psi_1'(t))$ be the normal vector pointing out the circle given by $\rho(\mathbb{S}^1)$. Taking all these definitions into account, ρ is said to be a permissible circle parametrization.

Let p be a singular point of vector field (2.1.1) and consider it defined in a compact neighbourhood U of p where all $q \in U$ such that $q \neq p$ satisfy $X(q) \neq 0$. Let ∂U be the boundary of U, which can be described in terms of a permissible circle parametrization as defined above, i.e. U is the image of ρ. Then, p is a center if ∂U is a periodic orbit and all orbits within $U \setminus \{p\}$ are periodic. Moreover, the restriction $X|_U$ is also called a center.

3.2 Local structure near periodic orbits

The aim of this subsection is to describe the composition of the phase portrait containing periodic orbits surrounding a center, based on the explanation given in [15]. With the notation introduced in section 2, let X be a planar $\mathcal{C}^r$ vector field with $1 \leq r \leq \infty$ or $r = \omega$, defined in an open subset $\Delta \subset \mathbb{R}^2$. Consider a periodic orbit contained in Δ with period τ_0 given by

$$\varphi = \{\varphi_p(t) : t \in \mathbb{R}\}. \tag{3.2.1}$$

Let Σ be a transverse section to vector field X. Since flow φ of X is continuous, for any $q \in \Sigma$ near p, φ_q is close enough to φ_p. A diagram of this situation is displayed in figure 3.1.

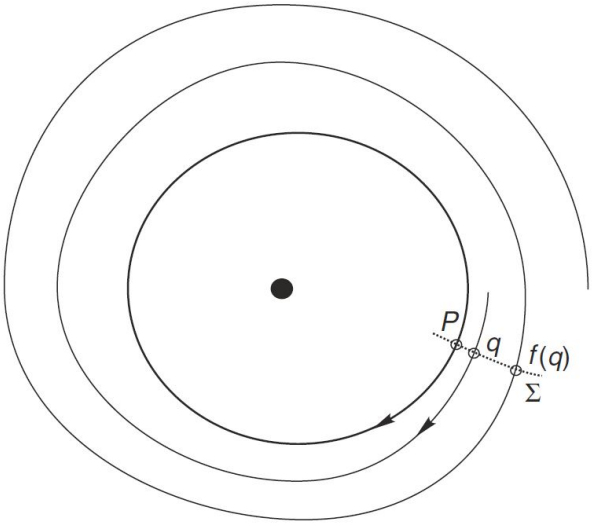

Figure 3.1: Local structure in a neighbourhood of a periodic orbit. Here, Σ denotes a transverse section to vector field X and $f(q)$ denotes the first point where orbit φ_q intersects the transverse section. Image extracted from [15].

As stated in the figure above, f maps each point q in the transverse section Σ to the first point such that $\varphi_q(t)$ intersects Σ considering a time interval containing increasing positive times t. Let Σ_0 be the domain of f. According to it, the definition of the Poincaré map must be introduced.

Definition 3.2.1. *Let Σ be a transverse section to vector field X as described formerly. The Poincaré map is defined as function $f : \Sigma_0 \longrightarrow \Sigma$ which maps each point in the transverse section with the first point where the orbit passing through this point intersects Σ taking positive times.*

There exists a particular type of periodic orbits when they appear isolated.

Definition 3.2.2. *Let γ be a periodic orbit of vector field X. If there exists a neighbourhood V of γ such that γ is the only periodic orbit contained on it, then γ is said to be a limit cycle.*

Let γ be a periodic orbit of a planar vector field X defined in an open subset $\Delta \subset \mathbb{R}^2$. The set of points contained in the unbounded component of $\mathbb{R}^2 \setminus \gamma$ is called the exterior of γ and denoted by $\mathrm{Ext}(\gamma)$ and the set of points contained in the bounded component of $\mathbb{R}^2 \setminus \gamma$ is called the interior of γ, denoted by $\mathrm{Int}(\gamma)$.

The following proposition allows a classification for limit cycles in planar vector fields defined in a subset of $\mathbb{R}^2$ [15]. According to it, only three cases are possible.

Proposition 3.2.3. *Let V be a neighbourhood of a limit cycle from a planar vector field defined in $\Delta \subset \mathbb{R}^2$. Then, the limit cycle can be either*

- *Stable. For all $q \in V$, $\omega(q) = \gamma$, i.e. the limit cycle "attracts" orbits contained in a neighbourhood.*
- *Unstable. For all $q \in V$, $\alpha(q) = \gamma$, i.e. the limit cycle "repels" orbits contained in a neighbourhood.*
- *Semi-stable. For all $q \in V \cap Ext(\gamma)$, $\omega(q) = \gamma$ and for all $q \in V \cap Int(\gamma)$, $\alpha(q) = \gamma$, or conversely. That is to say, the limit cycle "attracts" orbits contained in the unbounded component of $\mathbb{R}^2 \setminus \gamma$ and "repels" orbits contained in the bounded component of $\mathbb{R}^2 \setminus \gamma$, or conversely.*

3.3 First integrals

The notion of integrability of a vector field provides a way of characterising the phase portrait of a planar vector field by means of the so called first integrals, which are functions that are constant along the solutions of a planar vector field such as the one given by (2.1.1). Formally, let (2.1.1) be a polynomial vector field with coefficients in $\mathbb{R}$, i.e. (2.1.2) is a $\mathbb{R}$-polynomial system. Denote by m the degree of the polynomial vector field given by the maximum of the degrees of polynomials $X_1 = P(x, y)$ and $X_2 = Q(x, y)$, where $P, Q \in \mathbb{R}[x, y]$.

A first integral is an analytical function defined in the open subset $U \subset \mathbb{R}^2$ in which X is defined, $H : U \longrightarrow \mathbb{R}$, that is constant when evaluated in all solutions $(x_1(t), x_2(t))$ of (2.1.2) contained in U. Then,

$$H(x_1(t), x_2(t)) = C, \;\; C \in \mathbb{R}. \tag{3.3.1}$$

The former expression is accomplished for all $t \in I$. Constant functions H are excluded from the definition of a first integral. The differential equation system associated to the polynomial vector field (2.1.1) is said to be integrable on $U \subset \mathbb{R}$ if there exists a first integral defined in U.

Condition (3.3.1) allows an equivalent definition to characterise first integrals. Given a function H defined in an open subset of $U \subset \mathbb{R}^2$ in which X is defined, H is said to be a first integral if and only if

$$XH = P\frac{\partial H}{\partial x} + Q\frac{\partial H}{\partial y} \equiv 0. \tag{3.3.2}$$

Equivalence follows readily from condition (3.3.1).

There exists a characterisation of centres using first integrals which allows establishing sufficient and necessary conditions for the existence of a centre in a planar vector field by means of the existence of a first integral. Many references can be found for this characterisation. In this work, we cite the work made in 1987 by L. Mazzi and M. Sabatini [3].

Theorem 3.3.1. *Let X be a vector field of class $\mathcal{C}^k$ as defined in (2.1.1) and let p be an isolated singular point. Then p is a centre if and only if there exists a first integral $H \in \mathcal{C}^k$ with an isolated minimum at p. The result can be extended to a vector field of class $\mathcal{C}^\infty$ and the first integral is of class $\mathcal{C}^\infty$.*

3.4 Integrating factors, invariant algebraic curves and exponential factors

Consider now a polynomial system described by the vector field (2.1.1), in which X_1 and X_2 are polynomials in the variables x and y with real coefficients. Let $R : U \longrightarrow \mathbb{R}^2$ be a non-identically zero function and $U \subset \mathbb{R}^2$ an open subset. Let $\nabla = (\partial/\partial x, \partial/\partial y)$ and

$$XR = -R\nabla \cdot (P, Q), \qquad \frac{\partial(RP)}{\partial x} = -\frac{\partial(RQ)}{\partial y}, \qquad \nabla \cdot (RP, RQ) = 0. \tag{3.4.1}$$

If one of the previous equivalent conditions holds for function R and the polynomial vector field X in U, then R is said to be an integrating factor of system (2.1.2). The integrating factor, if exists, has a first integral defined in U associated given by,

$$H(x, y) = \int R(x, y)P(x, y)dy + h(x), \tag{3.4.2}$$

where $h(x)$ is found imposing $\partial H/\partial x = -RQ$.

Let $f \in \mathbb{R}[x, y]$ be a polynomial of degree m such that $f \not\equiv 0$, i.e. f is not identically zero. Then, f is said to be an invariant algebraic curve of the polynomial system (2.1.2) if there exists $K \in \mathbb{R}[x, y]$ such that

$$Xf = P\frac{\partial f}{\partial x} + Q\frac{\partial f}{\partial y} = Kf, \tag{3.4.3}$$

where K is known as the cofactor of $f = 0$.

On the other hand, [15] introduces the notion of exponential factor of a vector field. This definition will not be used for our interest but it is required to state the main theorem of Darboux theorem. Let g, h be polynomials in the ring $\mathbb{R}[x, y]$ which are relatively prime on it or such that $h \equiv 1$. Let $e(x, y) = \exp(g/h)$. Then, if

$$X\left(\exp\left(\frac{g}{h}\right)\right) = K\exp\left(\frac{g}{h}\right), \tag{3.4.4}$$

for some $K \in \mathbb{R}[x, y]$, function $e(x, y)$ is said to be an exponential factor of the polynomial system (2.1.2), with its corresponding cofactor K.

3.5 Darboux theory of integrability

Although Darboux results about integrability theory are extensive and some of them can be found detailed in [15], in this thesis only the result connecting integrating factors and cofactors from invariant algebraic curves and exponential factors will be stated. The importance lies in the fact that it provides a method for finding first integrals from integrating factors. The result is extracted from [15].

Theorem 3.5.1. *Let (2.1.2) be a polynomial system in $\mathbb{C}[x, y]$ and let m be the degree of the system. Assume that it admits p irreducible invariant algebraic curves $f_i = 0$ with cofactors K_i for $i = 1, \ldots, p$; q exponential factors $\exp(g_j/h_j)$ with cofactors L_j for $j = 1, \ldots, q$ and r independent singular points $(x_k, y_k) \in \mathbb{C}^2$ such that $f_i(x_k, y_k) \neq 0$ for $i = 1, \ldots, p$ and for $k = 1, \ldots, r$. Then, there exist $\lambda_i, \mu_j \in \mathbb{C}$ not all zero such that*

$$\sum_{i=1}^{p} \lambda_i K_i + \sum_{j=1}^{q} \mu_j L_j = -\mathrm{div}(P, Q), \tag{3.5.1}$$

if and only if

$$f_1^{\lambda_1} \cdots f_p^{\lambda_p} \left(\exp\left(\frac{g_1}{h_1}\right)\right)^{\mu_1} \cdots \left(\exp\left(\frac{g_q}{h_q}\right)\right)^{\mu_q}$$

is an integrating factor of the polynomial system.

Proof. Denoting by $F_i = \exp(g_i/h_i)$ for $i = 1, \ldots, q$, consider applying the vector field X to the

function given by $f_1^{\lambda_1}\cdots f_p^{\lambda_p}F_1^{\mu_1}\cdots F_q^{\mu_q}$. Then,

$$\begin{aligned}
X\left(f_1^{\lambda_1}\cdots f_p^{\lambda_p}F_1^{\mu_1}\cdots F_q^{\mu_q}\right) = \\
\frac{\lambda_1}{f_1}\left(f_1^{\lambda_1}\cdots f_p^{\lambda_p}F_1^{\mu_1}\cdots F_q^{\mu_q}\right)Xf_1+\cdots+\frac{\lambda_p}{f_p}\left(f_1^{\lambda_1}\cdots f_p^{\lambda_p}F_1^{\mu_1}\cdots F_q^{\mu_q}\right)Xf_p \\
+\frac{\mu_1}{F_1}\left(f_1^{\lambda_1}\cdots f_p^{\lambda_p}F_1^{\mu_1}\cdots F_q^{\mu_q}\right)XF_1+\cdots+\frac{\mu_q}{F_q}\left(f_1^{\lambda_1}\cdots f_p^{\lambda_p}F_1^{\mu_1}\cdots F_q^{\mu_q}\right)XF_q = \\
\left(f_1^{\lambda_1}\cdots f_p^{\lambda_p}F_1^{\mu_1}\cdots F_q^{\mu_q}\right)\left(\lambda_1\frac{Xf_1}{f_1}+\cdots+\lambda_p\frac{Xf_p}{f_p}+\mu_1\frac{XF_1}{F_1}+\cdots+\mu_q\frac{XF_q}{F_q}\right) = \\
\left(f_1^{\lambda_1}\cdots f_p^{\lambda_p}F_1^{\mu_1}\cdots F_q^{\mu_q}\right)\left(\lambda_1K_1+\cdots\lambda_pK_p+\mu_1L_1+\cdots+\mu_qL_q\right) = \\
-\left(f_1^{\lambda_1}\cdots f_p^{\lambda_p}F_1^{\mu_1}\cdots F_q^{\mu_q}\right)\cdot\mathrm{div}(P,Q).
\end{aligned}$$

In the third equality, invariant algebraic curves and exponential factors definitions have been used while the definition of integrating factor has been enforced in the last equality assuming $f_1^{\lambda_1}\cdots f_p^{\lambda_p}F_1^{\mu_1}\cdots F_q^{\mu_q}$ is an integrating factor by hypothesis. Hence, since the former expression is equivalent to that in (3.5.1), the statement is proved.

□

Chapter 4

Compactifications

This section constitutes a brief introduction to different compactifications, which may become a powerful tool to study exhaustively the flow of a given vector field X defined in an open subset of $\mathbb{R}^2$. By using concepts such as the stereographic projection or sending determinate subsets to the infinity, an appropriate change of coordinates provides a new representation of a vector field which can simplify and increase the accuracy of numerical results.

4.1 Poincaré-Lyapunov compactification

Let

$$\begin{aligned} \dot{x} &= P(x_1, x_2) \\ \dot{y} &= Q(x_1, y_2) \end{aligned} \tag{4.1.1}$$

be a differential equation system where $P(x, y)$ and $Q(x, y)$ are polynomials in the independent variables x and y of arbitrary degree. The vector field associated to this system is given by

$$X = P(x, y)\frac{\partial}{\partial x} + Q(x, y)\frac{\partial}{\partial y} \tag{4.1.2}$$

The degree d of (4.1.1) is given by the maximum degree of both $P(x, y)$ and $Q(x, y)$.

In order to obtain insight on the phase portrait of a real, bi-dimensional differential equation system, the study of the whole $\mathbb{R}^2$ plane must be carried out. This implies the analysis of orbits that may come from or tend to infinity. To gain knowledge of the behaviour of these orbits, different strategies can be followed with the aim of moving singular points or trajectories at the infinity to finite regions, such has the use of a compactification. In case of polynomial vector fields, the Poincaré compactification appears to be the most suitable option.

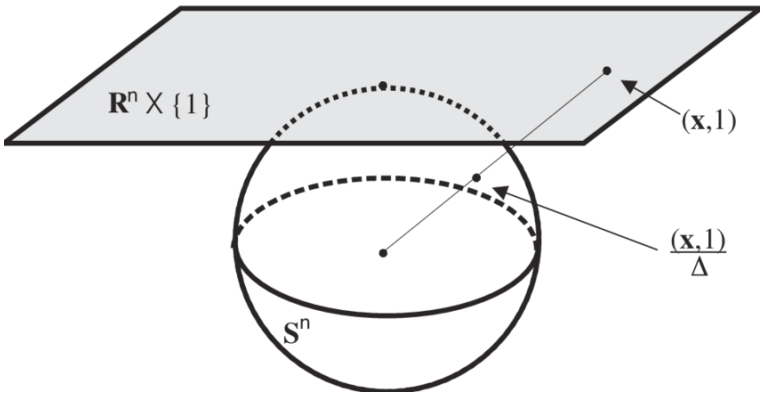

Figure 4.1: Projection of plane x_1x_2 onto the unit sphere centered in the origin. This projection is known as stereographic projection. Image extracted from [13].

In general lines, the Poincaré compactification allows the description of a polynomial vector field defined in the x_1x_2-plane by projecting it onto the unit sphere centered in the origin of $\mathbb{R}^3$, positioning the plane tangent to the north pole as shown in figure 4.1. Let p be a point of the x_1x_2-plane, then its projection onto the sphere is given by the intersection of the unit, centered sphere of $\mathbb{R}^3$ with the straight line joining the origin of $\mathbb{R}^3$ with the given point. As two intersections are possible, one for each hemisphere, the study can be reduced only to one of them including the equator. In this line, points at infinity in the x_1x_2-plane will lie on the equator.

Let (y_1, y_2, y_3) be any point of $\mathbb{R}^3$. The x_1x_2 plane can be then identified with $(y_1, y_2, y_3) = (x_1, x_2, 1)$ by the tangent condition previously stated and, consequently, $\mathbb{R}^2 \subset \mathbb{R}^3$. The unit sphere is given by

$$\mathbb{S}^2 = \{y \in \mathbb{R}^3 : y_1^2 + y_2^2 + y_3^2 = 1\}, \tag{4.1.3}$$

and it is tangent to the x_1x_2 plane at $(0, 0, 1)$. Consider now the division of the unit sphere $\mathbb{S}^2$ in the three following components:

$$\begin{aligned} H_+ &= \{y \in \mathbb{S}^2 : y_3 > 0\}, \\ H_- &= \{y \in \mathbb{S}^2 : y_3 < 0\}, \\ \mathbb{S}^1 &= \{y \in \mathbb{S}^2 : y_3\}, \end{aligned}$$

associated, respectively, to the northern hemisphere, the southern hemisphere and the equator. Let $f^+ : \mathbb{R}^2 \longrightarrow \mathbb{S}^2$ and $f^+ : \mathbb{R}^2 \longrightarrow \mathbb{S}^2$ be, respectively, the central projections for the northern and the southern hemisphere of the unit sphere. The central projection is defined, intuitively, as the intersection of the unit sphere $\mathbb{S}^2$ with the straight line resulting from the union of both the $\mathbb{R}^3$ origin and a given point $(y_1, y_2, y_3) = (x_1, x_2, 1) \in X \subset \mathbb{R}^2$. They are defined, respectively, as:

$$f^+(x) = \left(\frac{x_1}{\Delta(x)}, \frac{x_2}{\Delta(x)}, \frac{1}{\Delta(x)}\right), \tag{4.1.4}$$

$$f^-(x) = \left(\frac{-x_1}{\Delta(x)}, \frac{-x_2}{\Delta(x)}, \frac{-1}{\Delta(x)}\right), \tag{4.1.5}$$

where $\Delta(x) = \sqrt{x_1^2 + x_2^2 + 1}$. Therefore, each projection induces a vector field in each of the hemispheres which is analytically conjugate to X [15]. Denoting now $y = f^+(x)$ and $y = f^-(x)$ for each of the projections, these induced vector fields are given, pursuant to lemma 2.2.3, by:

$$H_+ : \overline{X}(y) = Df^+(x)X(x), \tag{4.1.6}$$

$$H_- : \overline{X}(y) = Df^-(x)X(x). \tag{4.1.7}$$

According to the previous reasoning, $\overline{X}$ is a vector field defined in $\mathbb{S}^2 \setminus \mathbb{S}^1$ which is tangent to the unit sphere at every point. Moreover, there exists a bijection between the points at infinity in $\mathbb{R}^2$ and points from $\mathbb{S}^1$. Due to this feature, in general $\overline{X}$ does not remain bounded when approaching to the equator. In order to extend $\overline{X}$ from $\mathbb{S}^2 \setminus \mathbb{S}^1$ to the whole unit sphere, the correction $\rho(x)\overline{X}$, where $\rho(x) = x_3^{d-1}$, must be applied since it makes possible the infinity to remain bounded. Now, $\overline{X}$ is no longer $\mathcal{C}^\omega$-conjugate to X but $\mathcal{C}^\omega$-equivalent.

Definition 4.1.1. *The extension $\overline{X}$ to the whole unit sphere $\mathbb{S}^2$ is called the Poincaré compactification of the vector field $X \subset \mathbb{R}^2$ and it is denotes by $p(X)$.*

In order to express vector field X with the new coordinates of the compactification, local charts covering all the unit sphere must be used. A local chart is a pair (U, ϕ) where U denotes a subset and ϕ a map to U. With the aim of covering it, 6 charts must be used, each of them given by:

$$U_k := \{y \in \mathbb{S}^2 : y_k > 0\}, \tag{4.1.8}$$

$$V_k := \{y \in \mathbb{S}^2 : y_k < 0\}, \tag{4.1.9}$$

where $k = 1, 2, 3$, with their corresponding local maps given by:

$$\phi_k : U_k \longrightarrow \mathbb{R}^2, \tag{4.1.10}$$

$$\psi_k : V_k \longrightarrow \mathbb{R}^2, \tag{4.1.11}$$

$$\phi_k(y) = -\psi_k(y) = \left(\frac{y_m}{y_k}, \frac{y_n}{y_k}\right) = (u, v), \tag{4.1.12}$$

for $m < n$ and $m, n \neq k$. Coordinates (u, v) are the coordinates of the vector field using the compactification. Points in $\mathbb{S}^1$ satisfy, in any chart, $v = 0$. Since two different projections have been defined, the study of the whole plane $\mathbb{R}^2$ is then reduced to one of the hemispheres together with equator $\mathbb{S}^1$. For out convenience, the northern hemisphere will be chosen. The union $H_+ \cup \mathbb{S}^1$ is the so-called *Poincaré disk* and it is fully covered by using charts (U_1, ϕ_1), (U_2, ϕ_2) and (U_3, ϕ_3). Thus, it is sufficient to derive the expression of the vector field in these three local charts.

For local chart (U_1, ϕ_1), applying lemma 2.2.3,

$$D\phi_1(y)\overline{X}(y) = D\phi_1(y) \circ Df^+(x)X(x) = D(\phi_1 \circ f^+)(x)X(x).$$

Denoting $\overline{X}|_{U_1} = D\phi_1(y)\overline{y}$, where $\overline{X}$ and $\overline{X}|_{U_1}$ are conjugate, coordinates (u, v) are given by:

$$(u, v) = (\phi_1 \circ f^+)(x) = \left(\frac{x_2}{x_1}, \frac{1}{x_1}\right), \tag{4.1.13}$$

and

$$D(\phi_1 \circ f^+)(x) = \begin{pmatrix} -\dfrac{x_2}{x_1^2} & \dfrac{1}{x_1} \\ -\dfrac{1}{x_1^2} & 0 \end{pmatrix}. \tag{4.1.14}$$

In this way,

$$\begin{aligned} \overline{X}|_{U_1} = D(\phi_1 \circ f^+)(x)X(x) &= \begin{pmatrix} -\dfrac{x_2}{x_1^2} & \dfrac{1}{x_1} \\ -\dfrac{1}{x_1^2} & 0 \end{pmatrix} \begin{pmatrix} P(x,y) \\ Q(x,y) \end{pmatrix} = \\ &= v^2 \left(-\frac{u}{v}P\left(\frac{1}{v}, \frac{u}{v}\right) + \frac{1}{v}Q\left(\frac{1}{v}, \frac{u}{v}\right), -P\left(\frac{1}{v}, \frac{u}{v}\right)\right)^T. \end{aligned} \tag{4.1.15}$$

Notice this expression may be ill-defined for $v = 0$ since polynomials P and Q in the new coordinates may contain denominator terms v^c with $c > 2$. Therefore, as stated above, in order to extend this vector field to the equator $\mathbb{S}^1$, factor $\rho(y)$ must be applied. Then,

$$\rho(y) = y_3^{d-1} = \frac{1}{\Delta(x)^{d-1}} = \frac{v^{d-1}}{\Delta(u,v)^{d-1}} = v^{d-1}m(u,v), \tag{4.1.16}$$

and $m(u,v) = (1+u^2+v^2)^{(1-d)/2}$. Then, $p(X)|_{U_1}$ is defined as

$$\rho \cdot \overline{X}|_{U_1}(u,v) = v^{d+1}m(u,v)\left(-\frac{u}{v}P\left(\frac{1}{v},\frac{u}{v}\right) + \frac{1}{v}Q\left(\frac{1}{v},\frac{u}{v}\right), -P\left(\frac{1}{v},\frac{u}{v}\right)\right). \tag{4.1.17}$$

Making a change in time variable, factor $m(u,v)$ can be removed while keeping the $\mathcal{C}^\omega$-equivalence. This change will not be stated in here, see chapter 5 in [15]. With a similar argument as described above, expressions for charts (U_2,ϕ_2) and (U_3,ϕ_3). Below, the expressions of the vector field for the three charts are displayed:

$$(U_1,\phi_1) \longrightarrow \dot{u} = v^d\left[-uP\left(\frac{1}{v},\frac{u}{v}\right) + Q\left(\frac{1}{v},\frac{u}{v}\right)\right] \tag{4.1.18}$$

$$\dot{v} = -v^{d+1}P\left(\frac{1}{v},\frac{u}{v}\right) \tag{4.1.19}$$

$$(x_1,x_2) = \left(\frac{1}{v},\frac{u}{v}\right) \tag{4.1.20}$$

$$(U_2,\phi_2) \longrightarrow \dot{u} = v^d\left[P\left(\frac{u}{v},\frac{1}{v}\right) - uQ\left(\frac{u}{v},\frac{1}{v}\right)\right] \tag{4.1.21}$$

$$\dot{v} = -v^{d+1}Q\left(\frac{u}{v},\frac{1}{v}\right) \tag{4.1.22}$$

$$(x_1,x_2) = \left(\frac{u}{v},\frac{1}{v}\right) \tag{4.1.23}$$

$$(U_3,\phi_3) \longrightarrow \dot{u} = P(u,v) \tag{4.1.24}$$

$$\dot{v} = Q(u,v) \tag{4.1.25}$$

$$(x_1,x_2) = (u,v) \tag{4.1.26}$$

Taking a look at the expressions of both charts (U_1,ϕ_1) and (U_2,ϕ_2) it is clear that points satisfying $v = 0$, which correspond to points at infinity in coordinates x_1, x_2, are now bounded due to the reescaling made. Expression for charts (V_k,ψ_k) are analogous to the ones above but multiplied by $(-1)^{d-1}$ for $k = 1,2,3$. Therefore, infinite singular points, defined as those lying at $\mathbb{S}^1$, appear in pairs of diametrally opposed singular points.

The main goal of this section is to understand how a compactification can be constructed in order to overcome some problems such as understanding the phase portrait of a planar vector field at the infinity. Multiple different compactifications may be built using different techniques and local charts.

4.2 $\mathbb{RP}^2$ compactification

Let $\mathbb{RP}^2$ be the projective real plane [19] and denote by $r : y = x - 2$ the straight line through $(0,-2)$ and slope equal to the unit. The general idea of the projective compactification lies on the idea of

sending line r to infinity in such a way that all the points contained on it lie at the infinity using the new coordinates. Let $\phi : \mathbb{R}^2 \longrightarrow \mathbb{R}^2 \setminus r$ the coordinates change such that

$$\phi(x, y) = (u(x, y), v(x, y)) = \left(\frac{1}{y - x + 2}, \frac{x - 1}{y - x + 2} \right), \tag{4.2.1}$$

where (u, v) denote the new coordinates in the $\mathbb{RP}^2$ compactification. The inverse function is given by

$$\phi^{-1}(u, v) = (x(u, v), y(u, v)) = \left(\frac{u + v}{u}, \frac{v - u + 1}{u} \right), \tag{4.2.2}$$

which is defined for $u \neq 0$. In here, only a single chart is presented since it will be the only one of interest for the purposes of this thesis.

Chapter 5

Loud systems

Focusing on quadratic vector fields, the following result provides a common expression for those containing a center at the origin as a singular point. For a proof, see chapter 8 in [15].

Lemma 5.0.1. *Let X be a quadratic vector field containing a center. Performing a translation, a linear transformation and a time rescaling, X can be written in the form below:*

$$\begin{cases} \dot{x} = -y - bx^2 - Bxy - dy^2, \\ \dot{y} = x + Dx^2 + Axy - Fy^2 \end{cases} \tag{5.0.1}$$

There exist five different families of quadratic centers [17]: reversible centers, Hamiltonians, generalized Lotka-Volterra, codimension four Q_4 and the Hamiltonian triangle. This thesis focuses on quadratic reversible centers since the period function associated is not monotonous in general. Chicone conjectured that any quadratic center whose period function is not monotonous, can be brought, by means of a rescaling of time and an affine transformation, to Loud normal form [24]:

$$\begin{cases} \dot{x} = -y + Bxy, \\ \dot{y} = x + Dx^2 + Fy^2, \end{cases} \tag{5.0.2}$$

where $(B, F, G) \in \mathbb{R}^3$. Assuming $B \neq 0$ and by means of a rescaling, the former system can be brought to the so-called dehomogenized Loud's system, with $B = 1$ [14]:

$$\begin{cases} \dot{x} = -y + xy = P(x, y), \\ \dot{y} = x + Dx^2 + Fy^2 = Q(x, y). \end{cases} \tag{5.0.3}$$

It follows readily that these systems are reversible with respect to the x-axis by means of the transformation $(x, y, t) \longmapsto (x, -y, -t)$, i.e. Loud systems are symmetric with respect to the x-axis and so their orbits. System (5.0.3) can be linearized obtaining the differential matrix below:

$$DX(x, y) = \begin{pmatrix} y & x - 1 \\ 1 + 2Dx & 2Fy \end{pmatrix}. \tag{5.0.4}$$

Evaluating it at the origin,

$$DX(0, 0) = \begin{pmatrix} 0 & -1 \\ 1 & 0 \end{pmatrix}, \tag{5.0.5}$$

which has eigenvalues $\pm i$, i.e. eigenvalues at the origin are purely imaginary and hence, taking into account the classification outlined in section 2.4, the origin is linearly a center. It must be noticed that this fact does not depend on the values of parameters D and F and hence the topology at the

origin remains invariable for all values of $\mu = (D, F) \in \mathbb{R}^2$. Consequently, the origin is non-degenerate (0 is not an eigenvalue).

In order to discern the qualitative nature of the origin for Loud systems, theorem 3.3.1 provides a sufficient and necessary condition for the existence of a center. Indeed, there exists a first integral defined at the origin of system (5.0.3) and, by extension, defined in the whole plane $\mathbb{R}^2$. It can be readily seen that $f_1 = x - 1 = 0$ is an invariant algebraic curve with cofactor

$$P\frac{\partial f_1}{\partial x} + Q\frac{\partial f_1}{\partial y} = -y + xy = y(x-1) \Longrightarrow K_1 = y.$$

Algebraic curve $f_1 = 0$ is irreducible since it is a polynomial with degree 1 in one variable over the real field. Actually, this invariant algebraic curve is enough to derive an integrating factor for Loud's system. Computing the condition stated in theorem 3.5.1,

$$\begin{aligned}\sum_{i=1}^{p} \lambda_i K_i + \sum_{j=1}^{q} \mu_j L_j = -\mathrm{div}(P, Q) \\ \Longleftrightarrow \lambda_1 K_1 = -\mathrm{div}(P, Q) \\ \Longleftrightarrow \lambda_1 \cdot y = -y(1 + 2F) \\ \Longleftrightarrow \lambda_1 = -1 - 2F.\end{aligned}$$

Hence, from theorem 3.5.1, $R(x) = f_1^{\lambda_1} = (x-1)^{-1-2F}$ is an integrating factor of system (5.0.3). The existence of other invariant algebraic curves or exponential factors is not necessary since the condition is fulfilled using only $f_1 = 0$. From expression (3.4.2), a first integral is given by

$$H(x, y) = \int R(x)P(x, y)dy + h(x) = \int (x-1)^{-1-2F} y(x-1)dy + h(x) = \frac{y^2}{2}(x-1)^{-2F} + h(x), \tag{5.0.6}$$

and

$$\begin{aligned}\frac{\partial H}{\partial x} = -Fy^2(x-1)^{-2F-1} + h'(x) = -RQ = -(x-1)^{-1-2F}(x + Dx^2 + Fy^2) \\ \Longleftrightarrow h'(x) = -(x-1)^{-2F-1}(x + Dx^2).\end{aligned} \tag{5.0.7}$$

Integrating the former expression with respect to x, the following expressions for $h(x)$ are obtained:

$$F \in \mathbb{R} \setminus \{1, 1/2, 0\} \longrightarrow h_1(x) = \frac{2DF^2x^2 - DF(x+2)x + D + (F-1)(2Fx-1)}{2F(F-1)(2F-1)} \cdot (x-1)^{-2F}, \tag{5.0.8}$$

$$F = 1 \longrightarrow h_2(x) = \frac{D(4x-3) - 2D(x-1)^2 \log(x-1) + 2x - 1}{2(x-1)^2}, \tag{5.0.9}$$

$$F = 0 \longrightarrow h_3(x) = -\frac{1}{2}(x-1)[D(x+3) + 2] - (D+1)\log(x-1), \tag{5.0.10}$$

$$F = \frac{1}{2} \longrightarrow h_4(x) = -\frac{D(x-2)x + (2D+1)(x-1)\log(x-1) - 1}{x-1}. \tag{5.0.11}$$

For the sake of simplicity, case $F \in \mathbb{R} \setminus \{1, 1/2, 0\}$, can be rewritten as [14]:

$$H(x, y) = (1-x)^{-2F}\left[\frac{y^2}{2} + a(D, F)x^2 + b(D, F)x + c(D, F)\right] \tag{5.0.12}$$

where

$$a(D,F)=\frac{D}{2(F-1)},\qquad b(D,F)=\frac{F-D-1}{(F-1)(2F-1)},\qquad c(D,F)=\frac{D-F+1}{2F(F-1)(2F-1)}. \tag{5.0.13}$$

For future purposes, term $(x-1)^{-2F}$ will be written as $(1-x)^{-2F}$. The first integral is then given by

$$H_i(x,y)=\frac{y^2(1-x)^{-2F}}{2}+h_i(x), \tag{5.0.14}$$

for $i=1,2,3,4$ depending on the value of parameter F. Condition (3.3.2) can be easily verified for expression (5.0.14). Then, since the origin is a singular point of the system, it is a solution and $H_1(0,0)=ct$ in accordance with the definition of first integral. Moreover, both

$$\frac{\partial H_1}{\partial x}(0,0)=0,\qquad \frac{\partial H_1}{\partial y}(0,0)=0.$$

Hence, the origin is a stationary point for the first integral. Computing second derivatives and evaluating at the origin, the minimum condition is fulfilled and therefore, the first integral of system (5.0.3) has an isolated minimum on it as required by theorem 3.3.1. Thus, the origin is a center for all values of D and F such that $D,F\in\mathbb{R}$.

From (5.0.3), it can be readily seen that $g_1\equiv x-1=0$ is an invariant subset for all values $D,F\in\mathbb{R}$ since $\dot{x}=0$ implies $y(x-1)=0$. Due to the uniqueness of solutions, the period annulus of the origin will be contained in the half-plane $\{x<1\}$. Moreover, taking into account the expression of the first integral of (5.0.3) given by (5.0.12), another invariant algebraic curve is obtained. Factor

$$g_2(x,y)\equiv\frac{1}{2}y^2+a(D,F)x^2+b(D,F)x+c(D,F), \tag{5.0.15}$$

where $a(D,F)$, $b(D,F)$ and $c(D,F)$ are defined in (5.0.13); is associated to the invariant algebraic curve $g_2(x,y)=0$, which is a conic curve. Indeed, condition (3.4.3) is satisfied for $g_2(x,y)$ and cofactor $K=2Fy$. A straightforward computation shows that

$$Xg_2=P\frac{\partial g_2}{\partial x}+Q\frac{\partial g_2}{\partial y}=2Fy\cdot g_2(x,y). \tag{5.0.16}$$

Thus, at every point along curve $g_2(x,y)=0$, since its gradient is orthogonal to the vector field X, X and $g_2(x,y)=0$ are tangent and therefore g_2 itself is a solution of (5.0.3). Furthermore, the line at infinity L_∞ in Cartesian coordinates is also an invariant curve of vector field X. To summarise, g_1, g_2 and L_∞ are invariant algebraic curves of vector field associated to system (5.0.3).

Invariant curve $g_2(x,y)=0$ intersects the x-axis at $g_2(x,0)=0$ and this equation has the following solutions:

$$p_1=\frac{-b-\sqrt{b^2-4ac}}{2a},\qquad p_2=\frac{-b+\sqrt{b^2-4ac}}{2a}. \tag{5.0.17}$$

When $0<p_1<1$ or $0<p_2<1$, invariant curve $g_2(x,y)=0$ may be part of the polycycle acting as the outer boundary of the period annulus of the center at the origin. For this reason, the study of these points is of major importance when determining the phase portrait and, specifically, the period annulus for a given value of $\mu=(D,F)\in\mathbb{R}^2$.

5.1 Period function and bifurcation diagram

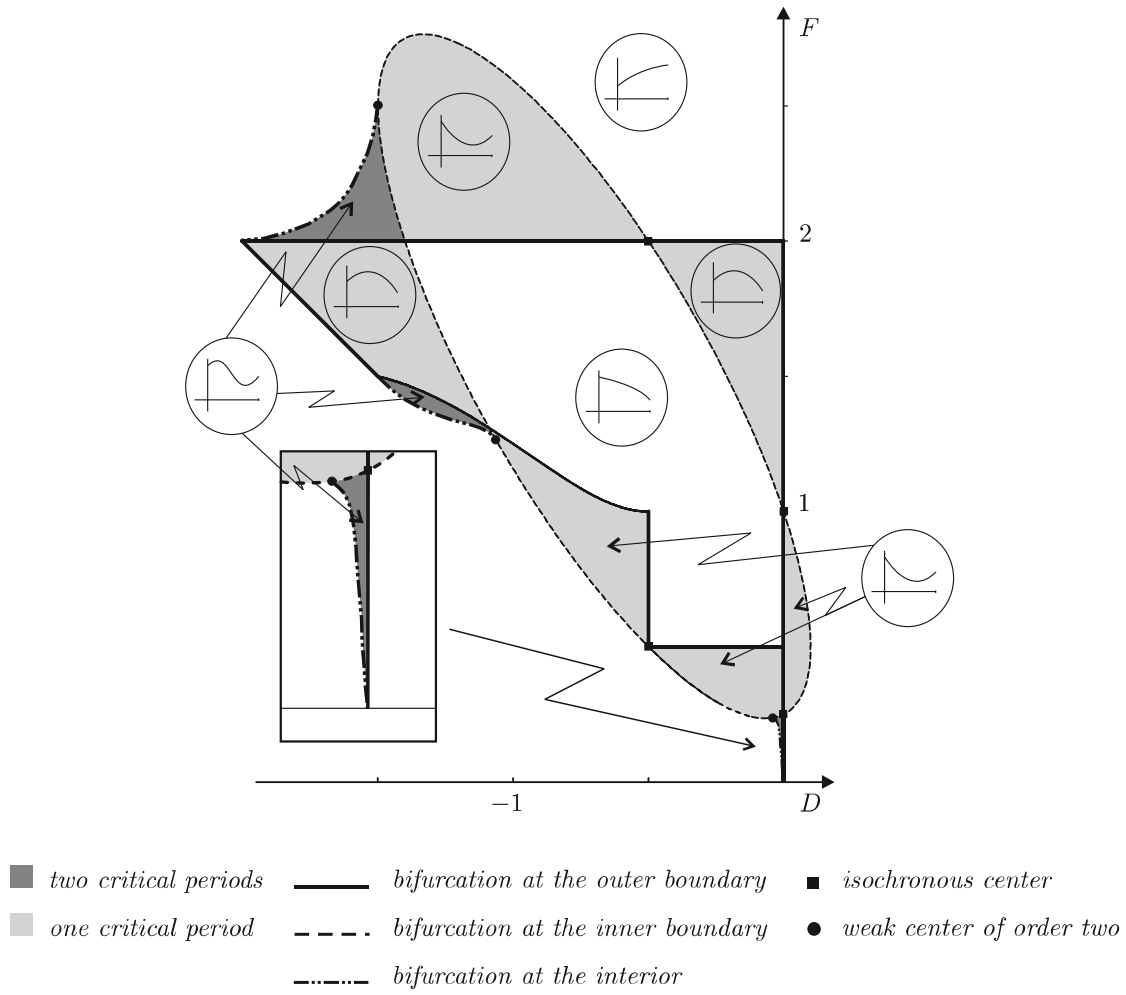

Figure 5.1: Conjectural bifurcation diagram of the period function. All parameter values $\mu := (D, F)$ within a common region have a period function with the same number of critical periods. Boundaries among different regions stand for different bifurcation types arising in the period function. Extracted from [14].

Figure 5.1 considers the first conjecture made in 2005 about the bifurcation diagram of the period function made by P. Mardešić, D. Marín and J. Villadelprat and whose work can be found in [14]. Period function in each different region has a given shape with different number of critical periods. In this paper, region displayed in light grey was proven to be associated to period functions with, at least, one critical period. Moreover, regions displayed in dark grey were conjectured to be associated to period functions with, at least, two critical periods. Despite the shape of the first region was analytically described, for the second regions the boundaries were uncertain and only for specific regions the existence of at least two critical periods was proven.

Later on, the conjectural bifurcation diagram in figure 5.1 was updated by the results reported in [23]. Specifically, regions conjectured to have exactly two critical periods were delimited with higher accuracy by defining the curve germs of some of the boundaries. This conjectural bifurcation diagram

is displayed in figure 5.2a.

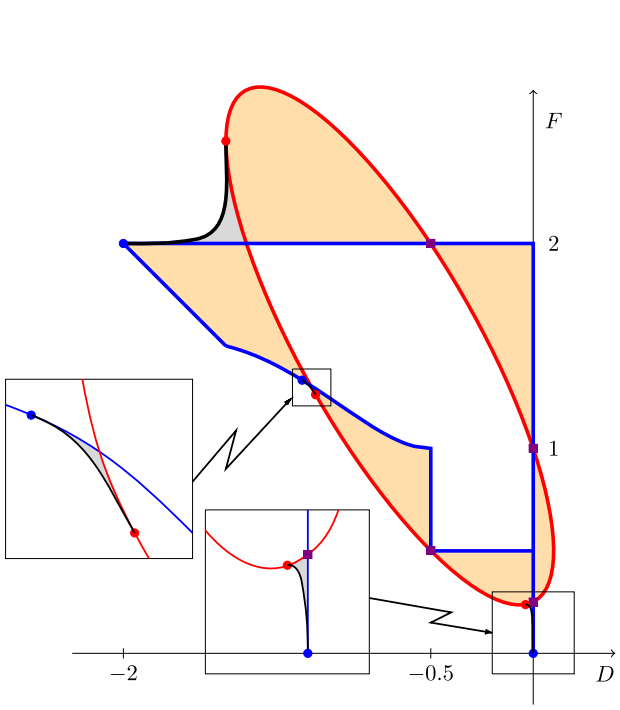

(a) Conjectured regions for the number of critical periods updated from the conjecture made in figure 5.1. White, orange and grey regions are associated, respectively, to those values of $\mu = (D, F)$ such that the period function of the center at the origin is conjectured to have, exactly, 0, 1 and 2 critical periods. Red, blue and black curves denote boundaries associated, respectively, to bifurcations at the inner boundary, outer boundary and the interior. Violet squares denote the isochronous centers. Image extracted from [23].

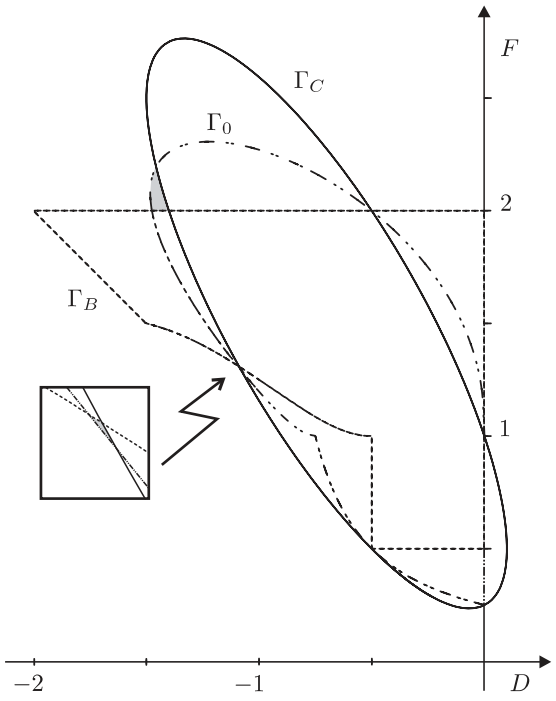

(b) In grey, regions for which the number of critical period has been proved to be, at least, two. A new curve, Γ_0 arises and constitutes one of the boundaries of these regions. Conjecture made in [23] says that, in fact, these regions contain at most two critical periods. Image extracted from [23].

Figure 5.2: Space of parameters with the different regions according to the number of critical periods of the period function and bifurcation curves.

The period function may undergo three different possible types of bifurcations when varying the value of $\mu = (D, F)$, defined as follows:

- Bifurcation at the inner boundary. A critical period arises near the origin or disappears by collapsing on it. These bifurcations are well understood since the period function extends analytically to the center at the origin as Chicone proved in [4]. These bifurcations take place for $\mu = (D, F)$ lying on the ellipse given by:

$$\Gamma_C := \left\{ \mu = (D, F) \in \mathbb{R}^2 : \frac{\pi}{12} \left(10D^2 + 10DF - D + 4F^2 - 5F + 1 \right) = 0 \right\}. \tag{5.1.1}$$

  For the sake of simplicity, the following notation will be used: $P_C(D, F) = \pi \cdot (10D^2 + 10DF - D + 4F^2 - 5F + 1)/12$.

- Bifurcation at the outer boundary. A critical period arises near the polycycle in the outer boundary or disappears by collapsing on it. These bifurcations were widely studied in [14]

and curve Γ_B, corresponding to the blue curve in figure 5.2a and associated to these kind of bifurcations, was determined. It will be introduced subsequently since some previous definitions are required.

- Bifurcation at the interior. A critical period disappears due to the collision of two different critical periods. Conversely, two critical periods arise very close to each other in a monotonous period function.

Notice that, according to the definitions above, transitions between regions containing 1 and 2 critical periods are not possible through bifurcations at the interior.

5.1.1 Main results within region W

Consider the following region within the space of parameters:

$$W \coloneqq \left\{(D,F) \in \mathbb{R}^2 : D \in (-1,0), F \in (0,1)\right\}, \tag{5.1.2}$$

and subregions

$$W_1 \coloneqq \left\{\mu \in W : \frac{1}{2} < F < 1\right\}, \quad W_2 \coloneqq \left\{\mu \in W : 0 < F < \frac{1}{2}\right\}. \tag{5.1.3}$$

Proposition below provides a series expansion for the period function in terms of a given parameter and $\mu = (D,F)$. In fact, since Loud systems are reversible, the proposition gives the expression for half of the period. Before stating it, some considerations must be made.

It is well known that for parameter μ in region W, the period annulus comprises the whole semi-plane $\{x < 1\}$. See, for instance, [7]. Denote by $P(s,\mu)$ the period of the periodic orbit passing through point $(1-s,0)$, where s is the parameter arising from a given parametrization of the period annulus of the center. At most, it will take value 1 and, at least, value 0. Values of $s \approx 0$ stand for orbits close to the outer boundary and $s = 1$ for the center itself. Let $T(s,\mu)$ be half of the period for a given s and a given μ. Moreover, consider the following set of functions [10]:

Definition 5.1.1. *Let U be an open subset of $\mathbb{R}^m$, where $m \in \mathbb{N}$. The set of analytic functions $h(s;\mu)$, where $\mu = (D,F)$, defined on $(0,\varepsilon) \times U$ for some $\varepsilon > 0$ and satisfying*

$$\lim_{s\to 0} h(s;\mu) = 0 \qquad \text{and} \qquad \lim_{s\to 0} s\frac{\partial h(s;\mu)}{\partial s} = 0,$$

uniformly on every compact subset of U is denoted by $\mathcal{I}(U)$.

The following proposition, extracted from [10], reads as:

Proposition 5.1.2. *Denote $\Delta_0(\mu) = \pi/(2\sqrt{F(D+1)})$ and $\lambda(\mu) = F/(1-F)$. Then the following holds:*

(a) If $\mu \in W_1$, then $T(s,\mu) = \Delta_0(\mu) + \Delta_1(\mu)s + sf_1(s,\mu)$, where $f_1 \in \mathcal{I}(W_1)$ and

$$\Delta_1(\mu) = \frac{\sqrt{\pi}(2D+1)}{2\sqrt{F(D+1)^3}} \frac{\Gamma((2\lambda-1)/(2\lambda))}{\Gamma((3\lambda-1)/(2\lambda))}. \tag{5.1.4}$$

(b) If $\mu \in W_2$, then $T(s,\mu) = \Delta_0(\mu) + \Delta_2(\mu)s^\lambda + s^\lambda f_2(s,\mu)$, where $f_2 \in \mathcal{I}(W_2)$ and

$$\Delta_2(\mu) = \frac{1}{1-F}\left(\frac{F}{D+1}\right)^{(\lambda+1)/2} \int_0^\infty \left(\left(\frac{D}{F-1}u^2 + 1\right)^{(\lambda-1)/2} - 1\right)\frac{du}{u^{\lambda+1}}. \tag{5.1.5}$$

For a proof of the previous proposition, refer, again, to [10]. Both cases have in common the asymptotic behaviour of $T(s,\mu)$ when s tends to 0, i.e. period orbits within the period annulus are approaching the invariant line $x = 1$, which is part, as mentioned above, of the outer boundary of the period annulus of the center at the origin. In this case, the period tends to

$$\Delta_0(\mu) = \frac{\pi}{\sqrt{F(D+1)}}, \tag{5.1.6}$$

as s tends to 0.

The following theorem describes the behaviour of the period function near the outer boundary within region W. This result can be found in [14] as well as its proof and it can be deduced from the previous proposition and theorem 5.1 in [10].

Theorem 5.1.3. *Let $\{X_\mu,\ \mu = (D,F) \in \mathbb{R}^2\}$ be the family of vector fields inducing Loud differential equation system given in (5.0.3). The period function is monotonous increasing near the outer boundary in the following subregions of W:*

$$\{\mu \in W : F < 1/2\},$$
$$\{\mu \in W : -1 < D < -1/2 \text{ and } F > 1/2\}.$$

On the other hand, near the outer boundary, the period function is monotonous decreasing within subset

$$\{\mu \in W : -1/2 < D < 0 \text{ and } F > 1/2\}.$$

5.1.2 Main results within region U

Consider now the following region within the space of parameters:

$$U \coloneqq \left\{(D,F) \in \mathbb{R}^2 : F > 1,\ F + D > 0 \text{ and } D < 0\right\}, \tag{5.1.7}$$

and the following subregions:

$$U_1 \coloneqq \{\mu \in U : F < 3/2\},$$
$$U_2 \coloneqq \{\mu \in U : F > 3/2\}.$$

Let $P(s,\mu)$ the period function for a given value of parameter $\mu = (D,F)$ evaluated in s, where s stands for a parametrization of the period annulus such that $s \in (0,1)$ and s near 1 is associated to periodic orbits near the center at the origin and values of s near 0 refer to those periodic orbits near the outer boundary of the period annulus. Then, the following theorem extracted from theorem 3.6 in [14] provides an expression of first order for the period function and, by extension, the value of the period function when $s \longrightarrow 0$ for all parameter values such that $\mu \in U$.

Theorem 5.1.4. *Let $P(s,\mu)$ be the period function of the center at the origin of system (5.0.3) for a given value of $\mu = (D,F) \in U$. Let $s \in (0,1)$ be a parametrization of the period annulus with the conditions given above. Define*

$$\Delta_0(\mu) = \frac{2\sqrt{2}}{\sqrt{a+b+c}} \operatorname{arctanh}\left(\frac{2a+b-\sqrt{b^2-4ac}}{2\sqrt{a(a+b+c)}}\right), \text{ and } \lambda(\mu) \coloneqq \frac{1}{2(F-1)}. \tag{5.1.8}$$

Then, the following statements hold:

(a) If $\mu \in U_1$, $P(s;\mu) = \Delta_0(\mu) + \Delta_1(\mu)s + sf_1(s;\mu)$, *where* $f_1 \in \mathcal{I}(U_1)$ *and*

$$\Delta_1(\mu) = \frac{-1/\sqrt{2a}}{(p_2-p_1)(1-p_1)} \cdot \left[2 - \int_0^1 \left(u^{-1/\lambda}\left(\frac{1-p_2}{1-p_1}(u-1)+1\right)^{1+\frac{1}{\lambda}} - 1\right)\frac{du}{(1-u)^{3/2}}\right], \tag{5.1.9}$$

where p_1 *and* p_2 *are defined in (5.0.17).*

(b) If $\mu \in U_2$, $P(s;\mu) = \Delta_0(\mu) + \Delta_2(\mu)s^\lambda + s^\lambda f_2(s;\mu)$, *where* $f_2 \in \mathcal{I}(U_2)$ *and*

$$\Delta_2(\mu) = \sqrt{\frac{2\pi}{a}}\frac{\lambda(p_2-p_1)^\lambda}{(1-p_1)^{2\lambda+1}}\frac{\Gamma\left(\frac{1}{2(1-F)}\right)}{\Gamma\left(\frac{F-2}{2(F-1)}\right)}, \tag{5.1.10}$$

where Γ *is the Euler's gamma function [1].*

Therefore, the period of an orbit near the outer boundary for $\mu \in U$ *tends to*

$$P(s,\mu) \xrightarrow[s\to 0]{} L(\mu) = \Delta_0(\mu). \tag{5.1.11}$$

The previous result is proved in [14] and, in fact, it provides 1st-order analytical expressions for the value of the period function in different subregions of U. Notice that terms containing function f_1 and f_2 may be understood as a sort of remainders.

Theorem 5.2 in [14] proves the existence of two subregions in the space of parameters containing, at least, two critical periods. These two regions are displayed in figure 5.2b. Both of them are delimited by the ellipse Γ_C; Γ_B, which is the disjoint union of different segments and curves; and curve Γ_0. The last one is given by:

$$\Gamma_0 \coloneqq \{\mu \in U : L(\mu) - 2\pi = 0\}, \tag{5.1.12}$$

where $L(\mu)$ is given by equation (5.1.11). Curve Γ_B is given by the union of the following subsets:

$$\begin{aligned}\Gamma_B \coloneqq &\{\mu \in \mathbb{R}^2 : D \in [-2,0], F = 2\}\cup\\ &\{\mu \in \mathbb{R}^2 : D = 0, F \in [1/2,2)\}\cup\\ &\{\mu \in \mathbb{R}^2 : D \in [-1/2,0), F = 1/2\}\cup\\ &\{\mu \in \mathbb{R}^2 : D = -1/2, F \in (1/2,1]\}\cup\\ &\Gamma_1\cup\\ &\{\mu \in \mathbb{R}^2 : D \in (-2,-3/2], F = -D\},\end{aligned} \tag{5.1.13}$$

where

$$\Gamma_1 \coloneqq \{\mu \in \mathbb{R}^2 : \Delta_1(\mu) = 0\}, \tag{5.1.14}$$

and $\Delta_1(\mu)$ is given by equation (5.1.9). Curve Γ_1 has proven to be the graphic of an analytical function of $D = \mathcal{G}(F)$ [14].

Assertion (e) in Theorem A from [23] states the existence of a curve δ_1 starting at $v = (D,F) = (-2,2)$ such that it is tangent to $F = 2$ exactly at v. Moreover, there also exists a curve δ_2 with initial point $L_1 = (D,F) = (-3/2,5/2)$, which corresponds to the red dot in figure 5.2a for $F > 2$. Black curve in figure 5.2a for $F > 2$ joining both v and L_1 is unknown and [23] conjectures the connection of both δ_1 and δ_2 delimiting this way a region containing exactly two critical periods. Notice that grey region in figure 5.2b within $F > 2$ is a subset of the aforementioned region for which it is proved that the

number of critical periods is, at least, two.

Another interesting property studied analytically of the period function of the center at the origin is its behaviour near the outer boundary of the period annulus. For some regions of the parameters space, the monotonicity of the period function near the polycycle is determined. The following theorem shows the monotonicity near the outer boundary for two different subregions of region U. The result below holds:

Theorem 5.1.5. *Let $\{X_\mu,\ \mu = (D, F) \in \mathbb{R}^2\}$ be the family of vector fields inducing Loud differential equation system given in (5.0.3). The period function of the center at the origin near the outer boundary of the period annulus shows the behaviour displayed in figure 5.3.*

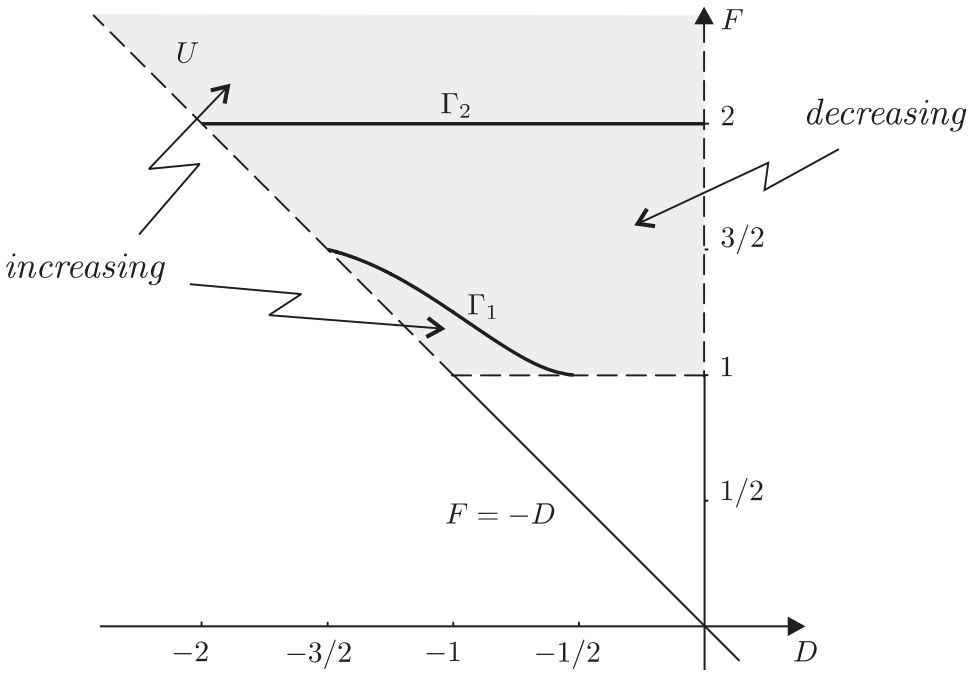

Figure 5.3: Monotonicity of the period function near the outer boundary of the period annulus for different subregions of region U. Following the notation, Γ_2 is the horizontal line $F = 2$. Image extracted from [14].

This theorem, along with other results concerning the behaviour of the period function, is proved in [14]. Since for $F = 2$ the period function undergoes a bifurcation at the outer boundary of the period annulus, a critical period arises or disappears very close to the polycycle.

Chapter 6

Methodology

Given the invariant algebraic curves of (5.0.3) stated in section 5, it is clear that the period annulus of the center at the origin must be contained in the real semi-plane $S_1 \equiv \{x < 1\}$. Therefore, a parametrization of the orbits given by the segment contained in the line $y = 0$ from $x = 0$ to $x = 1$ seems a reasonable way of identifying each of the periodic orbits within the period annulus. Moreover, notice that vector field inducing Loud systems is orthogonal to this segment and hence, it is a transverse section. However, the position of the invariant algebraic curve g_2 must be taken into account in order to identify the regions in the parameter's space $D - F$ for which this segment is crossed by g_2 and, therefore, the phase portrait varies.

6.1 Period using $\mathbb{RP}^2$ compactification

Section 4.2 provides the expression of the coordinates change for chart (u, v) using $\mathbb{RP}^2$ compactification. Since in x, y-coordinates the period annulus may be, for some combinations of D and F, the whole plane S_1, the period annulus may extend until the infinity. For this reason, periodic orbits very close to the invariant line $g_1 : x - 1 = 0$ may escape to infinity.

Using $\mathbb{RP}^2$ compactification in section 4.2, line $y = x - 2$ lies at infinity with the advantage that all periodic orbits within the period annulus of the origin will remain finite. Since $\phi(x, y) = (u(x, y), v(x, y))$ is a differentiable coordinates change, its Jacobian matrix is given by:

$$D\phi(x,y) = \begin{pmatrix} \partial u/\partial x & \partial u/\partial y \\ \partial v/\partial x & \partial v/\partial y \end{pmatrix} = \begin{pmatrix} \dfrac{1}{(y-x+2)^2} & -\dfrac{1}{(y-x+2)^2} \\ \dfrac{y+1}{(y-x+2)^2} & -\dfrac{x-1}{(y-x+2)^2} \end{pmatrix}. \tag{6.1.1}$$

In general terms, let h be a $\mathcal{C}^r$ coordinate change, where $1 \leq r \leq \infty$, operating over a vector field X_1 by describing it in terms of a new coordinate system as in lemma 2.2.3. Then, expression of X_1 in the new coordinates (u, v), denoted by X_2, is given by

$$X_2(u,v) = Dh_{h^{-1}(u,v)} X_1(h^{-1}(u,v)). \tag{6.1.2}$$

Therefore, in the chart (u, v) of the compactification, vector field associated to (5.0.3) has the expres-

sion given by $D\phi(x,y)\cdot X(x,y)^T$. Explicitly,

$$\begin{aligned} D\phi(x,y)\cdot X(x,y)^T &= \begin{pmatrix} \dfrac{1}{(y-x+2)^2} & -\dfrac{1}{(y-x+2)^2} \\ \dfrac{y+1}{(y-x+2)^2} & -\dfrac{x-1}{(y-x+2)^2} \end{pmatrix} \begin{pmatrix} f(x,y) \\ g(x,y) \end{pmatrix} \\ &= \begin{pmatrix} \dfrac{1}{(y-x+2)^2} & -\dfrac{1}{(y-x+2)^2} \\ \dfrac{y+1}{(y-x+2)^2} & -\dfrac{x-1}{(y-x+2)^2} \end{pmatrix} \begin{pmatrix} y(x-1) \\ x+Dx^2+Fy^2 \end{pmatrix} \\ &= \begin{pmatrix} \dfrac{y(x-1)}{(y-x+2)^2} - \dfrac{x+Dx^2+Fy^2}{(y-x+2)^2} \\ \dfrac{y(x-1)(y+1)}{(y-x+2)^2} - \dfrac{(x-1)(x+Dx^2+Fy^2)}{(y-x+2)^2} \end{pmatrix}. \end{aligned} \tag{6.1.3}$$

Identifying $h^{-1}(u,v)$ with $\phi^{-1}(u,v)$ given by (4.2.2), the expression of (5.0.3) in the coordinates of the compactification is obtained:

$$\dot{u} = -(D+F+1)u^2 - (D+F-1)v^2 + dFu - [2(D-F+1)u + 2F - 1]v - F = p(u,v), \tag{6.1.4}$$

$$\begin{aligned} \dot{v} &= -(D+F-1)\frac{v^3}{u} - 2[(D-F+1)u + F - 1]\frac{v^2}{u} - [(D+F+1)u^2 - (2F-1)u + F - 1]\frac{v}{u} \\ &= q(u,v). \end{aligned} \tag{6.1.5}$$

In the new coordinates, the center at the origin in x,y-coordinates is shifted to the coordinates $(u,v) = (1/2,-1/2)$ and the line $v = 0$ becomes invariant. Studying numerically Loud systems compactified in $\mathbb{RP}^2$ has the advantage of bounded period annulus, i.e. periodic orbits do not escape to infinity and thus, numerical errors due to overflow are easily controlled. For this reason, integrating Loud systems in the expressions given by (6.1.4) and (6.1.5) using a 4th-order Runge-Kutta method may be a suitable option specially for orbits near the outer boundary.

6.2 Period by numerical integration of a differential equation

This method uses the expression of the dehomogenized Loud system (5.0.3) to compute numerically the period of a given orbit using the existence of a first integral. By taking advantage of the derivative of variable x with respect to time t, variables in the differential equation can be easily separated and integration can be performed. Therefore, equation for $\dot{x}$ in (5.0.3) may be rewritten as:

$$\frac{dx}{dt} = \dot{x} = -y(1-x) \iff \frac{dx}{y(1-x)} = -dt. \tag{6.2.1}$$

First integral obtained in (5.0.14) is the key concept in order to obtain the period numerically. By definition, a first integral is constant on each solution of (5.0.3) contained within the period annulus of the center and, hence, each solution can be associated to a constant value h called the *energy level*. Then, we can identify each energy level with a given orbit according to:

$$H(x(t),y(t)) = h \longmapsto \gamma_h, \tag{6.2.2}$$

where $(x(t),y(t))$ is a solution in the definition domain of the first integral. Then, each orbit γ is associated to a given energy level $h \in \mathbb{R}$. Thus, integrating expression (6.2.1) over a periodic orbit

γ_h within the period annulus of the center at the origin, the expression for the period function is obtained:

$$\int_{\gamma_h} \frac{dx}{y(1-x)} = -\int_{\gamma_h} dt = P(h), \tag{6.2.3}$$

where $P(h)$ denotes the period function which depends, exclusively, on the energy level of the orbit considered. Since the left hand side of expression (6.2.3) is a line integral along curve γ_h in $\mathbb{R}^2$ and the expression within the integral is a function of both variables x and y, the first integral given by (5.0.14) provides the link among variables. Therefore, for $F \in \mathbb{R} \setminus \{0, 1, 1/2\}$ and a given energy level h,

$$H(x,y) = h \Longleftrightarrow (1-x)^{-2F}\left[\frac{y^2}{2} + a(D,F)x^2 + b(D,F)x + c(D,F)\right] = h. \tag{6.2.4}$$

Every expression of the form given by (6.2.4) with an added constant is a first integral of Loud systems since $H(x,y)$ is a first integral modulus a constant. Thus, for the purposes of this study, the following first integral will be considered:

$$H(x,y) = (1-x)^{-2F}\left[\frac{y^2}{2} + a(D,F)x^2 + b(D,F)x + c(D,F)\right] - c(D,F), \tag{6.2.5}$$

where

$$A(x) = \frac{1}{2}(1-x)^{-2F}, \tag{6.2.6}$$

$$E(x) = (1-x)^{-2F}\left[a(D,F)x^2 + b(D,F)x + c(D,F)\right] - c(D,F), \tag{6.2.7}$$

$A(0) \neq 0$ and $E(0) = 0$. Therefore, the first integral can be rewritten as $H(x,y) = A(x)y^2 + E(x)$. Since term $(1-x)^{-2F}$ is analytical in $x = 0$, there exists a Taylor's series containing quadratic an higher-order terms. This series takes the expression below:

$$(1-x)^{-2F} = \sum_{n=0}^{\infty} x^n (-1)^n \binom{-2F}{n} = 1 + 2Fx + F(2F+1)x^2 + O(x^3). \tag{6.2.8}$$

Consequently, $E(x)$ does not contain any independent term. Given the symmetry of periodic orbits within the period annulus of the center of Loud systems with respect to line $y = 0$ due to the property of reversibility, it is sufficient to take only the positive branch of the periodic orbit and integrate between the maximum and minimum values of x. These values, hereafter $x_l(h)$ and $x_r(h)$ for the left and the right intersection point of the orbit with the x-axis as displayed in figure 6.1, are solutions of equation

$$H(x,0) = h. \tag{6.2.9}$$

All the previous arguments constitute the proof of the following lemma:

Lemma 6.2.1. *With the notation introduced above, the expression of the period function is given by:*

$$P(h) = 2\int_{x_r(h)}^{x_l(h)} \frac{dx}{(1-x)\sqrt{\frac{h-E(x)}{A(x)}}}. \tag{6.2.10}$$

Since term $E(x)$ is only dependent on x and $H(x,y) = A(x)y^2 + E(x)$, at the extremes of integration $E(x_i(h)) = h$ for $i = r, l$ and therefore, the integral defined in lemma 6.2.1 is an improper integral since

$$\frac{h - E(x)}{A(x)} \xrightarrow[x \to x_i(h)]{} 0, \tag{6.2.11}$$

for $i = r, l$; and

$$\frac{1}{(1-x)\sqrt{\frac{h-E(x)}{A(x)}}} \xrightarrow[x \to x_i(h)]{} \infty.$$

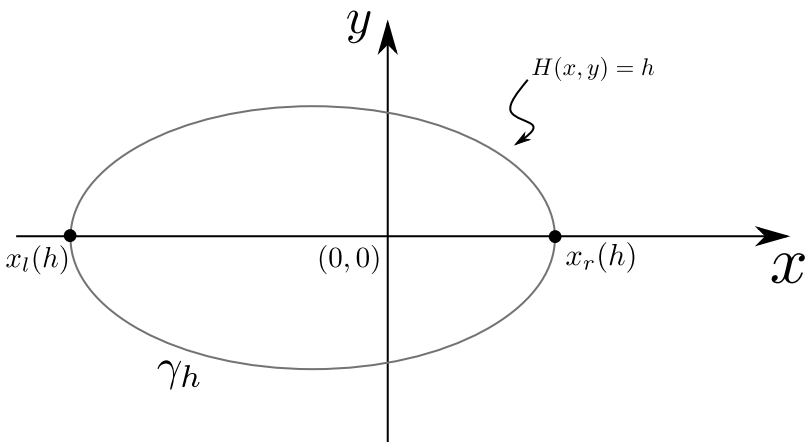

Figure 6.1: Schematic display of a periodic orbit within the period annulus of the center at the origin for a given energy level h. Points where the orbit intersects the x-axis are given by $x_l(h)$ and $x_r(h)$, where subscripts l and r stand for right ang left, respectively.

In order to overcome the improper integral issue, some manipulations of the function to be integrated are required. Consider the identity $d(fg) = fdg + gdf$ where $f, g : U \to \mathbb{R}$ and $U \subset \mathbb{R}$, given by the differential multiplication rule. Let γ_h be a closed orbit contained in the period annulus of the center at the origin, i.e. a closed curve. Then, integrating the former identity along γ_h, the line integral is given by:

$$\int_{\gamma_h} d(fg) = \int_{\gamma_h} (fdg + gdf) \tag{6.2.12}$$

From the result obtained in theorem B.1 (see appendix B), the integral above is exactly zero since γ_h is a closed simple curve. Therefore,

$$\int_{\gamma_h} (fdg + gdf) = 0 \iff \int_{\gamma_h} fdg = -\int_{\gamma} gdf \tag{6.2.13}$$

Term y dividing in expression (6.2.3) makes the function to be integrated to become infinite when the x value is near the intersection points $x_l(h)$ and $x_r(h)$. Thus, manipulations are oriented towards getting rid of this y dividing. From expression (6.2.3),

$$P(h) = \frac{h}{h}\int_{\gamma_h} \frac{dx}{y(1-x)} = \frac{1}{h}\int_{\gamma_h} \frac{A(x)y^2 + E(x)}{y(1-x)}dx, \tag{6.2.14}$$

where the fact that $H(x, y) = A(x)y^2 + E(x) = h$ along the curve γ_h has been used. The former integral can be split into the sum of two different integrals:

$$P(h) = \frac{1}{h}\int_{\gamma_h} \frac{A(x)y}{1-x}dx + \frac{1}{h}\int_{\gamma_h} \frac{E(x)}{y(1-x)}dx. \tag{6.2.15}$$

In the first integral above, y does not appear anymore dividing while in the second one it persists. Taking now the expression of the first integral and deriving with respect to x in both sides,

$$E'(x) + \frac{d}{dx}\left(A(x)y^2\right) = 0 \iff \frac{d}{dx}\left(A(x)y^2\right) = -E'(x). \tag{6.2.16}$$

Since $\sqrt{A(x)}$ is well-defined locally in a neighbourhood of 0, it is possible to write $l = y\sqrt{A(x)}$ and so,

$$\frac{d}{dx}\left(A(x)y^2\right) = \frac{d}{dx}(l^2) = -E'(x), \tag{6.2.17}$$

$$2ll' = E'(x), \tag{6.2.18}$$

$$\frac{d}{dx}\left(y\sqrt{A(x)}\right) = -\frac{E'(x)}{2y\sqrt{A(x)}}. \tag{6.2.19}$$

The second integral in expression (6.2.15) can be written as:

$$\int_{\gamma_h} \frac{E(x)}{y(1-x)}dx = \int_{\gamma_h} \frac{E(x)}{E'(x)(1-x)} \cdot \frac{E'(x)}{y}dx, \tag{6.2.20}$$

where term $E(x) \cdot E'(x)^{-1}$ is well-defined in $x = 0$ since the multiplicity of $E'(x)$ in $x = 0$ is always lower than the multiplicity of $E(x)$ in $x = 0$ according to the Taylor series expansion provided before. Moreover, since the center at the origin of Loud systems is non-degenerate, the first integral starts in quadratic terms of x and y. Multiplying and dividing the former expression by a factor 2 and $\sqrt{A(x)}$,

$$\int_{\gamma_h} \frac{E(x)}{y(1-x)}dx = 2\int_{\gamma_h} \frac{E(x)}{E'(x)} \frac{\sqrt{A(x)}}{(1-x)} \cdot \frac{E'(x)}{2y\sqrt{A(x)}}dx. \tag{6.2.21}$$

By identifying f and dg and using the identity given in (6.2.13),

$$f(x) = \frac{E(x)}{E'(x)} \frac{\sqrt{A(x)}}{(1-x)}, \qquad dg(x) = \frac{E'(x)}{2y\sqrt{A(x)}}dx = -\frac{d}{dx}\left(y\sqrt{A(x)}\right), \tag{6.2.22}$$

$$\int_{\gamma_h} \frac{E(x)}{y(1-x)}dx = 2\int_{\gamma_h} f dg = -2\int_{\gamma_h} g df = 2\int_{\gamma_h} y\sqrt{A(x)}f'(x)dx. \tag{6.2.23}$$

Returning to expression (6.2.15), the following lemma provides the suitable expression of the period function in order to integrate numerically. Its proof is deduced from all the arguments above.

Lemma 6.2.2. *With the notation introduced formerly, the period function for Loud systems can be written as:*

$$P(h) = \frac{1}{h}\int_{\gamma_h} \frac{A(x)y}{1-x}dx + \frac{2}{h}\int_{\gamma_h} y\sqrt{A(x)}f'(x)dx, \tag{6.2.24}$$

where the expression of $f'(x)$ is given by:

$$f'(x) = -\frac{(x-1)EE'A' + 2(x-1)A(E')^2 - 2(x-1)AEE'' - 2AEE'}{2(x^2-2x+1)\sqrt{A}(E')^2}. \tag{6.2.25}$$

Thereby, equation provided by lemma 6.2.2 provides the analytical expression for the period function of the center at the origin in terms of the sum of two different integrals which do not diverge in a neighbourhood of it. However, term $1 - x$ dividing in the first integral may diverge for values of x

near the invariant subset $x = 1$ but since period annulus extends, at most, until invariant line $x = 1$, it will be assumed that case $x = 1$ will not be studied since it belongs to the outer boundary of the period annulus. Both integrals can be computed numerically giving an approximation of the period of each periodic orbit surrounding the origin.

In practice, however, one must take into account that, for some combinations in the parameters space $D-F$, the period annulus of the center at the origin may comprise all the semi-plane given by $\{x < 1\}$. For such cases, the boundary of the period annulus escapes towards infinite and, consequently, the orbits near the inner boundary of the period annulus also escape to infinity. For this reason, the numerical problem of integrating vector field (5.0.3) may induce large numerical errors for orbits escaping to infinity. Since the method explained in this section deals with Cartesian coordinates, integration of γ_h numerically using methods such as the Trapezium's rule or Simpson's rule may be extremely inaccurate.

Due to the advantages and disadvantages of both methods presented above, it seems reasonable to use both of them combined: the period function near the inner boundary will be studied using the integration of the period function while for periodic orbits near the outer boundary, which may escape to infinity, compactification will be used.

6.3 Parametrization of the period annulus

In order to transform the analytical problem of obtaining the value of the period function of the period annulus for a given combination of parameters (D, F) into a numerical problem, one must find a strategy to identify each orbit within the period annulus of the center. As mentioned previously, depending on the value of parameter $\mu := (D, F)$, invariant curves take different relative positions and, therefore, the phase portrait varies. Phase portraits are displayed in figure 6.2. Assume the phase portrait varies continuously with $\mu = (D, F)$. Taking advantage of the symmetry of periodic orbits in Loud systems with respect to x-axis, cases of interest are listed below:

- Region $W = \{(D, F) \in \mathbb{R}^2 : D \in (-1, 0), F \in (0, 1)\}$. As mentioned in section 5.1, it is well-known (see [7]) that the period annulus extends through the whole semi-plane $\{x < 1\}$. In this case, the vector field defining Loud systems is transverse to the x-axis when $y = 0$. Then, segment $\{(x, 0) : 0 < x < 1\}$ can be taken as a transverse section in order to perform a parametrization of the periodic orbit within the period annulus.

- Region $U = \{(D, F) \in \mathbb{R}^2 : D < 0, D + F > 0, F > 1\}$. In this case the period annulus does not extend through the whole semi-plane $\{x < 1\}$ [14] since the invariant curve given by expression (5.0.15) crosses the x-axis for $x \in (0, 1)$. The intersection point is given by setting $y = 0$:

$$g_2(x, 0) \equiv a(D, F)x^2 + b(D, F)x + c(D, F) = 0, \tag{6.3.1}$$

  where, for the sake of simplicity, $a(D, F) = a$, $b(D, F) = b$ and $c(D, F) = c$,

$$x = \frac{-b \pm \sqrt{b^2 - 4ac}}{2a}. \tag{6.3.2}$$

  The discriminant $\Delta = b^2 - 4ac$ indicates the number of intersection points: for $b^2 > 4ac$, the conic curve intersects twice line $y = 0$, for $b^2 = 4ac$ just once and for $b^2 < 4ac$, the hyperbola has no intersections. Indeed, the intersection point satisfies $x \in (0, 1)$. Let x^* be this point, then the conic curve is an hyperbola intersecting $y = 0$ at $(x^*, 0)$. All the periodic orbits within the

period annulus then cross the x-axis in the interval $(0, x^*)$, which provides a parametrization of the period annulus.

In conclusion, the outer boundary of the period annulus for $\mu = (D, F) \in U$ contains the invariant curve $g_2(x, y) = 0$ and extends through the left plane induced by it.

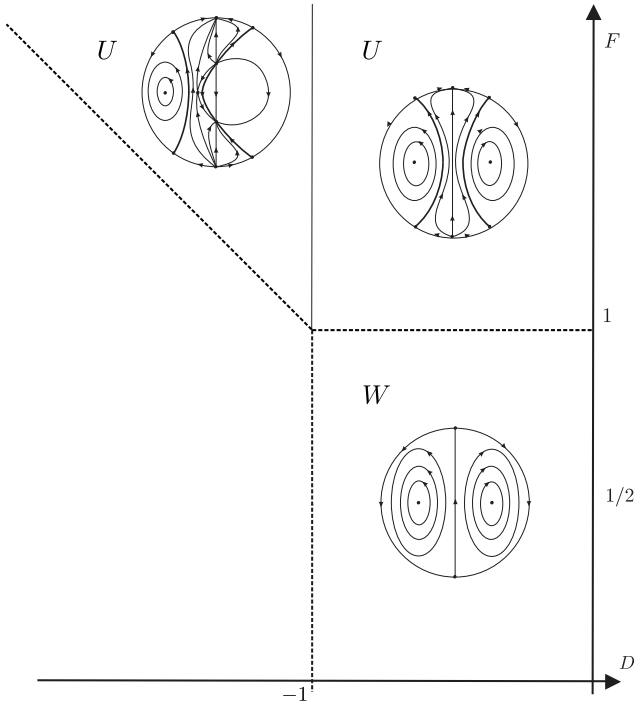

Figure 6.2: Phase portraits in the space of parameters $D - F$ for the regions of interest. Image extracted from [14].

For each of the regions listed above, the parametrization of the period annulus associated to the center at the origin provides one of the conditions needed to study the period function numerically. The period function for a given pair $\mu = (D, F)$ will be computed by discretizing the orbits within the period annulus as described. Notice that the maximum interval of definition of the period function will be $(0, 1)$ for those period annulus extending through all the semi-plane $\{x < 1\}$. Therefore, for a given pair $\mu = (D, F)$ a loop must be performed in order to go across all the orbits in the parametrization. Then, for each of the orbits, a 4th-order Runge-Kutta (see Appendix A for a detailed explanation of the numerical method) with N iterations and a step size h is performed, providing the value of half of the period, taking into account the reversibility of Loud systems. Analogously when the integration of the period function method is used.

6.4 Determining critical periods numerically

The problem of finding critical periods in the period function is equivalent to that of finding where its derivative equals to zero, i.e. the slope of the tangent line is 0. Since the problem is being tackled from the numerical point of view, two different methods for determining the number of critical periods will be stated.

Let T_1, T_2 and T_3 be the values of half of the period for three consecutive periodic orbits in the discretization of the period annulus (taking increasing values from $x = 0$ for the parameter). Then,

- $T_1 > T_2$ and $T_2 < T_3$. Period function has a minimum for that value of the parameter associated to the periodic orbit such that half of its period equals to T_2.
- $T_1 < T_2$ and $T_3 < T_2$. Period function has a maximum for that value of the parameter associated to the periodic orbit such that half of its period equals to T_2.

This method is the simplest one since it takes directly the values for $T(x)$ computed by numerical approach. However, it considers a neighbourhood of the critical period containing just two additional points, i.e. two adjacent periodic orbits in the parametrization of the period annulus. For this reason, this method is extremely sensible to possible numerical fluctuations, which may lead to misreporting critical periods. That is to say, for each value of $\mu = (D, F)$, fluctuations of the value of the period of a given periodic orbit may arise due to numerical errors and hence, erroneous increasing or decreasing regions may be found. Moreover, since the fluctuations' order is unknown *a priori*, a tolerance for declaring a critical period may not be a solution for the problem.

Another approach considered concerns the number of points within the neighbourhood of the critical period. Since the period function is assumed to be as smooth as the vector field X [23] and in this case X is polynomial, it can be assumed that taking a sufficiently refined discretization of the period annulus the conditions below are equivalent to those of a maximum and a minimum. Let T_1, T_2, T_3, T_4 and T_5 be the values of half of the period for five consecutive periodic orbits in the discretization of the period annulus taking increasing values of the parameter. Then,

- If $T_1 > T_2 > T_3$ and $T_3 < T_4 < T_5$, then the period function contains a minimum for that value of the parameter x associated to the periodic orbit such that half of its period equals to T_3.
- If $T_1 < T_2 < T_3$ and $T_3 > T_4 > T_5$, then the period function contains a maximum for that value of the parameter x associated to the periodic orbit such that half of its period equals to T_3.

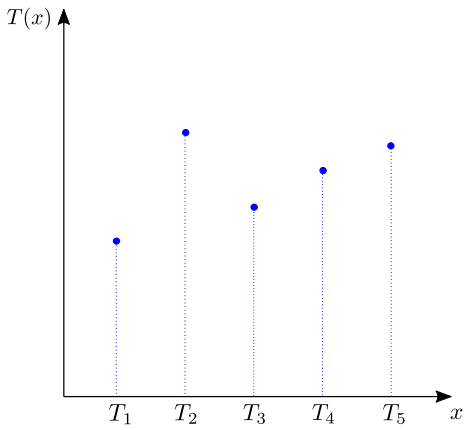

Figure 6.3: Example of erroneous critical periods due to numerical fluctuations. By taking neighbourhoods containing five consecutive orbits with the conditions above, this critical periods are not computed given the smothness of the period function.

By taking neighbourhoods of the critical period containing four additional points, single point fluctuations are directly removed. For instance, consider a subdomain of the period function where it is

monotonous increasing and there is a numerical fluctuation such that $T_1 < T_2$, $T_2 > T_3$, $T_3 < T_4$ and $T_4 < T_5$, where T_1, T_2, T_3, T_4 and T_5 as defined formerly. This case is illustrated in figure 6.3. Then, by using a neighbourhood containing four additional points, this fluctuations will not be computed as a critical period.

On the other hand, and as stated at the beginning of this section, the numerical derivative of the period function may also be used to determine critical periods. An expression using 5 points has been used. Let x_0 be the value of the parameter associated to a periodic orbit within the period annulus for a given parametrization and let h be the step-size of this parametrization. Then, a five-points formula for the numerical derivative is given by [12]:

$$T'(x_0) \approx \frac{T(x_0 - 2h) - 8T(x_0 - h) + 8T(x_0 + h) - T(x_0 + 2h)}{12h}, \tag{6.4.1}$$

with an error of $O(h^4)$, [12]. Notice that five consecutive values of $T(x)$ are needed in order to approximate the derivative using (6.4.1). Therefore, for the first and second orbits and the ultimate and penultimate orbits within the discretization of the period annulus, forward, centered, backward and centered expressions for the derivative will be used, respectively. Their expressions are given by:

$$T'(x_0) \approx \frac{T(x_0 + h) - T(x_0)}{h} \longrightarrow \text{1st orbit (forward difference)}, \tag{6.4.2}$$

$$T'(x_0) \approx \frac{T(x_0 + h) - T(x_0 - h)}{2h} \longrightarrow \text{2nd and penultimate orbits (centered difference)}, \tag{6.4.3}$$

$$T'(x_0) \approx \frac{T(x_0) - T(x_0 - h)}{h} \longrightarrow \text{last orbit (bacward difference)}. \tag{6.4.4}$$

Error of each of the previous expressions is $O(h)$, $O(h^2)$ and $O(h)$ respectively. By determining a change in the sign of the derivative, a critical period can be declared. Let $T_1(x_1)$ and $T_2(x_2)$ be the values of half of the period associated to periodic orbits with parameter values $x_1 < x_2$. Assume $T_1'(x_1) > 0$ and $T_2'(x_2) < 0$. Then, by linear interpolation, the critical period is declared at

$$x_0 = \frac{x_2 + x_1}{2}, \tag{6.4.5}$$

and its value is given by $T(x_0) = (T(x_2) - T(x_1))/2$. Certainly, higher-order interpolation may be used to declare critical periods but, for the sake of simplicity, it is assumed that for a sufficiently refined discretization of the period annulus, the linear interpolation is a good approximation of the critical period.

Chapter 7

Numerical results

Given the reversible property of Loud systems, only half of the period of each orbit within the period annulus will be computed numerically. Following the notation introduced in former sections, it will be denoted by $T(x)$, where x is the parameter associated to a given orbit according to section 6.3. Thus, the period of a periodic orbit within the period annulus of the center at the origin is $P(x) = 2T(x)$. Hereafter, plots and calculus corresponding to periods will display values for $T(x)$.

7.1 $D \in (-1, 0)$, $F \in (0, 1)$

Before studying the numerical bifurcation diagram for region $W \coloneqq \{(D, F) \in \mathbb{R}^2 : D \in (-1, 0) \text{ and } F \in (0, 1)\}$, a particular case will be analysed in order to see how critical periods bifurcate and distinguishing among different bifurcation types.

7.1.1 Bifurcations for a specific case: $D = -0.2$ and $F \in (0, 1)$

The goal is to verify the behaviour of the period function when the value of $F \in \mathbb{R}$ increases within region W, defined in section 6.3. Taking into account the theoretical result provided by figure 5.2a, for $D = -0.2$ three different regions may be distinguished taking increasing values of F: a region where the period function is monotonous, i.e. no critical periods are reported; a region with at least one critical period, conjectured to have exactly one critical period; and another region with zero critical periods. By setting $D = -0.2$ in equation (5.1.1), the boundary point between the first and second region can be found by solving

$$P_C(-0.2, F) = \frac{\pi}{12}\left(4F^2 - 7F + \frac{8}{5}\right) = 0 \iff \begin{cases} F_1 = -\frac{3\sqrt{65}}{40} + \frac{7}{8}, \\ F_2 = \frac{3\sqrt{65}}{40} + \frac{7}{8}, \end{cases} \tag{7.1.1}$$

where P_C is defined in (5.1.1). Since $F_1 < 1$, for $D = -0.2$ the ellipse is reached in $P_1(D, F) = (-0.2, F_1)$. Subsequently, the next boundary -between the second and third region, orange and white regions, respectively, with blue straight line boundary according to figure 5.2a- is reached when $P_2(D, F) = (-0.2, 0.5)$. Figure 5.2a conjectures that, along this domain of parameter F, two bifurcations of the period function arise: the first one when crossing the ellipse, which is a bifurcation at the inner boundary; the second one at $F = 1/2$, where the period function bifurcates at its outer boundary.

Figure 7.1 displays the numerical results of the period function for different values of $\mu = (D, F)$ along line $D = -0.2$. Specifically, values of F around bifurcation values have been chosen in order to verify that the period function undergoes a bifurcation. Results have been obtained integrating

numerically (5.0.3), compactified using coordinates introduced in section 4.2, using a 4th-order Runge-Kutta method for different values of $\mu = (D, F)$ and integrating the period function near the inner boundary. The algorithm used can be found in appendices C and D, corresponding to the use of $\mathbb{RP}^2$ compactification for orbits near the outer boundary and integration of the period function for orbits near the origin, respectively.

Bifurcation at the inner boundary takes place for $F = F_1$, when the period function (taking increasing values of F) is monotonic increasing for $F < F_1$, it bifurcates at $F = F_1$ and a minimum arises near the inner boundary, i.e. the center, which corresponds to values of the parameter near 0. This transition is displayed in the numerical results plotted in figure 7.1a. In here, for $F = 0.28$ the minimum in the period function is greatly shifted to the right despite of $|F_1 - 0.28| \approx 0.0097$. For this reason, a fast shift of the critical period towards the interior of the period annulus is expected. Values plotted have been chosen in order to provide a visual understanding of the bifurcation. However, in order to verify numerically the bifurcation at the inner boundary, some period values for $F^* = 0.2701$ ($|F_1 - F^*| < 10^{-3}$), where the minimum is considerably nearer to the origin, are listed below:

x	$T(x)$
0.00100000	3.14159265
0.02000000	3.14159264
0.09000000	3.14159241
0.10000000	3.14159240
0.12000000	3.14159244

Table 7.1: Minimum in the period function at $x = 0.1$ for $D = -0.2$ and $F = 0.2701$ obtained numerically by integrating the period function as described in section 6.2 and using the algorithm stated in appendix D.

Although not displayed explicitly in table 7.1, $T(x)$ is monotonic decreasing for $x < 0.1$ and monotonic increasing for $x > 0.1$ according to the numerical results obtained.

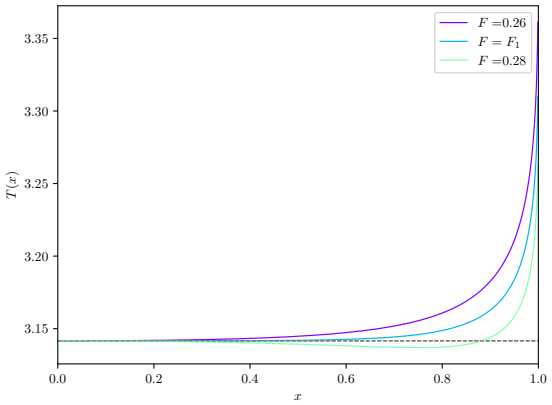

(a) Bifurcation at the inner boundary for $F = F_1$. A critical period arises near the center and it moves rapidly towards the outer boundary. Values of F very close to F_1 are needed in order to, effectively, observe the new critical period near the origin.

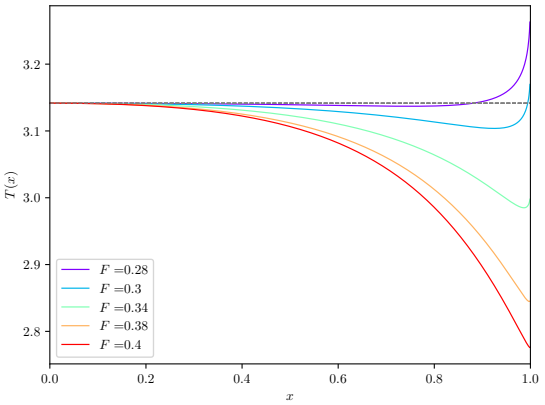

(b) Bifurcation at the outer boundary for $F = 1/2$. Critical period approaches the outer boundary of the period annulus when F value is near the bifurcation value. Visually, for $0.4 < F < 0.5$, the critical period is extremely near $x = 1$ and can not be observed at first sight .

Figure 7.1: Bifurcations arising for $D = -0.2$ when F varies its value from 0 to 1 within region $W = \{(D, F) \in \mathbb{R}^2 : D \in (-1, 0), F \in (0, 1)\}$. Bearing in mind the reversibility of Loud systems, figures above display, for each value of x, the value of half of the period, $T(x)$.

On the other hand, figure 7.1b displays the bifurcation at the outer boundary, i.e. for periodic orbits approaching the invariant line $x = 1$, which is, in this case, part of the outer boundary of the period annulus. Within region $\{(D, F) \in \mathbb{R}^2 : D = -0.2 \text{ and } F \in (F_1, 1/2)\}$, period function contains a minimum shifting between $x = 0$ (bifurcation at $F = F_1$) and $x = 1$ (bifurcation at $F = 1/2$). According to the hypothesis aforementioned, the minimum shifts to the right rapidly for increasing values of F. In fact, for $F = 0.4$, the minimum in the period function is not perceptible in figure 7.1b. For this reason, figure 7.2 displays it by amplifying the region of the parameter near the outer boundary.

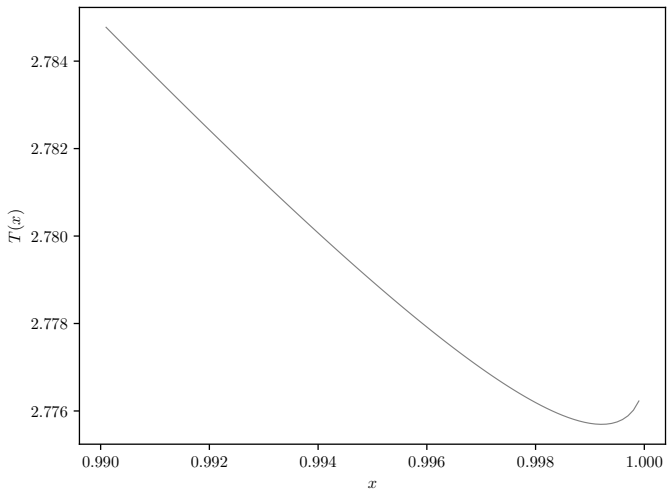

Figure 7.2: $T(x)$ for $D = -0.2$ and $F = 0.4$ in the region near the outer boundary of the period annulus. In this case, the minimum emerges in orbits very close to $x = 1$, i.e. near the polycycle.

Therefore, two different types of bifurcations have been found: those at the inner boundary for critical values of $\mu \in \Gamma_C$ and those at the outer boundary for $F = 1/2$. For increasing values of F between F_1 and $F = 1/2$, a rapid shift of the critical period is observed from the inner boundary to the outer boundary in such a way that it appears very close to the invariant line $x = 1$ even for values of F far from the bifurcation curve.

7.1.2 General case for region W

Figure 7.3 displays the numerical result (figure 7.3a) and the theoretical conjecture in [23] (figure 7.3b) for the number of critical periods for $D \in (-1, 0)$ and $F \in (0, 1)$, i.e. within region W. Period annulus in this region of the parameters space extends through all the semi-plane $\{x < 1\}$ as stated in section 6.3 and, therefore, compactification in $\mathbb{RP}^2$ has been used as explained in section 6.1 in order to avoid periodic orbits escaping to infinity near the outer boundary (algorithm in appendix C). For orbits close to the origin within the period annulus, algorithm in appendix D has been used.

All values of $\mu = (D, F)$ which do not exhibit the same number of critical periods as values around it for regions far from bifurcation boundaries are identified as wrong results due to numerical fluctuations inducing numerical errors. They correspond to light red dots. For some of them, an analysis has been carried out showing critical periods declared from fluctuations of the period function of 10^1 order.

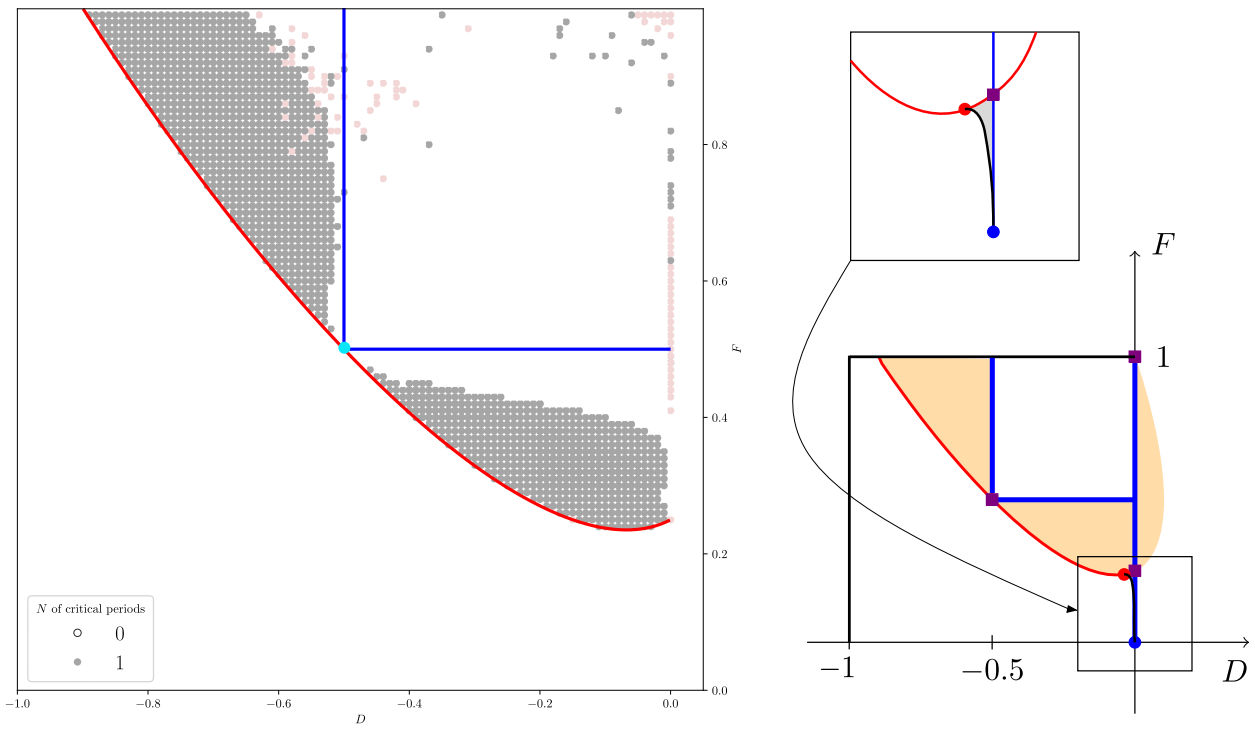

(a) Numerical result for the number of critical periods of the period function within region W. White region displays period functions which are monotonous increasing or decreasing, i.e. they do not contain critical periods; grey region displays values of $\mu = (D, F)$ such that the period function contains a single critical period; and light red points are those for which the numerical methods employed are not able to determine the number of critical periods due to an excessive number of fluctuations in the period function. Boundaries between regions are bifurcations in the period function. Red line displays the ellipse Γ_C and blue lines denote the theoretical boundaries for the bifurcation at the outer boundary of the period annulus. Light blue circle denotes the isochronous center found for $\mu = (D, F) = (-0.5, 0.5)$. The grid used to compute these results numerically contains 100×100 points.

(b) Conjecture for the number of critical periods within region W. Orange, white and grey regions correspond, respectively, to one, zero and two critical periods regions. Blue, red and black curves correspond, respectively, to bifurcations at the outer boundary, inner boundary and the interior of the period function. Violet squares stand for those values of μ such that the center is isochronous, i.e. all periodic orbits within the period annulus have, exactly, the same period. Red and blue points correspond, respectively, to values of μ with criticality 2 at the inner and outer boundary. Image extracted from [23].

Figure 7.3: Number of critical periods within region W.

Focusing in figure 7.3a, due to the computational cost, a grid consisting of 100×100 points has been used by discretizing the parameters space. For each pair $\mu = (D, F)$, a numerical integration using the modified 4th-order Runge-Kutta is performed for each of the orbits in the period annulus following the algorithm described in appendix A.1, which is, in turn, discretized as in section 6.3 with parameter $x \in (0, 1)$. The period annulus has been discretized studying 10000 periodic orbits using an equispaced value of the parameter. At first, it must be noticed that the small grey region conjectured theoretically at the bottom of the ellipse is not observed numerically (figure 7.3b). This region is conjectured to be associated to period functions with exactly two critical periods.

At first sight, remark that the ellipse given by (5.1.1) is probably well-approximated using the numerical approach. This ellipse corresponds to the bifurcation at the inner boundary of the period annulus, i.e. close to the center (value of the parameter $s = 0$). Therefore, numerical methods used are able to detect the appearance of the critical period (a minimum in the period function in this case) when

crossing from the unbounded component of the ellipse Γ_C to the bounded component. Furthermore, this behaviour near the ellipse Γ_C has already been predicted for the particular case $D = -0.2$, where numerical approach is able to detect the bifurcation in the ellipse.

Notice that, according to the numerical result in figure 7.3a, bifurcation at the inner boundary of the period annulus are much better identified than those at the outer boundary, specially for the region $D \in (-0.5, 0)$. This is mainly due to:

- The rapid shift of the critical period from the inner to the outer boundary of the period annulus once the period function undergoes a bifurcation at the inner boundary (taking increasing values of F).
- Proximity of the critical period to the outer boundary for values of F far from the bifurcation line at $F = 0.5$.

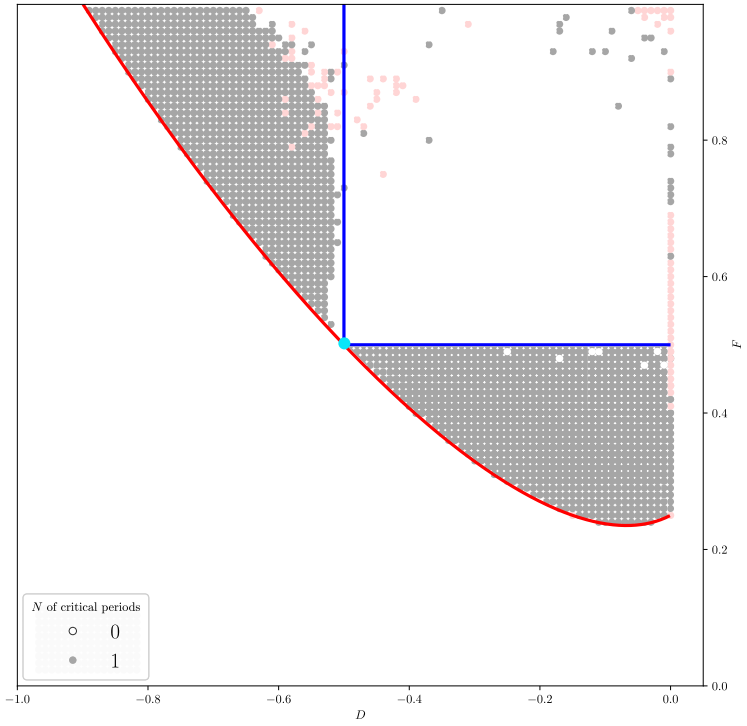

Figure 7.4: Numerical result for the number of critical periods of the period function for $D \in (-1, 0)$ and $F \in (0, 1)$ applying the theoretical result given by theorem 5.1.3 in the region $-1/2 < D < 0$ and $F < 1/2$. The meaning of each curve is exactly the one given in the caption of figure 7.3a.

However, the analytical result given in theorem 5.1.3 describing the behaviour of the period function near the outer boundary for $\mu \in W$ provides a method in order to improve results in figure 7.3a. Period function for $-1/2 < D < 0$ and $F < 1/2$ near the bifurcation boundary $F = 1/2$ is expected to be monotonous increasing near the outer boundary, i.e. there exists a neighbourhood of parameter $x = 1$ (by definition of the period function this set only contains points such that $x < 1$) such that the period function is monotonous increasing. Numerically, a slight modification will be introduced to the algorithm in appendix C: if the period function is monotonous decreasing for the last five orbits within the discretization of the period annulus, an additional minimum will be computed according to the result in theorem 5.1.3. In this situation, the minimum is so close to the outer boundary that the

discretization of the period annulus chosen is not able to identify the orbit with the minimum period. Applying it, the result obtained is displayed in figure 7.4.

Comparing both figure 7.3a and figure 7.4, the modification introduced in the algorithm by using the analytical result induces a much better approximation to the theoretical result in figure 7.3b. The difference means that, within region $-1/2 < D < 0$, $F < 1/2$ and close to $F = 1/2$, for all those values of $\mu = (D, F)$ associated to 0 critical periods in figure 7.3a, the period function near the outer boundary is monotonous decreasing while it should be monotonous increasing according to theorem 5.1.3. Again, in this region the only critical period, which is a minimum, is greatly shifted to the outer boundary and a highly refined discretization of the period annulus is needed in order to detect it. Since it is not feasible due to the computational cost, the modification introduced, combining both numerical and analytical techniques provides a result verifying the theoretical prediction.

7.2 $D \in (-2, -1.4)$, $F \in (2, 2.5)$

Within this region, the period annulus does not extend through the whole semi-plane $x < 1$ as stated in section 6.3. According to the parametrization of the period annulus for this region, from the center, and taking increasing values of parameter x, the period annulus extends through the interval $(0, p)$, where p is given by equation (6.3.2). Then, $x = 0$ is the center itself, i.e. the inner boundary of the period annulus and $x = p$ is part of the polycycle acting as outer boundary.

According to figure 5.2a, semi-plane $F > 2$ is bounded in $-2 < D < 0$ by $F = 2$, corresponding to a bifurcation of the period function at the outer boundary of the period annulus. In fact, this segment is the union of different segments and some particular points such as isochronous points. For values of $D < -2$, there is no conjectured boundary since for all values of F, the conjecture says that period function has no critical periods and it is monotonous increasing.

Ellipse (5.1.1) intersects horizontal line $F = 2$ at two different points that will be denoted as D_r and D_l, standing for right and left points such that $D_l < D_r$. From equation (5.1.1),

$$\frac{\pi}{12}(10D^2 + 19D + 7) = 0 \iff \begin{cases} D_l = -7/5 \\ D_r = -1/2 \end{cases} \tag{7.2.1}$$

Focusing on the conjectured region with two critical periods, its lower boundary is the segment $-2 < D < D_l$. The union of this segment with the ellipse Γ_C, points v and L_1 defined at the end of section 5.1 and the unknown curve joining both of them constitute the boundary of the region.

7.2.1 Bifurcations for specific cases

At first, the period function for three different values of $\mu = (D, F)$ within this region will be studied in order to see whether the numerical approximation is able to find two critical periods in this region. The values chosen are:

$$\begin{aligned} \mu_1 &= (D_1, F_1) = (-1.47, 2.05), \\ \mu_2 &= (D_2, F_2) = (-1.52, 2.10), \\ \mu_3 &= (D_3, F_3) = (-1.47, 2.15). \end{aligned}$$

Remark that these values have been chosen arbitrarily. They are displayed in figure 7.5.

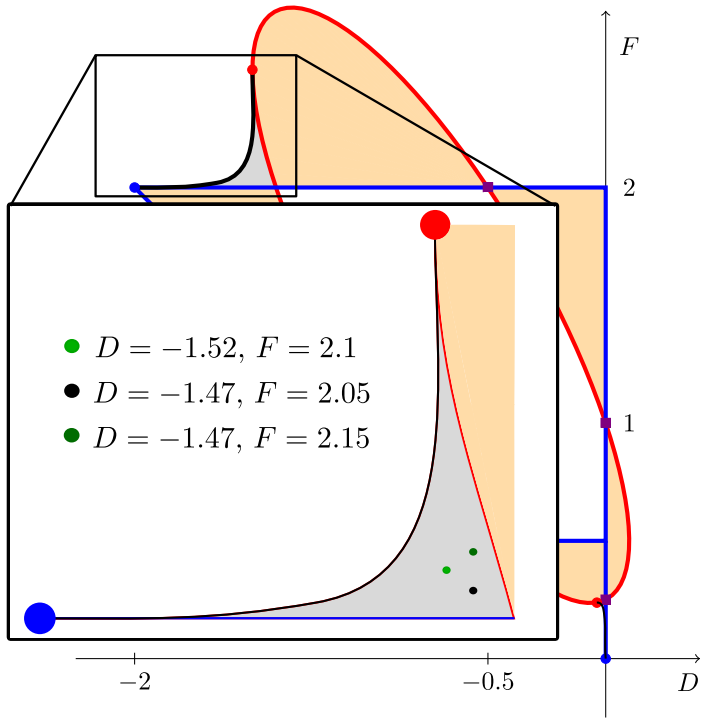

Figure 7.5: Conjectured region for those values of $\mu = (D, F)$ such that the period function of the center at the origin contains, exactly, two critical periods. Light green, dark green and black dots denote particular cases whose period function has been analysed numerically. Red and blue circles denote, respectively, values of $\mu = (D, F)$ with criticality 2 at the inner and outer boundaries, respectively. The meaning of each curve is the same as the one stated in figure 5.2a. Figure has been created using figure 5.2a extracted from [23].

In this region, the period annulus escapes to infinity in x, y-coordinates and it is bounded by invariant curve $g_2(x, y) = 0$. Numerically, the integration of the period function has been the method used to find the period for orbits near the origin (section 6.2) and the compactification stated in section 6.1 for the rest of the orbits within the period annulus (see appendices D and C, respectively) . For the discretization of the orbits of the period annulus, a total number of $N = 10000$ orbits with equally spaced parameter have been chosen.

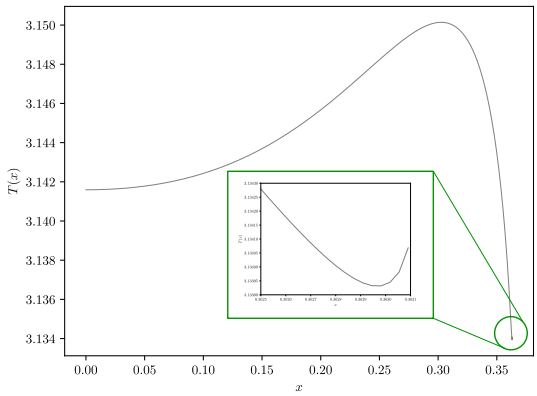

(a) $T(x)$ for $D = -1.47$ and $F = 2.05$.

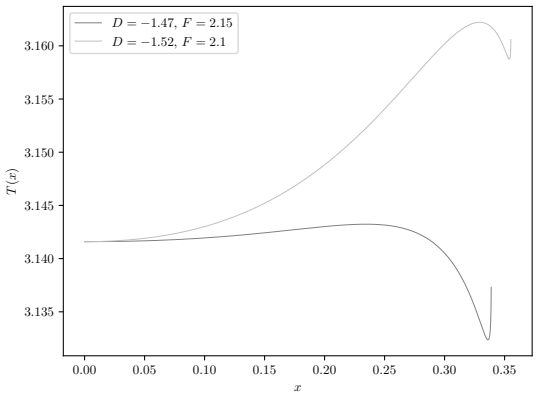

(b) $T(x)$ for $D = -1.52$ and $F = 2.1$ and $D = -1.47$ and $F = 2.15$.

Figure 7.6: Period function obtained numerically using algorithms described in appendices C and D for three different values of parameter $\mu = (D, F)$ in figure 7.5.

Figure 7.6 displays the period function obtained for values of μ_1, μ_2 and μ_3. At first sight, indeed, the three of them show exactly two critical periods as conjectured theoretically: a maximum and a minimum near the outer boundary of the period annulus. For μ_1, the minimum is greatly shifted to the outer boundary of the period annulus since μ_1 is near the bifurcation line at the outer boundary given by $F = 2$. Figure 7.6a displays the region near the outer boundary amplified where the second critical period arises.

Figure 7.6b displays the period function for $T(x)$ for values μ_2 and μ_3. Value μ_3 is the nearest one to the bifurcation curve at the inner boundary given by ellipse Γ_C. For this reason, the maximum of the period function is the one closer to the origin. Exactly as observed in the previous section, a fast shift of the critical period arising in the bifurcation curve at the inner boundary towards the outer boundary is identified. That is to say, moving away from the bifurcation curve induces a rapid movement of the position of the critical period. Moreover, the maximum gets flatter when approaching the ellipse. On the other hand, comparing the period function for μ_3 and μ_1, the nearest critical period to the outer boundary is further from the outer boundary of the period annulus for μ_3 since μ_1 is closer to the bifurcation at the outer boundary.

Finally, for μ_2, both critical periods can be easily seen graphically since this value of the parameter is far enough away from any bifurcation curve. The maximum arising from a bifurcation at the inner boundary is already shifted to the outer boundary of the period function.

With a view to understand the bifurcation at the interior of the period annulus predicted by the black curve in figure 7.5, two additional specific values of $\mu = (D, F)$ have been studied. Setting the value of $F = 2.18$ constant and changing the value of D along the interval $(-2, -1.4)$, the bifurcation at the inner boundary can be easily observed. Figure 7.7 displays the period function for $T(x)$ for the limit values of D: $D = -1.53$ is within the region containing two critical periods (figure 7.7a) and for $D = -1.54$, $T(x)$ does not contain any critical period (figure 7.7b).

When $\mu = (D, F)$ approaches the bifurcation curve at the interior of the period annulus from within the region with two critical periods, both the maximum and the minimum get closer and they collide

exactly at the bifurcation curve annihilating each other in such a way that the period function becomes monotonous increasing.

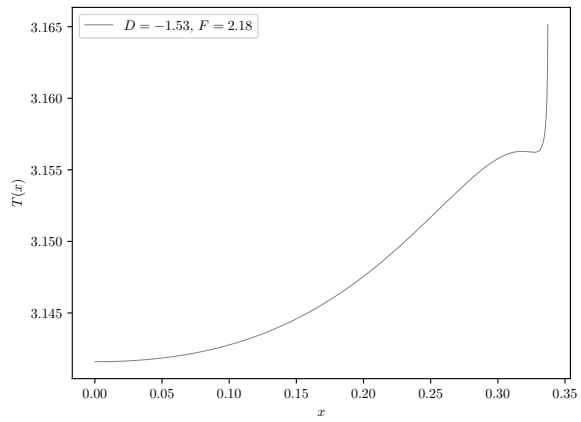

(a) $T(x)$ for $D = -1.53$ and $F = 2.18$.

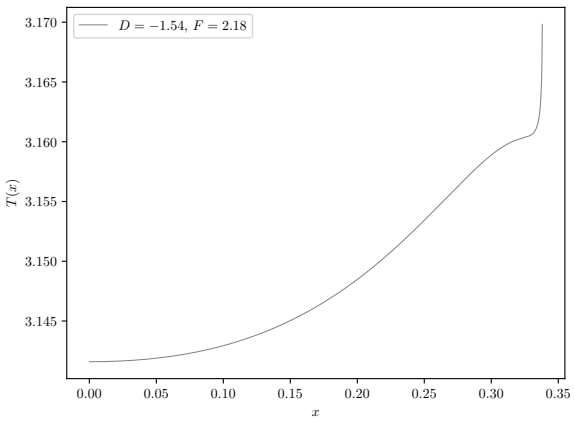

(b) $T(x)$ for $D = -1.54$ and $F = 2.18$.

Figure 7.7: Bifurcation at the inner boundary of the period annulus in the region $D \in (-2, -1.4)$ and $F \in (2, 2.5)$. Transition from $D = -1.53$ to $D = -1.54$ fixing the value of $F = 2.18$ implies crossing the black bifurcation curve conjectured in [23].

7.2.2 General case for region $D \in (-2, -1.4)$, $F \in (2, 2.5)$

Once some particular cases have been studied and the bifurcation at the interior of the period annulus has been analysed for a particular case of parameter $\mu = (D, F)$, this section aims to assess whether the numerical approximation is sufficiently accurate compared to the theoretical prediction. For this purpose, and using algorithms in appendices C and D to study the period function near the outer boundary and the inner boundary, respectively, the number of critical periods is computed for values of $\mu = (D, F)$ in the following region

$$Z = \{\mu = (D, F) \in \mathbb{R}^2 : D \in (-2, -1.4) \text{ and } F \in (2, 2.5)\}. \tag{7.2.2}$$

The grid used to discretize the space of parameters contains 60×50 values of μ and, for each of them, the period annulus has been discretized according to section 6.3 using 10^4 orbits. Figure 7.8 displays the number of critical periods within region Z for two different methods used. Both in figure 7.8a and 7.8b, bounded region enclosed by red, blue and black curves displays a region where it is proved that the period function contains, at least, two critical periods. This result can be found together with its proof in theorem 5.2 from [14]. In accordance with the notation introduced in section 5.1, red curve denotes ellipse Γ_C, and black curve is given by Γ_0 in (5.1.12).

Figure 7.8a shows the results obtained by executing algorithms in appendices C and D. At first sight, the following regions may be distinguished:

A_1 Large region containing zero critical periods, i.e. for these values of μ the period function of the center at the origin is monotonous. In fact, it is monotonous increasing.

A_2 A well-bounded region by ellipse Γ_C and straight line $D = -1.4$ containing, exactly, one critical period. Values of $\mu = (D, F)$ within this region and associated to two critical periods, after an

exhaustive analysis have been discarded as acceptable results since the additional critical period declared was due to a fluctuation in the period function breaking its smoothness.

A_3 Black region associated to period functions with two critical periods bounded by ellipse Γ_C and a small subregion containing one critical period.

A_4 Small region between black region and $F = 2$ containing, exactly, one critical period. This region is close to the bifurcation at the outer boundary and it is not predicted in the theoretical bifurcation diagram.

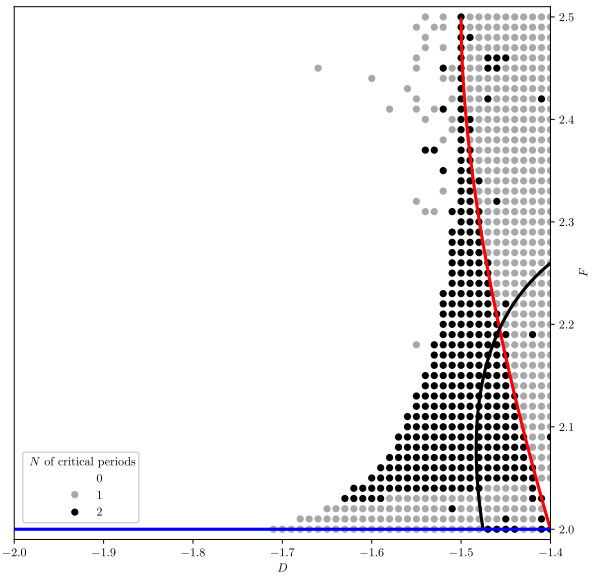

(a) Number of critical periods obtained without modifications. Since blue straight line displays a bifurcation at the outer boundary of the period annulus, a critical period arises very close to it and can not be detected numerically. For this reason, there exists a region for $F > 2$ near $F = 2$ such that only a critical period is found.

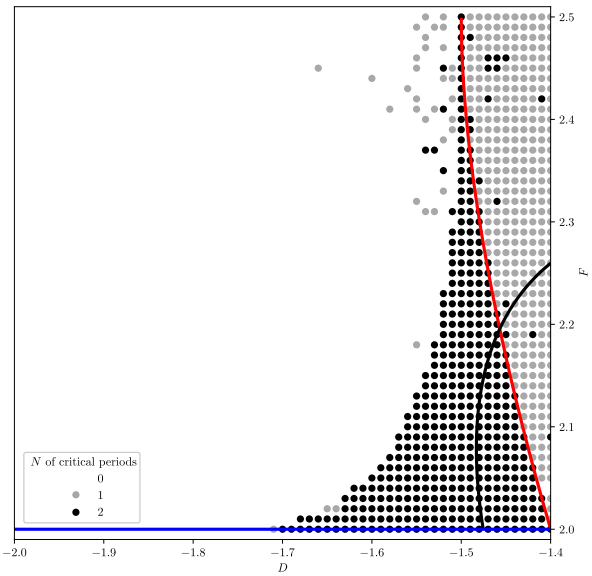

(b) Number of critical periods obtained when applying corrections by virtue of the fact that the period function is monotonous increasing near the outer boundary of the period annulus for $F > 2$. Values of μ near $F = 2$ that were classified as parameter values with only one critical period in figure 7.8a, now are classified as values with two critical periods due to the numerical-analytical method used.

Figure 7.8: Numerical result for the number of critical periods for the region $D \in [-2, -1.4]$ and $F \in [2, 2.5]$, where there exists a conjectured subregion whose period function contains, exactly, two critical periods. White, light grey and black regions stand for those values of $\mu = (D, F)$ such that the period function of the center contains, respectively, 0, 1 and 2 critical periods. Red line displays the ellipse Γ_C. Boundaries between regions are bifurcations in the period functions, i.e. in the number of critical periods: red curve stands for bifurcations at the inner boundary of the period annulus and blue line stands for bifurcations at the outer boundary. Black curve corresponds to Γ_0. The grid used contains 60×50 points and a discretization of 10000 orbits of the period annulus has been chosen.

Focusing on region A_4, it, indeed, does not exist. Its proximity to the bifurcation line at $F = 2$, which stands for a bifurcation at the outer boundary of the period annulus, implies the existence of a critical period sharply shifted towards the outer boundary, as it is the case studied in figure 7.6a. Thus, numerically it can not be identified with the discretization of the period annulus chosen.

However, bearing in mind the result in theorem 5.1.5, where it is proved analytically that there exists a neighbourhood of the outer boundary of the period annulus for which the period function is monotonous increasing, one may improve the results obtained in figure 7.8a. Consider all those values of $\mu \in Z$ such that the last two orbits in the discretization of the period annulus, associtaed to parameters x_{n-1} and x_n, have a value of $T(x)$ such that $T(x_{n-1}) > T(x_n)$, i.e. the period function is decreasing near the outer boundary. Therefore, in this situation, an additional critical period will be computed for the period function although not being detected numerically considering the result aforementioned. The outcome is displayed in figure 7.8b.

In this case, the region with exactly one critical period completely disappears and it integrates within the region containing exactly two critical periods. Remark that, theoretically, it has only been proven that this region contains at least two critical periods, however, there is conjecture that it in fact contains exactly two critical periods [23]. Given the results obtained numerically, this conjecture is reinforced although region boundaries may not be predictable due to the discretization of the space of parameters.

Black dots within region A_2 are mainly distributed near the boundary Γ_C. Indeed, since Γ_C corresponds to a bifurcation at the inner boundary, fluctuations are more likely to appear near boundaries than far from them. Numerically, period of the orbits near the origin is more sensitive to fluctuations since the integration interval gets narrower and composite Simpson's rule is $\mathcal{O}(h^4)$, where h is the step size.

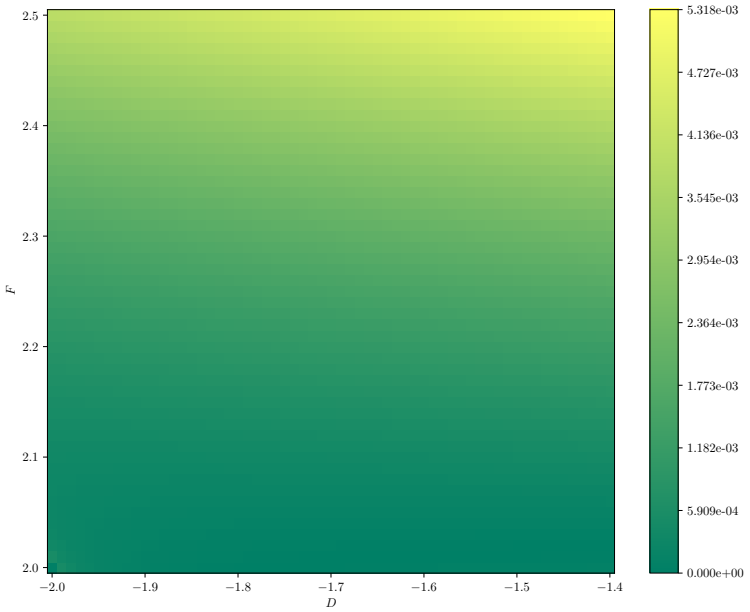

Figure 7.9: Relative error of the period near the outer boundary of the period annulus for $\mu = (D, F) \in Z$.

Finally, using the grid above, it is not observed that boundary between regions A_1 and A_3 is tangent to $F = 2$ at $v = (-2, 2)$, result which is analytically proven in [23]. Due to the computational cost of getting a finer grid, only a slight intuition of this tangency can be found. On the other hand, boundary bifurcation curve starting at $L_1 = (-3/2, 5/2)$ is not numerically detectable due to both the resolution of the grid and the proximity between bifurcation curves, which induces a lot of noise in the numerical results.

The final numerical test performed in this region consists in comparing the period of the last orbit in the discretization of the period annulus with the theoretical vale for each $\mu \in Z$. This limit value is given by equation (5.1.11). Relative error between numerical and theoretical value has been computed and figure 7.9 displays in a heat map the magnitude of this error.

The largest error obtained is in the order of 10^{-3}, i.e. difference with the theoretical value is lower than 1%. Notice that the smallest errors are given for those values of $\mu \in Z$ near $F = 2$, where the period function undergoes a bifurcation at the outer boundary. Notice that were precisely these values of μ those such that the bifurcation was more difficult to be identified numerically due to the proximity of the critical period to the outer boundary. This situation may be explained by the fact that the difference between the last period before the critical period and the actual value of the period near the outer boundary may differ in a relative error in the order of 10^{-4}, i.e. after reaching the critical period, period function increases just in a magnitude of 10^{-4}.

7.3 $D \in (-3/2, -1)$, $F \in (1, 1.5)$ and $F + D > 0$

This section aims to study the third and last region of the space of parameters containing at least two critical periods in accordance with the theoretical results from [14]. It focuses in the triangular region given by

$$Z_2 = \left\{\mu = (D, F) \in \mathbb{R}^2 : D \in (-3/2, -1), F \in (1, 3/2) \text{ and } F + D > 0\right\}, \tag{7.3.1}$$

where there exists a region containing, at least, two critical periods (theorem 5.2 in [14]). Period annulus for $\mu \in Z_2$ is bounded by invariant curve $g_2(x, y) = 0$ and extends towards decreasing values of x until the infinity. Therefore, in order to study the period function for a given value of $\mu \in Z_2$, the parametrization in section 6.2 for region U will be chosen.

Within Z_2, curves Γ_C, Γ_0 and Γ_1, defined, respectively, by equations (5.1.1), (5.1.12) and (5.1.14), intersect each other and the bounded area enclosed by them is a subregion which contains, at least, two critical periods. Paper [23] conjectures that, in fact, this region may be extended and this extension contains exactly two critical periods.

At first, an execution has been carried out in order to determine the number of critical periods within triangle Z_2. The result is displayed in figure 7.10. The resolution of the grid used, with step-size in each dimension equal to 0.01, is not enough to discern a region containing two critical periods. However, there exists a value of $\mu = (D, F)$ near the bounded area enclosed by the intersection of curves Γ_C, Γ_0 and Γ_1 such that two critical periods are found. Notice that boundary Γ_1 does not fit exactly the numerical boundary provided by the number of critical periods. This is mainly due to the numerical errors arising from the computation of this curve. Its expression is given by (5.1.14), i.e. this curve is the zero level of expression $\Delta_1(\mu)$ given by (5.1.9), which is defined by a definite integral. In order to compute it, for each value of $\mu = (D, F)$, the integral has been calculated numerically using the composite Simpson's rule, which introduced a source of error that induces the use of a tolerance in order to define the zero level of $\Delta_1(\mu) = 0$.

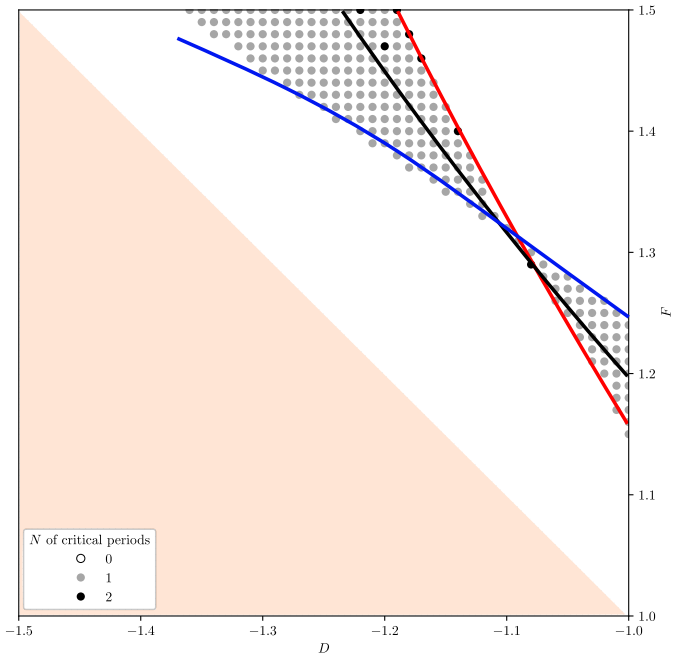

Figure 7.10: Numerical result for the number of critical periods for the region $D \in [-1.5, -1]$, $F \in [1, 1.5]$ and $F + D > 0$, where there exists a conjectured subregion whose period function contains, exactly, two critical periods.

In order to enhance the comprehension of the theoretically predicted region containing two critical periods, computations have focused on the bounded region enclosed by the intersection of curves Γ_C, Γ_1 and Γ_0. For this purpose, region

$$Z_3 = \{\mu = (D, F) \in \mathbb{R}^2 : D \in [-1.14, -1.07] \text{ and } F \in [1.27, 1.34]\} \tag{7.3.2}$$

has been studied using a discretization of the space of parameters with step-size 0.001, i.e. making the grid finer comparing to the former case. This change has led to a considerable increase in computing time but still assumable. In figure 7.11, the number of segments used to integrate numerically the definite integral in the expression of Γ_1 has increased in order to get a higher accuracy. Result obtained with this new changes is displayed in figure 7.11a.

Now, a region containing two critical periods arises in the bounded area enclosed by Γ_C, Γ_1 and Γ_0, which is proven that contains, at least, two critical periods. However, some values, displayed in light red dots within this region, are points such that the numerical computation of the number of critical periods could not be ascertained due to numerical fluctuations in the value of the period. Moreover, as conjectured in [23], this region extends beyond Γ_0 and a boundary curve separating the black region and the region of monotonous period functions appears more clearly as in figure 5.2a. Remark that the analytical expression of this curve is still unknown. Only the initial and final points are computed and the tangency of the curve to these points is also proven [23]. Thus, the numerical result obtained reinforces the conjecture of the existence of this curve, tangent to Γ_C and Γ_1, delimiting a region with two critical periods. Furthermore, bifurcations at the inner and outer boundaries are well-identified despite the errors in the number of critical periods increases near them.

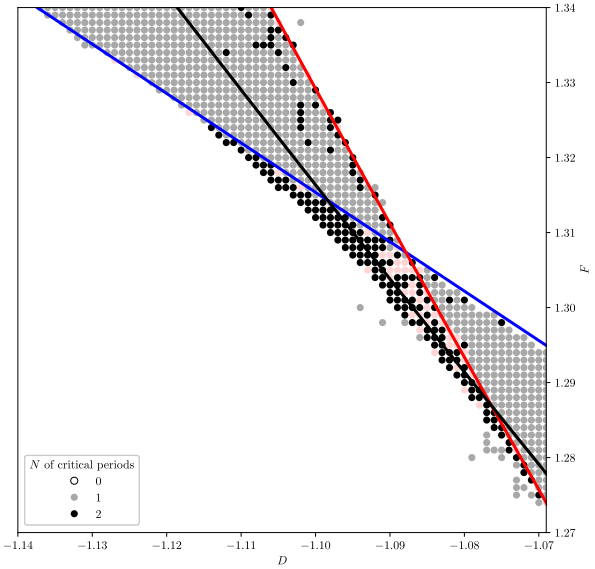

(a) Number of critical periods using only numerical methods to find them.

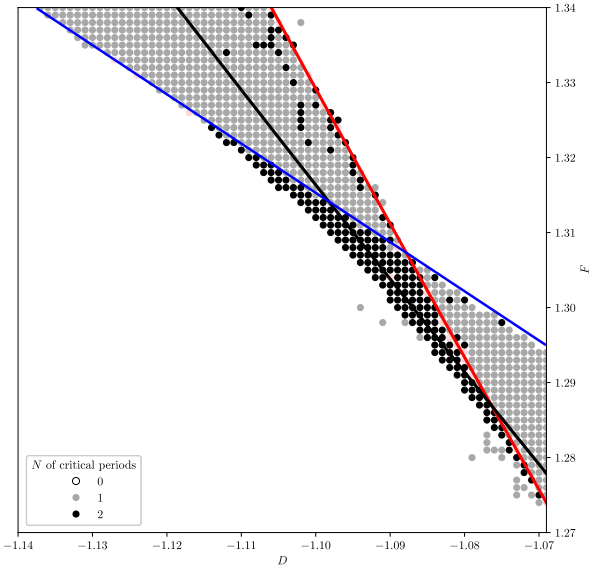

(b) Number of critical periods using both numerical methods and some theoretical results to find them.

Figure 7.11: Number of critical periods of the period function obtained numerically focused on the region where three different curves intersect each other. Red, blue and black curves denote, respectively, curves Γ_C, Γ_1 and Γ_0, described in equations (5.1.1), (5.1.14) and (5.1.12). Red and blue curves stand for bifurcations at the inner and outer boundary of the period annulus, respectively. Light red dots stand for those values of $\mu = (D, F)$ for which the number of critical periods could not be computed.

In order to overcome some of the errors generated by fluctuations in the period function as shown in figure 7.11a, the result given by theorem 5.1.5, concerning to the monotonicity of the period function near the outer boundary, will be used to determine the number of critical periods. For this purpose, algorithm in appendix C will be modified in such a way that, if the period function near the outer boundary exhibits the opposite monotonicity as the predicted in theorem 5.1.5 for each value of $\mu = (D, F)$, an additional critical point will be added or removed. Notice that, within the region studied and according to figure 5.3, there is a region with increasing period function near the outer boundary and another one decreasing, separated by Γ_1. In order to classify μ values between these two regions, the asymptotic expansion of the period function given by theorem 5.1.4 will be used. Let

$$P(s; \mu) = \Delta_0(\mu) + \Delta_1(\mu)s + sf_1(s; \mu),$$

where $f_1 \in \mathcal{I}(U_1)$ and the rest of the terms as defined in the statement of the theorem. Deriving with respect to parameter s,

$$\frac{dP(s;\mu)}{ds} = P'(s;\mu) = \Delta_1(\mu) + f_1(s;\mu) + s\frac{\partial f_1(s;\mu)}{\partial s} \xrightarrow[s\to 0]{} \Delta_1(\mu).$$

In the last equality, definition 5.1.1 and the fact that parameter s near the outer boundary is $s \approx 0$, have been applied. Therefore, the sign of the derivative provides the monotonicity of the period function near the outer boundary for a given value of $\mu = (D, F)$.

The result obtained applying this modification is displayed in figure 7.11b. Region containing exactly two critical periods is far better delimited than in the previous case reinforcing the conjecture of having, at most two critical periods, since those values that could not be determined before, now are

computed within region with two critical periods. Moreover, the bounded area enclosed by Γ_C, Γ_0 and Γ_1 is far better defined as a region with exactly two critical periods, removing the error points in the former case. Since generating figure 7.11b has required a higher number of computations, the computational cost of obtaining this results has increased considerably.

Numerical results in figure 7.11b show that curve separating regions with zero and two critical periods may reach Γ_1 and Γ_C tangentially, as it is proven analytically. Although the resolution used to discretize the space of parameters does not allow to assert, indeed, this tangency, there exists evidence of it. For this reason, we could conjecture that this region containing two critical periods will be delimited by Γ_C, Γ_1 and an unknown curve tangent to the previous ones following, approximately, the boundary obtained numerically.

Chapter 8

Conclusions

Once all the study has been carried out and all the topics that wanted to be covered have been analysed, the aim of this section is to summarise and outline the most important results obtained and the principal conclusions that can be drawn. For this purpose, and consistently with the order used in this thesis, the most remarkable facts will be enumerated.

One of the main objectives that this thesis tried to achieve was to evaluate the scope of the numerical approach in studying the bifurcation diagram of the period function associated to the center at the origin in Loud systems. Using numerical techniques and some results already proven analytically, the goal was to reproduce the different regions and bifurcation curves stated and conjectured in former works. For the latter case, providing solid evidence of formulated conjectures has been of major importance in such a way that it has constituted a step forward in the study of this period function. The main conclusions are listed below.

a) The use of compactifications in order to study the period of periodic orbits within the period annulus of the center escaping towards the infinity allows numerical integration in a bounded region. Therefore, both the computational cost and numerical errors reduce due to the absence of overflow errors. In this way, compactifications reveal themselves to be a powerful tool to study non-bounded period annulus, which has been the case for all the regions in the space of parameters analysed.

b) While compactifications enhance the study of periodic orbits near infinity, integrating directly the differential equation in x, y-coordinates to obtain the period function provides a higher accuracy in the period for periodic orbits near the origin. This fact implies less fluctuations in the period function for values of the parameter near the inner boundary of the period annulus. Thus, combination of both methods -using 4th-order Runge-Kutta methods in the compactified space and integrating the period function- are shown to be the ones achieving results with the highest accuracy. The exhaustive comparison between methods has not been developed in this thesis since it escaped the main objectives.

c) The existence of a first integral defined in the period annulus of the center at the origin provides very useful information for the study of the phase portrait. For instance, invariant algebraic curves have been identified from the expression of the first integral and some bifurcation curves depend on coefficients extracted from the expression of the first integral.

d) Three different types of bifurcations have been identified as mechanisms to create or destroy critical periods within the period function: bifurcations at the inner boundary, bifurcations at the outer boundary and bifurcations at the interior. For all of them, particular cases have been

studied and graphs of the period function displayed to observe how critical periods were created or annihilated. Moreover, bifurcations at the interior of the period annulus have been identified to be possible only as a mechanism of transition between two critical periods and zero critical periods (or conversely). That is to say, a single critical period may not arise or disappear by means of a bifurcation at the interior of the period annulus. Bifurcations at the inner boundary are easily detected due to a rapid shift of the critical period towards the interior of the period annulus while bifurcations at the outer boundary are more difficult to find due to the proximity of the critical period to the outer boundary even when far from the bifurcation curve.

e) For region $W = \big\{(D, F) \in \mathbb{R}^2 : D \in (-1, 0), F \in (0, 1)\big\}$, bifurcations at the inner boundary have been reasonably well identified as well as the bifurcation curve, which is associated to ellipse Γ_C. The resolution used for the grid is able to determine this boundary between regions. This is not the case of bifurcations at the outer boundary, where the problem has found to be more complicated due to the proximity of a critical period to the outer boundary, which makes it more difficult to be detected. Numerical approach has not been able to identify a conjectured region with two critical periods: making finer the discretization of the period annulus increases fluctuations and, therefore, inaccuracy when declaring critical periods. Regions identified contained, exactly, zero or one critical period, reinforcing Chicone's conjecture.

f) Within region $Z = \{\mu = (D, F) \in \mathbb{R}^2 : D \in (-2, -1.4)$ and $F \in (2, 2.5)\}$, a region containing exactly two critical periods and bounded by ellipse Γ_C, $F = 2$ and an unknown curve has been identified providing solid evidence to the conjecture formulated within this area. The three different types of bifurcations have been identified and collision of critical points annihilating each other has been found to be the mechanism of bifurcations in the interior of the period annulus. A critical period near $F = 2$ has been identified to be very close to the outer boundary and, thus, difficult to find numerically. Numerical noise has been detected in the confluence region of the ellipse Γ_C and the unknown bifurcation curve at the interior due to the proximity of bifurcations. Furthermore, numerical approach has revealed to be appropriate in predicting the value of the period near the outer boundary of the period annulus, with relative errors of magnitude 10^{-3} or lower.

g) Numerical methods have reproduced with acceptable accuracy the number of critical periods within region $\big\{\mu = (D, F) \in \mathbb{R}^2 : D \in (-3/2, -1)$ and $F \in (-D, 3/2)\big\}$. As in region Z, numerical results provide solid evidence of the existence of a region such that the period function contains, exactly, two critical periods. Although the exact boundaries are difficult to determine due to fluctuations near bifurcation curves, boundaries given by Γ_C and Γ_1 are well-determined while the bifurcation curve at the inner boundary seems reasonably tangent to both of them.

h) Combination of both numerical and analytical results allows an improvement in the numerical results standing for the number of critical periods for a given value of $\mu = (D, F)$. Results stating the monotonicity of the period function near the outer boundary enable the detection of additional critical periods. Thus, a mixed approach to the problem increases the accuracy of the results.

i) The computational cost has been found to be assumable for the regions studied, the resolution of the grid chosen and the computing power used. However, reducing one order of magnitude the step-size in the grid of the space of parameters implied unaffordable computing times. Thus, it must be concluded that the resolution studied for the discretization of the space of parameters is the highest that could be studied.

For the case of the parametrization of the period annulus, a balance between the computational cost and the accuracy has been found. Increasing the number of orbits studied within the period annulus does not necessarily imply a better accuracy in the period obtained. Specially near the inner boundary, fluctuations arise when increasing the resolution of the parametrization of the period annulus due to numerical errors induced by numerical integration. This fact is extremely important when computing the number of critical periods since fluctuations may induce wrong critical periods. Moreover, these wrong critical periods have been identified as such based on the smoothness of the period function.

Hence, this thesis has been able to reproduce numerically with acceptable accuracy the bifurcation diagram of the period function of the center at the origin in Loud systems. Although not providing new results related to the regions which are still under study, evidence about some conjectures has been provided from a numerical point of view.

Bibliography

[1] M. Abramowitz and I.A. Stegun. *Handbook of Mathematical Functions: With Formulas, Graphs, and Mathematical Tables*. Applied mathematics series. Dover Publications, 1965. ISBN: 9780486612720. URL: https://books.google.es/books?id=MtU8uP7XMvoC.

[2] Jörg Waldvogel. "The period in the Lotka-Volterra system is monotonic". In: *Journal of Mathematical Analysis and Applications* 114.1 (1986), pp. 178–184. ISSN: 0022-247X. DOI: https://doi.org/10.1016/0022-247X(86)90076-4. URL: https://www.sciencedirect.com/science/article/pii/0022247X86900764.

[3] Luisa Mazzi and Marco Sabatini. "A CHARACTERIZATION OF CENTRES VIA FIRST INTEGRALS". In: *Journal of Differential Equations* 76 (1988), pp. 222–237.

[4] Carmen Chicone and Marc Jacobs. "Bifurcation of Critical Periods for Plane Vector Fields". In: *Transactions of the American Mathematical Society* 312.2 (1989), pp. 433–486. ISSN: 00029947. URL: http://www.jstor.org/stable/2000999 (visited on 08/02/2023).

[5] D.K. Arrowsmith and C.M. Place. *Dynamical Systems: Differential Equations, Maps, and Chaotic Behaviour*. Chapman & Hall mathematics. Chapman & Hall, 1992. ISBN: 9780412390708. URL: https://books.google.es/books?id=nHWzQgAACAAJ.

[6] H. Zoladek. "Quadratic Systems with Center and Their Perturbations". In: *Journal of Differential Equations* 109.2 (1994), pp. 223–273. ISSN: 0022-0396. DOI: https://doi.org/10.1006/jdeq.1994.1049. URL: https://www.sciencedirect.com/science/article/pii/S0022039684710497.

[7] Grzegorz Świrszcz. "Cyclicity of Infinite Contour around Certain Reversible Quadratic Center". In: *Journal of Differential Equations* 154.2 (1999), pp. 239–266. ISSN: 0022-0396. DOI: https://doi.org/10.1006/jdeq.1998.3538. URL: https://www.sciencedirect.com/science/article/pii/S0022039698935380.

[8] Jordi Villadelprat Yagüe. "Index of vector fields on manifolds and isochronicity for planar hamiltonian differential systems". In: 1999.

[9] Yulin Zhao. "The Monotonicity of Period Function for Codimension Four Quadratic System Q4". In: *Journal of Differential Equations* 185.1 (2002), pp. 370–387. ISSN: 0022-0396. DOI: https://doi.org/10.1006/jdeq.2002.4175. URL: https://www.sciencedirect.com/science/article/pii/S0022039602941756.

[10] Pavao Mardesic, David Marin, and Jordi Villadelprat. "On the time function of the Dulac map for families of meromorphic vector fields". In: *Nonlinearity* 16 (Mar. 2003), p. 855. DOI: 10.1088/0951-7715/16/3/305.

[11] Armengol Gasull, Toni Grabolosa, and Jordi Villadelprat. "The period function for second-order quadratic ODEs is monotone". In: *Qualitative Theory of Dynamical Systems* 4 (Sept. 2004), pp. 329–352. DOI: 10.1007/BF02970864.

[12] W.Y. Yang et al. *Applied Numerical Methods Using MATLAB*. Wiley, 2005. ISBN: 9780471698333. URL: https://books.google.es/books?id=f-9QAAAAMAAJ.

[13] Antonio Garcia, Ernesto Pérez-Chavela, and Toni Susin. "A Generalization of the Poincaré Compactification". In: *Archive for Rational Mechanics and Analysis* 179 (Feb. 2006), pp. 285–302. DOI: 10.1007/s00205-005-0389-y.

[14] P. Mardešić, D. Marín, and J. Villadelprat. "The period function of reversible quadratic centers". In: *Journal of Differential Equations* 224.1 (2006), pp. 120–171. ISSN: 0022-0396. DOI: https://doi.org/10.1016/j.jde.2005.07.024. URL: https://www.sciencedirect.com/science/article/pii/S0022039605002500.

[15] Freddy Dumortier, Jaume Llibre, and Joan Artés. *Qualitative Theory Of Planar Differential Systems*. June 2007. ISBN: 978-3-540-32893-3. DOI: 10.1007/978-3-540-32902-2.

[16] J. Villadelprat. "On the Reversible Quadratic Centers with Monotonic Period Function". In: *Proceedings of the American Mathematical Society* 135.8 (2007), pp. 2555–2565. ISSN: 00029939, 10886826. URL: http://www.jstor.org/stable/20534856 (visited on 08/30/2023).

[17] J. Villadelprat. "The period function of the generalized Lotka–Volterra centers". In: *Journal of Mathematical Analysis and Applications* 341.2 (2008), pp. 834–854. ISSN: 0022-247X. DOI: https://doi.org/10.1016/j.jmaa.2007.10.053. URL: https://www.sciencedirect.com/science/article/pii/S0022247X07012966.

[18] David Griffiths and Desmond Higham. *Numerical methods for ordinary differential equations. Initial value problems*. Jan. 2010. ISBN: 978-0-85729-147-9. DOI: 10.1007/978-0-85729-148-6.

[19] A.A. Albert and R. Sandler. *An Introduction to Finite Projective Planes*. Dover Books on Mathematics. Dover Publications, 2015. ISBN: 9780486789941. URL: https://books.google.es/books?id=%5C_E-RBQAAQBAJ.

[20] Christian Gorski. *Math 20860: Honors Calculus IV*. Accessed June 15, 2023. https://www3.nd.edu/~jdiller/teaching/archive/spring15_20860/Integrals_over_Curves_and_Surfaces.pdf. University of Notre Dame. 2015.

[21] *Equacions diferencials i modelització*. Apunts de les assignatures d' *Equacions diferencials i modelització I i II* impartides al grau de Matemàtiques, 2020.

[22] Pablo Pedregal. *Hilbert's 16th problem*. 2021. arXiv: 2103.07193 [math.DS].

[23] D. Marín and J. Villadelprat. "The criticality of reversible quadratic centers at the outer boundary of its period annulus". In: *Journal of Differential Equations* 332 (2022), pp. 123–201. ISSN: 0022-0396. DOI: https://doi.org/10.1016/j.jde.2022.05.026. URL: https://www.sciencedirect.com/science/article/pii/S002203962200359X.

[24] C. Chicone. In: *Review in MathSciNet* (). Ref. 94h:58072.

Appendices

A Numerical methods. Fourth-order Runge-Kutta

The Euler's method contains the basis of many other numerical methods for resolve ordinary differential equations [18]. Let $\dot{x} = f(x)$, where $f : \Omega \longrightarrow \mathbb{R}^n$ and $\Omega \subset \mathbb{R} \times \mathbb{R}^n$, be an autonomous ordinary differential equation and $x_0 = x(t_0)$ an initial condition given. The problem to be dealt with consists of finding an approximation for $x(t)$.

The results in this section will be discussed for $n = 1$ but they can be easily extrapolated for $n > 1$. A Taylor series expansion of $x(t)$ at t_0 suggests

$$x(t_0 + h) = x(t_0) + \frac{dx}{dt}(t_0)h + \frac{1}{2}\frac{d^2x}{dt^2}(t_0)h^2 + O(h^3) \tag{A.1}$$

The Euler's method takes a first order approximation, that is to say, neglecting terms of second and higher orders. As $x'(t_0) = f(x_0)$, then $x(t_0 + h) \approx x(t_0) + hx'(t_0) = x(t_0) + hf(x_0)$ and this is the approximation that is used in the iterative methods. Given the initial condition, x_1 is taken as $x(t_0 + h)$ and, iterating

$$x_{n+1} = x_n + hf(x_n) \tag{A.2}$$

where h is called the step-size. The iteration given by (A.2) is the equation of a straight line where the slope is $f(x_n)$.

The local truncation error for this method -the error committed after one iteration of the process- is given by the difference between the numerical value and the exact value. Taking as the exact solution for the first iteration the expression given by (A.1), the local truncation error, denoted by e, is:

$$e = \frac{h^2}{2}x''(t_0) + O(h^3) \tag{A.3}$$

Therefore, for small values of h, the error after one iteration is directly proportional to h^2. For this reason, Euler's method usually is not convenient as a smal step-size is needed and this implies a high computational cost.

As said before, Euler's method estimates the value of the $(n + 1)$-iteration by the straight line (A.2) and the slope of this line is approximated by the value of f in the previous iteration, that is, the slope is computed taking into account only the left end of the interval $[t_0, t_0 + h]$. This is why a way of improving the method consists of computing this slope taking into account more points of the interval. Although an enhancement in the result is intuitive, the more points considered, the more computational cost associated. Thus, a balance between computational cost and accuracy must be achieved.

The 4th order Runge-Kutta method [18], which will not be deduced here, is based on the intuitive idea of calculating a better approximation for the slope of the iterative line by using more points of the interval $(t_0, t_0 + h)$ and giving greater weight to those in the middle. The following numbers are required in each iteration in an autonomous ODE system:

$$\begin{aligned} k_1 &= f(x_n)h \\ k_2 &= f\left(x_n + \frac{1}{2}k_1\right)h \\ k_3 &= f\left(x_n + \frac{1}{2}k_2\right)h \\ k_4 &= f(x_n + k_3)h \end{aligned}$$

Then the iterative method is given by the following expression:

$$x_{n+1} = x_n + \frac{1}{6}(k_1 + 2k_2 + 2k_3 + k_4) \tag{A.4}$$

The local truncation error produced by this method is of the order of $O(h^5)$, which considerably reduces the error produced by Euler's method. Each iteration is obtained by multiplying the interval length h by the estimated slope. The time interval corresponding to the n-th iteration is (t_n, t_{n+1}), then for non-autonomous ODE systems

$$\begin{aligned} k_1 &= f(t_n, x_n) \\ k_2 &= f\left(t_n + \frac{h}{2}, x_n + \frac{h}{2}k_1\right) \\ k_3 &= f\left(t_n + \frac{h}{2}, x_n + \frac{h}{2}k_2\right) \\ k_4 &= f(t_n + h, x_n + hk_3) \end{aligned}$$

Therefore, k_1 can be interpreted as the slope at the initial point of the time interval (the one used by Euler's method), k_2 and k_3 the slopes at the middle time point but different spatial point and k_4 the slope at the end point of the interval. As equation (**??**) states, the slopes in the middle point have a greater weight in the average.

A.1 Modified 4th-order Runge Kutta for Loud systems

Numerically, the solution of $\dot{x} = f(x)$ for a given initial condition $x_0 = x(t_0)$ is obtained by iterating equation (A.4) N times with a given step-size h. At each step of the iterative process, for $f : \Omega \longrightarrow \mathbb{R}^2$ in Loud systems, three values are obtained, namely (t_n, x_n, y_n), where x and y stand for the usual Cartesian coordinates. When studying the period function, the main interest lies on the value of t_n.

The reversible property of Loud systems constitutes a powerful shortcut in terms of increasing the accuracy of the numerical period since it is not necessary to iterate along a complete periodic orbit but only along half of it. Bearing this in mind, the symmetry with respect to the x-axis provides a condition to stop the iterative process and therefore, saving up computational cost.

The main idea of the modified algorithm remains on implementing a buffer that constitutes a kind of memory in such a way that at each iteration, the algorithm is saving both the current computed value y_n and the previous computed value y_{n-1}. So, by comparing at each iteration the sign of y_n and y_{n-1}, it is possible to find whether the numerical method has crossed or not the x-axis by only detecting a

change in the sign, i.e. the numerical orbit crosses from semi-plane $\{y > 0\}$ to semi-plane $\{y < 0\}$. Below, the main steps of the algorithm are listed:

1. Initialize the iterative process by providing the initial conditions (t_0, x_0, y_0).
2. At each step, compute $(t_{n+1}, x_{n+1}, y_{n+1})$ using the value of the previous iteration (t_n, x_n, y_n) as stated in equation (A.4) and save it to the buffer. Since the buffer considered is tridimensional, it will contain, at each step, the current value (t_n, x_n, y_n) and the value of the previous iteration $(t_{n-1}, x_{n-1}, y_{n-1})$.
3. Verify if condition $y_{n-1} \cdot y_n < 0$ is fulfilled. If true, the orbit has crossed the x-axis. Move back to the former step and reduce the time step h in order to increase the accuracy, i.e.
$$(t_n, x_n, y_n) \longrightarrow (t_{n-1}, x_{n-1}, y_{n-1}), \qquad t_{n-1} = t_n \cdot 0.01$$
4. Repeat the process from step 2 until the total number of iterations has been reached or a desired accuracy has been achieved.
5. Stop the iterative process. The value of t_N, where N is the last iteration performed, is half of the period of the periodic orbit.

At first, a stop condition was introduced in order to stop the Runge-Kutta method once the orbit had crossed the x-axis. However, this condition depended on a tolerance whose efficacy varied enormously depending on the value of the parameter $\mu = (D, F)$. For this reason, and despite increasing the computational time, this stop condition was decided to be removed in order to obtain more accurate results.

B Line integrals

Let $U \subset \mathbb{R}^2$ be an open subset. A function $\omega : U \to (\mathbb{R}^2)^*$ such that

$$\omega(x) = \sum \omega_i(x) dx_i, \tag{B.1}$$

for all $x \in U$, where $\omega_i : U \to \mathbb{R}$ are scalar functions, is said to be a *differential 1-form*. The following theorem is a fundamental result of calculus for curves [20]:

Theorem B.1. *(The Fundamental Theorem of Calculus for Curves) Let $U \subset \mathbb{R}^n$ be an open set and $[a, b] \subset \mathbb{R}$ a compact interval. If $f : U \to \mathbb{R}$ is a $\mathcal{C}^1$ functon and $\gamma : [a, b] \to U$ a $\mathcal{C}^1$ curve, then*

$$\int_\gamma df = f(\gamma(b)) - f(\gamma(a)).$$

Therefore, the value of the integral of a given function over a curve only depends on the extreme points where the curve is defined and its orientation, i.e. the line integral is independent of the path used to travese the curve. Thus, the line integral along a closed curve is exactly zero since the initial and end points coincide, i.e. assuming γ is a closed curve,

$$\int_\gamma df = f(\gamma(a)) - f(\gamma(a)) = 0. \tag{B.2}$$

C General algorithm to find the period function using $\mathbb{RP}^2$ compactification

Algorithm used to perform all computations related to obtain the number of critical periods in the period function for each value of $\mu = (D, F)$ is displayed explicitly below. Code is implemented using C programming language and the whole executable consists of three main files: two C files and a header file. File `main.c` is the driver of the execution where main variables for execution are declared, text files needed are managed and different functions are called. These functions are defined in `orbit.c` file and are linked to the main execution through the header file `orbit.h`.

Since the study of the period annulus in the parameters space has required multiple tests, the main program is structured in different modes, numbered with integers, and each one is selected at the beginning of the execution by the user. Comments in the code are stated after a // symbol. Below, the content of file `main.c` is stated.

```
#include<stdio.h>
#include<math.h>
#include<stdlib.h>

#include "orbit.h"
#define pi 3.14159265359

int main()
{
    int mode;
    int min_it, n_orbits;
    int i, j;
    double D, F, param, tol, h;

    param = 0.54;       // parameter in Cartesian coordinates to identify a periodic orbit
    h = 1e-4;           // step-size for the 4th order Runge-Kutta method

    printf("Choose the mode you want: ");
    scanf("%d", &mode);

    FILE* file;         // declaration of text file
    FILE* extremes;     // declaration of text file
    FILE* derivative;   // declaration of text file
    const char* title;  // declaration of a variable containing the title of a text file

    // Given the value of the parameter, computes position and time values for each
    // iteration. It is a single execution of the 4th-order Runge-Kutta method for
    // a given value of D, F and the parameter.
    if (mode == 0)
    {
        D = -0.01;
        F = 0.99;
```

```
    go_single_orbit(D, F, param,h);
}

// This mode performs a double loop to compute the extremes and the value of the
// period function in a certain region of the parameters space.
else if (mode == 1)
{
    double int_point;
    D = 0; F = 0;
    extremes = fopen("extremes.txt", "w");
    for (i = 0; i < 10; i++)
    {
        D = -i*0.1;
        for (j = 0; j < 10; j++)
        {
            F = j*0.1;
            title = get_title(D, F);
            file = fopen(title, "w");
            free(title);
            int_point = intersection_point(D, F);
            go_period_annulus(D, F, h, file, extremes, 10000, int_point);
            fclose(file);
        }
    }
    fclose(extremes);
}

// This mode computes the value of the period function and the number of critical
// periods for a given value of parameters D and F. Values of D, F and the number
// of orbits required for the discretization of the period annulus are introduced
// by the user.
else if (mode == 2)
{
 double int_point;

    printf("Introduce D: ");
    scanf("%lf", &D);
    printf("Introduce F: ");
    scanf("%lf", &F);
    printf("Introduce the number of orbits: ");
    scanf("%d", &n_orbits);

    title = get_title(D, F);
    derivative = fopen("derivative.txt", "w");
    file = fopen(title, "w");
    free(title);
    int_point = intersection_point(D, F);
    go_period_annulus(D, F, h, file, derivative, n_orbits, int_point);
    fclose(file);
```

```
    fclose(derivative);
}

// This method is analogous to mode 1 but it just computes the number of critical
// periods for each pair D and F using a double loop. It calls function
// go_period_annulus_extremes, which is a slight variation of function
// go_period_annulus in such a way that it only produeces as output the file
// containing critical values.
else if (mode == 6)
{
    double int_point;

    n_orbits = 10000;
    D = 0; F = 0;
    extremes = fopen("D_-2_-1.4_F_2_2.5.txt", "w");

    for (i = 0; i < 61; i++)
    {
        D = -1.4 - i * 0.01;
        for (j = 0; j < 51; j++)
        {
            F = 2.0 + j * 0.01;
            int_point = intersection_point(D, F);
            go_period_annulus_extremes(D, F, h, extremes, n_orbits, int_point);
        }
    }
    fclose(extremes);
}

// Method analogous to mode 2 but using the variation of go_period_annulus_extremes.
else if (mode == 7)
{
    double int_point;

    printf("Introduce D: ");
    scanf("%lf", &D);
    printf("Introduce F: ");
    scanf("%lf", &F);
    printf("Introduce the number of orbits: ");
    scanf("%d", &n_orbits);

    extremes = fopen("prova_2_períodes.txt", "w");
    int_point = intersection_point(D, F);
    go_period_annulus_extremes(D, F, h, extremes, n_orbits, int_point);
    fclose(extremes);
}
else
{
    printf("There is no mode associated to value %d.", mode);
```

```
    }
    return 0;
}
```

Below, the algorithm used to compute the period function for a given value of parameter $\mu = (D, F)$ is displayed. It is presented as a function called `go_period_annulus` which does not return any variable and receives as input parameters:

- `D` and `F`. Values of parameter $\mu = (D, F)$ as double type variables.
- `h`. Step-size for the 4th-order Runge-Kutta numerical method. It is a double type variable.
- `*txt` and `*txt2`. Text files as pointers to write the period of each periodic orbit within the period annulus and the value of the derivative of the period function for each value of the parameter, respectively.
- `n_orbits`. Specifies the number of orbits into which the period annulus will be divided in its discretization. It is an integer type variable.
- `int_point`. Value of $x \in (0, 1]$ where invariant curve $g_2(x, y) = 0$ (see equation (5.0.15)) intersects axis $y = 0$. The study carried out in this thesis contemplates regions of the parameters space such that the period annulus of the center at the origin contains this invariant curve at its outer boundary. See phase portraits in figure 4 from [14]. It is a double type variable.

As stated in the code of `main.c` above, there exists an implemented slight variation of this method called `go_period_annulus_extremes` which just produces as output a text file containing the number of critical periods in the period function for each value of $\mu = (D, F)$ computed. For the sake of similarity, only the code of method `go_period_annulus` will be displayed in this appendix. In this code, compactification explained in section 6.1 is used and hence, Loud system is defined in coordinates $u - v$. Content below is included in `orbit.c`.

```
#include "orbit.h"

double g1(double u, double v, double D, double F)
{
    return -(D + F + 1) * u * u - (D + F - 1) * v * v + 2 * F * u
           - (2 * (D - F + 1) * u + 2 * F - 1) * v - F;
}
double g2(double u, double v, double D, double F)
{
    return -(1. / u) * ((D + F - 1) * v * v * v + 2 * ((D - F + 1) * u + F - 1) * v * v
           + ((D + F + 1) * u * u - (2 * F - 1) * u + F - 1) * v);
}

typedef double (*func)(double, double, double, double);
func g[2] = { *g1,*g2 };
```

```
void go_period_annulus(double D, double F, double h, FILE * txt, FILE * txt2,
                       int n_orbits, double int_point)
{
    double Tf;                          // theoretical final period
    int n = 100000, d = 2;              // n -> number of iterations, d -> dimension
    int i, j, k;                        // counters
    double k1[2], k2[2], k3[2], k4[2];  // rk4 coefficients

    int max = 0, min = 0;               // counters for the number of relative extremes
    double dT_buffer[] = {0,0};         // buffer for the derivative of the period function
    double T_buffer[] = {0,0,0,0,0};    // buffer containing time of 5 consecutive orbits
    double s_buffer[] = {0,0,0,0,0};    // buffer containing the parameter associated to 5
                                        // consecutive orbits
    double err_rel;                     // relative error between the numerical final
                                        // period and the theoretical final period Tf


    double s = 0;                       // orbit parameter
    double der;                         // value of the derivative
    double step = int_point / n_orbits; // step-size discretization period annulus

    // Values of a, b and c given by the expression of the first integral
    double a, b, c;
    a = D / (2 * (1 - F));
    b = (D - F + 1) / ((1 - F) * (1 - 2 * F));
    c = (F - D - 1) / (2 * F * (1 - F) * (1 - 2 * F));

    // Loop through all periodic orbits within the discretization of the period annulus
    for (j = 1; j < n_orbits; j++)
    {
        double x1[] = { 0,0,0 };
        double time = 0;
        s = j * int_point / n_orbits;   // parameter value in x,y coordinates

        // Initial conditions in u,v coordinates (compactification)
        double x00[] = { 1. / (2 - s),(s - 1) / (2 - s),0 };
        double x0[] = { x00[0],x00[1],x00[2] }; // initial conditions

        // 4th order Runge-Kutta method
        for (i = 0; i < n; i++)
        {
            // Save the previous iteration
            for (k = 0; k < d; k++)
            {
                x1[k] = x0[k];
            }
            x1[d] = x0[d];
```

```
    // RK4 using compactification
    for (k = 0; k < d; k++) { k1[k] = h * g[k](x0[0], x0[1], D, F); }
    for (k = 0; k < d; k++)
    {
        k2[k] = h * g[k](x0[0] + k1[0] * 0.5, x0[1] + k1[1] * 0.5, D, F);
    }
    for (k = 0; k < d; k++)
    {
        k3[k] = h * g[k](x0[0] + k2[0] * 0.5, x0[1] + k2[1] * 0.5, D, F);
    }
    for (k = 0; k < d; k++)
    {
        k4[k] = h * g[k](x0[0] + k3[0], x0[1] + k3[1], D, F);
    }

    for (k = 0; k < d; k++)
    {
        x0[k] = x0[k] + (k1[k] + 2. * k2[k] + 2. * k3[k] + k4[k]) * (1. / 6.);
    }
    x0[d] = x0[d] + h;
    time = time + h;

    // Si travessem la recta, fem tornem a la iteració anterior i reduïm el pas de
    // temps per tal d'aconseguir el període més acurat possible. La regió u-v < 1
    // correspon a estar per sobre de la recta v = u-1 i la regió u-v > 1 a estar
    // per sota.

    if (x0[0] - x0[1] > 1)
    {
        for (k = 0; k < d + 1; k++)
        {
            x0[k] = x1[k];
        }
        time = time - h;
        h = h * 0.01;
        i = i - 2;
    }
}

// Update period and parameter buffers values
for (int i = 0; i < 4; i++)
{
    T_buffer[i] = T_buffer[i+1];
    s_buffer[i] = s_buffer[i+1];
}
T_buffer[4] = x0[d];
s_buffer[4] = s;
```

```
// Compute the number of relative extremes by comparing values
if (T_buffer[0] != 0 && T_buffer[1] != 0 && T_buffer[2] != 0
    && T_buffer[3] != 0 && T_buffer[4] != 0)
{
    // MAXIMUM CONDITION (4 POINTS NEIGHBOURHOOD)
    if (T_buffer[0] < T_buffer[2] && T_buffer[1] < T_buffer[2] &&
        T_buffer[3] < T_buffer[2] && T_buffer[4] < T_buffer[2] &&
        T_buffer[0] < T_buffer[1] && T_buffer[3] > T_buffer[4])
        {
            if (fabs(T_buffer[2] - T_buffer[1]) > 0.01 ||
            fabs(T_buffer[3] - T_buffer[2]) > 0.01){}
            else{max++;}
        }
    // MINIMUM CONDITION (4 POINTS NEIGHBOURHOOD)
    if (T_buffer[0] > T_buffer[2] && T_buffer[1] > T_buffer[2] &&
        T_buffer[3] > T_buffer[2] && T_buffer[4] > T_buffer[2] &&
        T_buffer[0] > T_buffer[1] && T_buffer[3] < T_buffer[4])
        {
            if (fabs(T_buffer[2] - T_buffer[1]) > 0.01 ||
            fabs(T_buffer[3] - T_buffer[2]) > 0.01){}
            else{min++;}
        }
}

// Compute the derivative
// first orbit, 2nd iteration
if (T_buffer[0] == 0 && T_buffer[1] == 0 && T_buffer[2] == 0 && T_buffer[3] != 0)

{
    // FORWARD DIFFERENCES NUMERICAL DERIVATIVE
    der = (T_buffer[4] - T_buffer[3]) / step;
    dT_buffer[0] = dT_buffer[1];
    dT_buffer[1] = der;
    fprintf(txt2, "%.8lf \t\t %.10lf \n", s_buffer[3], der);
}
// second orbit, 3rd iteration
else if (T_buffer[0] == 0 && T_buffer[1] == 0 && T_buffer[2] != 0)
{
    // CENTERED DIFFERENCES NUMERICAL DERIVATIVE
    der = (T_buffer[4] - T_buffer[2]) / (2*step);
    dT_buffer[0] = dT_buffer[1];
    dT_buffer[1] = der;
    fprintf(txt2, "%.8lf \t\t %.10lf \n", s_buffer[3], der);
}
// rest of periodic orbits within the period annulus
else if (T_buffer[0] != 0 && T_buffer[1] != 0 && T_buffer[2] != 0
        && T_buffer[3] != 0 && T_buffer[4] != 0)
{
    // FIVE POINTS NUMERICAL DERIVATIVE
```

```
        der = (T_buffer[0] - 8*T_buffer[1] + 8*T_buffer[3] - T_buffer[4]) / (12*step);
        dT_buffer[0] = dT_buffer[1];
        dT_buffer[1] = der;
        fprintf(txt2, "%.8lf \t\t %.10lf \n", s_buffer[2], der);
    }

    fprintf(txt, "%.8lf \t\t", s);      // print orbit parameter to the text file
    fprintf(txt, "%.8f \t\t", x00[0]);
    fprintf(txt, "%.10lf \n", x0[d]);   // print period of the orbit to the text file

    // Compare the theoretical value of the period near the outer boundary
    // with the obtained value using the numerical approach
    if (j == n_orbits-1)
    {
        if (D < 0 && D > -1 && F > 0 && F < 1)
        {
            Tf = pi / (2 * sqrt(F * (D + 1)));
        }
        else if (F > 2)
        {
            Tf = sqrt(2)*atanh((2*a + b
            - sqrt(b*b - 4*a*c))/(2*sqrt(a*(a+b+c)))) / sqrt(a+b+c);
        }

        err_rel = fabs(Tf-x0[d])/Tf;

        // In order to plot the values of the relative error, we will distinguish
        // among several cases. Each case is a range of the relative error.
        if (err_rel < 0.01)
        {
         fprintf(minmax,"%lf \t\t %lf \t\t %lf \t\t %lf \t\t %lf \t\t %lf \t\t %d \n",
            D, F, Tf,x0[d],fabs(Tf-x0[d]),err_rel,1);
         printf("%lf \t\t %lf \t\t %lf \t\t %lf \t\t %lf \t\t %lf \t\t %d \n", D, F,
            Tf,x0[d],fabs(Tf-x0[d]),err_rel,1);
        }
        else if (err_rel < 0.05 && err_rel > 0.01)
        {
         fprintf(minmax,"%lf \t\t %lf \t\t %lf \t\t %lf \t\t %lf \t\t %lf \t\t %d \n",
            D, F, Tf,x0[d],fabs(Tf-x0[d]),err_rel,5);
         printf("%lf \t\t %lf \t\t %lf \t\t %lf \t\t %lf \t\t %lf \t\t %d \n", D, F,
            Tf,x0[d],fabs(Tf-x0[d]),err_rel,5);
        }
        else if (err_rel < 0.1 && err_rel > 0.05)
        {
         fprintf(minmax,"%lf \t\t %lf \t\t %lf \t\t %lf \t\t %lf \t\t %lf \t\t %d \n",
            D, F, Tf,x0[d],fabs(Tf-x0[d]),err_rel,10);
         printf("%lf \t\t %lf \t\t %lf \t\t %lf \t\t %lf \t\t %lf \t\t %d \n", D, F,
            Tf,x0[d],fabs(Tf-x0[d]),err_rel,10);
        }
```

```
            else if (err_rel < 0.5 && err_rel > 0.1)
            {
             fprintf(minmax,"%lf \t\t %lf \t\t %lf \t\t %lf \t\t %lf \t\t %lf \t\t %d \n",
                D, F, Tf,x0[d],fabs(Tf-x0[d]),err_rel,50);
             printf("%lf \t\t %lf \t\t %lf \t\t %lf \t\t %lf \t\t %lf \t\t %d \n", D, F,
                Tf,x0[d],fabs(Tf-x0[d]),err_rel,50);
            }
            else
            {
             fprintf(minmax,"%lf \t\t %lf \t\t %lf \t\t %lf \t\t %lf \t\t %lf \t\t %d \n",
                D, F, Tf,x0[d],fabs(Tf-x0[d]),err_rel,-1);
             printf("%lf \t\t %lf \t\t %lf \t\t %lf \t\t %lf \t\t %lf \t\t %d \n", D, F,
                Tf,x0[d],fabs(Tf-x0[d]),err_rel,-1);
            }
        }
    }
    // Print the number of critical periods computed by comparing values in a
    // 4-points neighbourhood
    printf("%lf \t\t %lf \t\t %d \t\t %d \t\t %d \n", D, F, max, min, max + min);
}
```

D General algorithm to find the period function by numerical integration of a differential equation

As stated in section 6.2, in order to obtain the value of half the period of a periodic orbit within the period annulus, the extremes of integration are needed. Using the reversible property of Loud systems and its first integral, both points are given by the intersection of the periodic orbit with the x-axis. Intersection point in the interval $(0, 1)$ is given by the parameter according to the parametrization of the period annulus. For the other intersection point, since $x < 0$, Newton-Raphson method must be used to find it. This method is implemented by means of a function which returns the value of the intersection point as a double type variable and receives the following parameters as input:

- `x0`. It is the initial seed needed to start the iterative process. Since the intersection point sought satisfies $x < 0$, the initial seed will be set to -1.
- `h`. It is the energy level of a given orbit according to the first integral.
- `D` and `F`. Values of the parameter $\mu = (D, F)$.

```
double NewtonRaps(double x0, double h, double D,double F)
{
    // Variables needed for Newton's method
    double eps, N, df, f, dx, x1;
    int i;
    N = 10000;
    eps = 0.001;
```

```
    f = H(x0, 0, D, F, h);                          // Initial value
    for (i = 0; i < N; i++)
    {
        df = dH(x0, D, F);                           // Value of the derivaitve evaluated
        f = H(x0, 0, D, F, h);                       // Value of the function evaluated
        dx = -f / df;                                // Quotient between the function and
                                                     // its derivative
        x1 = x0 + dx;                                // Value of the new iteration
        f = H(x1, 9, D, F, h);
        if (fabs(f) < eps || fabs(dx) < eps)         // Stop condition
        {
            break;
        }
        x0 = x1;                                     // Update variables for next iteration
    }
    return x1;
}
```

Next, once the integration extremes are computed, integration of the period function is carried out as stated in section 6.2. Composite Simpson's rule [12] is used to integrate expression (6.2.2). The code implemented in C is displayed below as a function called `comp_simpson` returning a double type variable. As input parameters, function receives:

- `a` and `b`. Double type arguments referring to lower and upper limits of integration, respectively.
- `N`. Integer type argument associated to the number of subdivisions within the integration interval.
- `D` and `F`. Double type arguments associated to parameter value $\mu = (D, F)$.
- `h`. Double type argument referring to the energy level of the periodic orbit whose period is intended to be computed.
- `*f`. Pointer to a function `f` which returns a double type variable and receives as input arguments, four double type variables. It is the function to be integrated.

Since the number of subdivisions for the composite Simpson's rule must be even by definition, an error message is shown by screen if `N` is an odd integer number.

```
// Composite Simpson's rule
double comp_simpson(double a, double b, int N, double D, double F, double h,
       double (*f)(double,double,double,double))
{
    double integral, sum1 = 0, sum2 = 0, step;
    step = (b - a) / N;
    if (N % 2 != 0)
    {
     printf("An even number of segments is required
```

```
        for the composite Simpson's rule. \n");
     integral = 0.0;
    }
    else
    {
     for (int i = 0; i < (N / 2); i++)
     {
     sum1 = sum1 + f(a + (2 * i + 1) * step,D,F,h);
     }
     for (int j = 1; j < N; j++)
     {
     sum2 = sum2 + f(a + j * step,D,F,h);
     }
     // integral = (step / 3) * (f(a,D,F,h) + f(b,D,F,h) + 2 * (sum1 + sum2));
     integral = step * (2 * (sum1 + sum2)) / 3;
    }
    // printf("%.8f \n", integral);
    return integral;
}
```

Bearing both functions `NewtonRaps` and `comp_simpson` in mind, in order to compute half of the period of a given periodic orbit with energy level h, expression (6.2.2) can be calculated as follows. Variable `param` refers to the parameter associated to periodic orbit with energy level h, variable `hh` is the energy level, `xl` is the intersection point of the periodic orbit with the x-axis and `I1` and `I2` are, respectively, expressions to be integrated according to (6.2.2), which are declared in a different C file.

```
    double D, F, param, hh, xl, T;
    int N = 10000;

    D = -0.25;
    F = 0.25;
    param = 0.0001;
    hh = H(param, 0, D, F, 0);
    xl = NewtonRaps(-1, hh, D, F);

    T = comp_simpson(xl, param, N, D, F, hh, I1) / hh
    + 2 * comp_simpson(xl, param, N, D, F, hh, I2) / hh;
```